REFERENCES

Allen, P. G. 2003. Actin filament uncapping localizes to ruffling lamellae and rocketing vesicles. Nat. Cell Biol. 5: 972-979.

Allingham, J. S., Tanaka, J., Marriott,G., and Rayment, I. 2004. Absolute stereochemistry of ulapualide A. Org. Lett. 6: 597-599.

Barkalow, K., Witke, W., Kwaiatkowski, D. J., and Hartwig, J. H. 1996. Coordinated regulation of platelet actin filament barbed ends by gelsolin and capping protein. J. Cell Biol. 134: 389-399.

Breinbauer, R., and Köhn, M. 2003. Azide-alkyne coupling: A powerful reaction for bioconjugate chemistry. ChemBioChem 4: 1147-1149.

Bubb, M. R., Senderowicz, A. M. J., Sausville, E. A., Duncan, K. L. K., and Korn, E. D. 1994. Jasplakinolide, a cytotoxic natural product, induces actin polymerization and competitively inhibits the binding of phalloidin to F-actin. J. Biol. Chem. 269: 14869-14871.

Bubb, M. R., Spector, I., Bayer, B. B., and Fosen, K. M. 2000. Effects of jasplakinolide on the kinetics of actin polymerization. J. Biol. Chem. 275: 5163-5170.

Chattopadhyay, S. K., and Pattenden, G. 2000. A total synthesis of the unique tris-oxazole macrolide ulapualide A produced by the marine nudibranch *Hexabranchus sanguineus*. J. Chem. Soc. 1: 2429-2454.

Choidas, A., Jungbluth, A., Sechi, A., Murphy, J., Ullrich, A., and Marriott. G. 1998. The suitability and application of a GFP-actin fusion protein for long-term imaging of the organization and dynamics of the cytoskeleton in mammalian cells. Eur. J. Cell Biol. 77: 81-90.

Cooper, J. A. 1987. Effects of cytochalasin and phalloidin on actin. J. Cell Biol. 105: 1473-1478.

Cooper, J. A., and Schafer. D. A. 2000. Control of actin assembly and disassembly at filament ends. Curr. Opin. Cell Biol. 12: 97-103.

Coue, M., Brenner, S. L., Spector, I., and Korn, E. D. 1987. Inhibition of actin polymerization by latrunculin A. FEBS Lett. 213: 316-318.

De La Cruz, E. M., and Pollard, T. D. 2001. Actin' Up. Science 293: 616-618.

Doi, Y. K., Banba, M., and Vertut-Doi, A. 1991. Cysteine-374 of actin resides at the gelsolin contact site in the EGTA-resistant actin-gelsolin complex. Biochemistry 30: 5769-77.

Faulstich, H., Zobeley, S., Rinnerthaler, G., Small, J. V. 1988. Fluorescent phallotoxins as probes for filamentous actin. J. Muscle Cell Motil. 9: 370-383.

Fernández, R., Dherbomez, M., Letourneux, Y., Nabil, M., Verbist, J. F., and Biard, J. F. 1999. Antifungal metabolites from the marine sponge *Pachastrissa* sp.: New bengamide and bengazole derivatives. J. Nat. Prod. 62: 678-680.

Forscher, P., and Smith, S. J. 1988. Actions of cytochalasins on the organization of actin filaments and microtubules in a neuronal growth cone. J. Cell Biol. 107: 1505-1516.

Fox, J. E. B., and Phillips, D. R. 1981. Inhibit of actin polymerization in blood platelet by cytochalasins. Nature 292: 650-652.

Fusetani, N., Yasumuro, K., Matsunaga, S., and Hashimoto, K. 1989. Mycalolides A-C, hybrid macrolides of ulapualides and halichondramide, from a sponge of the genus *Mycale*. Tetrahedron Lett. 30: 2809-2812.

Gordon, D. J., Yang, Y. Z., and Korn, E. D. 1976. Polymerization of Acanthamoeba actin. Kinetics, thermodynamics, and co-polymerization with muscle actin. J. Biol. Chem. 251: 7474-7479.

Groweiss, A., Shmueli, U., and Kashman, Y. 1983. Marine toxins of *Latrunculia magnifica*. J. Org. Chem. 48: 3512-3516.

Heidecker, M., Yan-Marriott, Y., and Marriott. G. 1995 Proximity relationships and structural dynamics of the phalloidin binding site of actin filaments in solution and on single actin filaments on heavy meromyosin. Biochemistry 34: 11017-11025.

Holmes, K. C., Popp, D., Gebhard, W., and Kabsch, W. 1990. Atomic model of the actin filament. Nature 347: 44-49.

Hooper, J. N. A. 2000. Sponguide: Guide to sponge collection and identification [online]. Available from: http://www.qmuseum.qld.gov.au/organisation/sections/SessileMarineInvertebrates/index.asp[2003, June 12]

Horne, W. S., Stout, C. D., and Ghadiri, M. R. 2003. A heterocyclic peptide nanotube J. Am. Chem. Soc. 125: 9372-9376.

Invitrogen Corporation 2004. Fluorescence polarization technical resource guide [online]. Available from: http://www.invitrogen.com/downloads/FP1.pdf #search='invitrogen%20anisotropy[2004, November 20].

Janmey, P. A., Chapporier, C., Lind, S. E., Zaner, K. S., Stossel, T. P., and Yin, H. L. 1985. Interactions of gelsolin and gelsolin-actin complexes with actin. Effects of calcium on actin nucleation, filament severing, and end blocking. Biochemistry 24: 3714-3723.

Kabsch, W., Mannherz, H. G., Suck, D., Pai, E. F., and Holmes, K. C. 1990. Atomic structure of the actin: DNase I complex. Nature 347: 37-44.

Kernan, M. R., and Faulkner, D. J. 1987. Halichondramide, an antifungal macrolide from the sponge *Halichondria* sp. Tetrahedron Lett. 28: 2809-2812.

Kernan, M. R., Molinski, T. F., and Faulkner, D. J. 1988. Macrocyclic antifungal metabolites from the Spanish dancer nudibranch *Hexabranchus sanguineus* and sponges of the genus *Halichondria*. J. Org. Chem. 53: 5014-5020.

Klenchin, V. A., Allingham, J. S., King, R., Tanaka, J., Marriott, G., and Rayment, I. 2003. Trisoxazole macrolide toxins mimic the binding of actin-capping proteins to actin. Nat. Struc. Biol. 10: 1058-1063.

Ko, S. Y. 2002. Unusual regioselection in the Mitsunobu reactions of *syn*-2,3-dihydroxy esters: synthesis of statine and its diastereomer. J. Org. Chem. 67: 2689-2691.

Kobayashi, J., Murata, O., and Shigemori, H. 1993. Jaspisamides A-C, new cytotoxic macrolides from the Okinawan sponge *Jaspis* sp. J. Nat. Prod. 56: 787-791.

Kobayashi, J., Tsuda, M., Fuse, H., Sasaki, T., and Mikami, Y. 1997. Halishigamides A-D, new cytotoxic oxazole-containing metabolites from Okinawan sponge *Halichondria* sp. J. Nat. Prod. 60: 150-154.

Kuroda, I., Musman, M., Ohtani, I. I., Ichiba, T., Tanaka, J., Gravalos, D. G., and Higa, T. 2002. Pachastrissamine, a cytotoxic anhydrophytosphingosine from a marine sponge, *Pachastrissa* sp. J. Nat. Prod. 65: 1505-1507.

Lodish, H., Berk, A., Matsudaira, P., Kaiser, C. A., Krieger, M., Scott, M. P., Zipursky, S. L., and Darnell, J. 2003. Molecular cell biology, 5th ed. New York: W. H. Freeman and Company.

Lorenz, M., Popp, D., and Holmes, K. C. 1993. Refinement of the F-actin model against X-ray fiber diffraction data by the use of a directed mutation algorithm. J. Mol. Biol. 234: 826-836.

Lorian, V. 1980. Antibiotics in laboratory medicine, pp 161-207. Baltimore: William & Wilkins.

Marriott, G.; Zechel, K.; Jovin T. M. 1988. Spectroscopic and functional characterization of an environmentally sensitive fluorescent actin conjugate. Biochemistry 27: 6214-6220.

Matsunaga, S., Fusetani, N., Hashimoto, K. Koseki, K., and Noma, M. 1986. Kabiramide C, a novel antifungal macrolide from nudibranch eggmasses. J. Am. Chem. Soc. 108: 847-849.

Matsunaga, S., Fusetani, N., Hashimoto, K., Koseki, K., Noma. M. Noguchi, H.; and Sankawa, U. 1989. Further kabiramides and halichondramides, cytotoxic macrolides embracing trisoxazole, from the *Hexabranchus* egg masses. J. Org. Chem. 54: 1360-1363.

Matsunaga, S., Liu, P., Celatka, C. A., Panek, J. S., and Fusetani, N. 1999. Relative and absolute stereochemistry of mycalolides, bioactive macrolides from the marine sponge *Mycale magellanica*. J. Am. Chem. Soc. 121: 5605-5606.

Matsunaga, S., Nogata, Y. and Fusetani, N. 1998a. Thiomycalolides: new cytotoxic trisoxazole-containing macrolides isolated from a marine sponge *Mycale* sp. J. Nat. Prod. 61: 663-666.

Matsunaga, S., Sugawara, T., and Fusetani, N. 1998b. New mycalolides from the marine sponge *Mycale magellanica* and their interconversion. J. Nat. Prod. 61: 1164-1167.

McLaughlin, P. J., Gooch, J. T., Mannherz, H. G., and Weeds, A. G. 1993. Structure of gelsolin segment 1-actin complex and the mechanism of filament severing. Nature 364: 685-692.

Mejillano, M. R., Kojima, S., Applewhite, D. A., Gertler, F. B., Svitkina, T. M., and Borisy, G. G. 2004. Lamellipodial versus filopodial mode of the actin nanomachinery: Pivotal role of the filament barbed end. Cell 118: 363-373.

Mitsunobu, O. 1981. The use of diethyl azodicarboxylate and triphenylphosphine in synthesis and transformation of natural products. Synthesis 1: 1-28.

Mujumdar, R. B., Ernst L. A., Mujumdar, S. R., Lewis, C. J., and Waggoner, A. S. (1993) Cyanin dye labeling reagents: Sulfoindocyanine succinimidyl esters. Bioconjugate Chem. 4: 105-111.

Olympus America Inc. 2005. Basic concepts in fluorescence[online]. Available from: http://www.olympusmicro.com/primer/techniques/fluorescence/fluorescenceintro.html[2005, April 6].

Otterbein, L. R., Graceffa, P., and Dominguez, R. 2001. The crystal structure of uncomplexed actin in the ADP state. Science 293: 708-711.

Phuwapraisirisan, P., Matsunaga, S., Van Soest, R. W. M., and Fusetani, N. 2002. Isolation of a new mycalolide from the marine sponge *Mycale izuensis*. J. Nat. Prod. 65: 942-943.

Pollard, T. D. 2003. The cytoskeleton, cellular motility and the reductionist agenda. Nature 422: 741-745.

Pollard, T. D., and Borisy, G. G. 2003. Cellular motility driven by assembly and disassembly of actin filaments. Cell 112: 453-465.

Rashid, M. A., Gustafson, K. R., Cardellina II, J. H., and Boyd, M. R. 1995. Mycalolides D and E, new cytotoxic macrolides from a collection of the stony coral *Tubastrea faulkneri*. J. Nat. Prod. 58: 1120-1125.

Roesener, J. A., and Scheuer, P. J. 1986. Ulapualide A and B, extraordinary antitumor macrolides from nudibranch eggmasses. J. Am. Chem. Soc. 108: 846-847.

Rostovsev, V. V., Green, L. G., Fokin, V. V., and Sharpless, K. B. 2002. A stepwise Huisgen cycloaddition process: copper (I)-catalyzed regioselective "ligation" of azides and terminal alkynes Angew. Chem. Int. Ed. 41: 2596-2599.

Roy, P., Rajfur, Z., Jones, D., Marriott, G., Loew, L., and Jacobson. K. 2001. Local photorelease of caged thymosin β4 in locomoting keratocytes causes cell turning. J. Cell Biol. 153: 1035-1047.

Saito, S., Watabe, S., Ozaki, H., Fusetani, N., and Karaki, H. 1994. Mycalolide B, a novel actin depolymerizing agent. J. Biol. Chem. 269: 29710-29714.

Schutt, C. E., Myslik, J. C., Rozycki, M. D., Goonesekere, C. W., and Lindberg, U. 1993. The structure of crystalline profilin-β-actin. Nature 365: 810-816.

Shin, J., Lee, H., Kim, J., Shin, H. J., Ahn, J., and Paul, V. J. 2004. New macrolides from the sponge *Chongrosia corticata*. J. Nat. Prod. 64: 1889-1892.

Small, J. V., Isenberg, G., and Celis, J. E. 1978. Polarity of actin at the leading adge of cultured cells. Nature 272: 638-639.

Spector, I., Shochet, N. R., Kashman, Y., and Groweiss A. 1983. Latrunculins: Novel marine toxins that disrupt microfilament organization in cultured cells. Science 219: 493-495.

Spudich, J. A., and Watt, S. 1971. The Regulation of Rabbit Skeletal Muscle Contraction. J. Biol. Chem. 246(15): 4866-4871.

Stachel, S. J., Chappell, M. D., Lee, C. B., Danishefsky, S. J., Chou, T., He, L., and Horwitz, S. B. 2000. On the total synthesis and preliminary biological evaluations of 15(*R*) and 15(*S*) aza-dEpoB: a Mitsunobu inversion at C15 in pre-epothilone fragments. Org. Lett. 2: 1637-1639.

Sun, H. Q., Kwiatkowska, K., and Yin, H. L. 1996. β-Thymosins are not simple actin monomer buffering proteins. J. Biol. Chem. 271: 9223-9239.

Suwanborirux, K. 2002. Bioactive marine natural products. In Yusoff, F. M., Shariff, M., Ibrahim, H. M., Tan, S. G., and Tai, S. Y. Tropical marine environment: charting strategies for the millennium, pp. 577-595. Malaysia: Universiti Putra Malaysia.

Tanaka, J., Yan, Y., Choi, J, Bai, J., Klenchin, V. A., Rayment, I., and Marriott, G. 2003. Biomolecular mimicry in the actin cytoskeleton: Mechanisms underlying the cytotoxity of kabiramide C and related macrolides. Proc. Natl. Acad. Sci. U.S.A. 100: 13851-13856.

Thale, Z., Kinder, F. R., Bair, K. W., Bontempo, J., Czuchta, A. M., Versace, R. W., Phillips, P. E., Sanders, M. L., Wattanasin, S., and Crews, P. 2001. Bengamides revisited: New structures and antitumor studies. J. Org. Chem. 66: 1733-1741.

Tornøe, C. W., Christensen, C., and Meldal, M. 2002. Peptidotriazoles on solid phase: [1,2,3]-Triazoles by regiospecific copper(I)-catalyzed 1,3-dipolar cycloadditions of terminal alkynes to azides. J. Org. Chem. 67: 3057-3064.

Valeur, B. 2002. Molecular fluorecence principle and applications. Weinheim: Wiley-VCH.

Wada, S., Matsunaga, S., Saito, S., Fusetani, N., and Watabe, S. 1998. Actin-binding specificity of marine macrolide toxins, mycalolide B and kabiramide D. J. Biochem. 123: 946-952.

Wang, Z. and Qin, H. 2003. Regioselective synthesis of 1,2,3-triazole derivatives *via* 1,3-dipolar cycloaddition reactions in water. Chem. Commun. 19: 2450-2451.

Weber, G., and Farris, F. 1979. Synthesis and spectral properties of hydrophobic fluorescent probe: 6-Propionyl-2-(dimethylamino)naphthalene. Biochemistry 18: 3075-3078.

Yan, Y. and Marriott, G. 2003. Analysis of protein interactions using fluorescence technologies. Curr. Opin. Chem. Biol. 7: 635-640.

Yarmola, E. G., Somasundaram, T., Boring T. A., Spector, I., and Bubb, M. R. 2000. Actin-latrunculin A structure and function. J. Biol. Chem. 275: 28120-28127.

Yeung, K. and Paterson, I. 2002. Actin-binding marine macrolides: Total synthesis and biological importance. Angew. Chem. Int. Ed. 41: 4632-4653.

APPENDIX

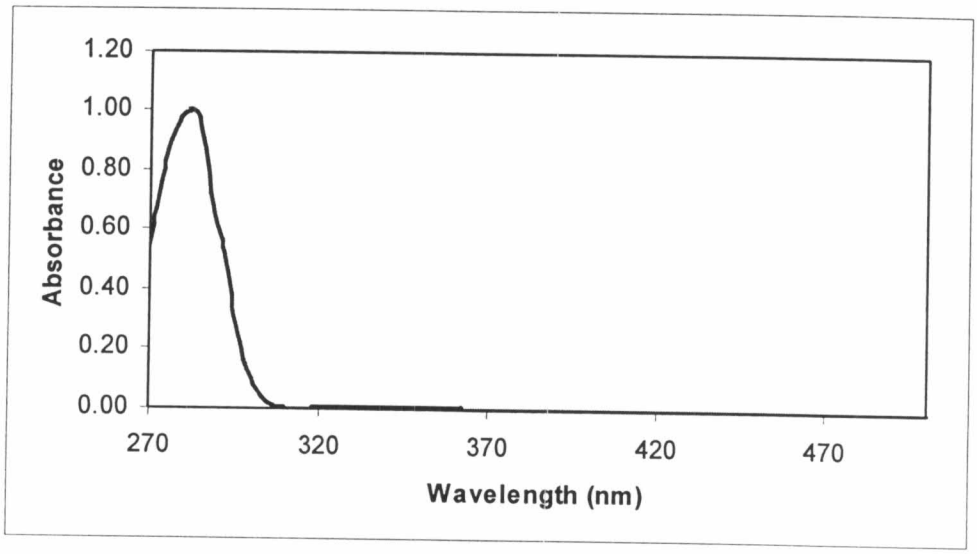

Figure 36 The UV spectrum of G-actin in G-buffer.

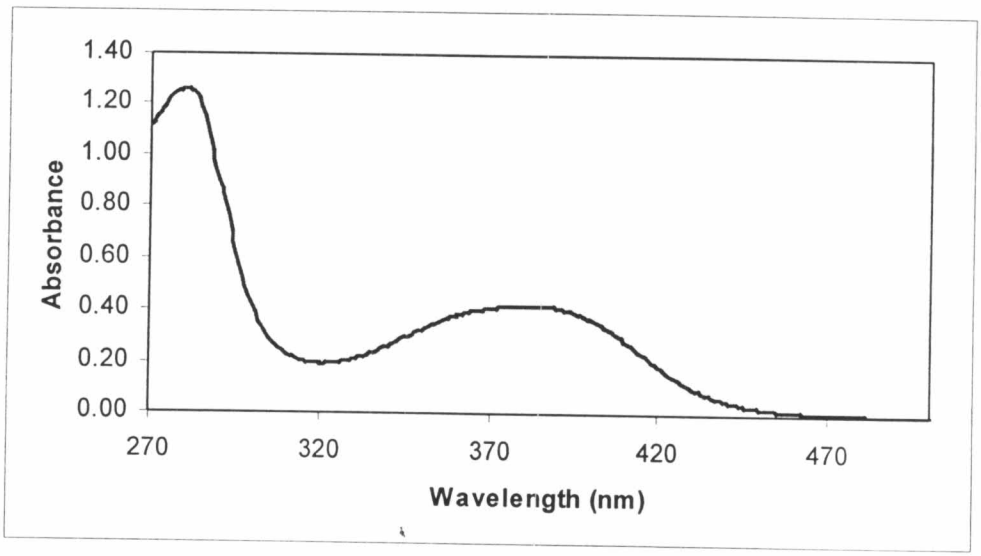

Figure 37 The UV spectrum of prodan-G-actin in G-buffer.

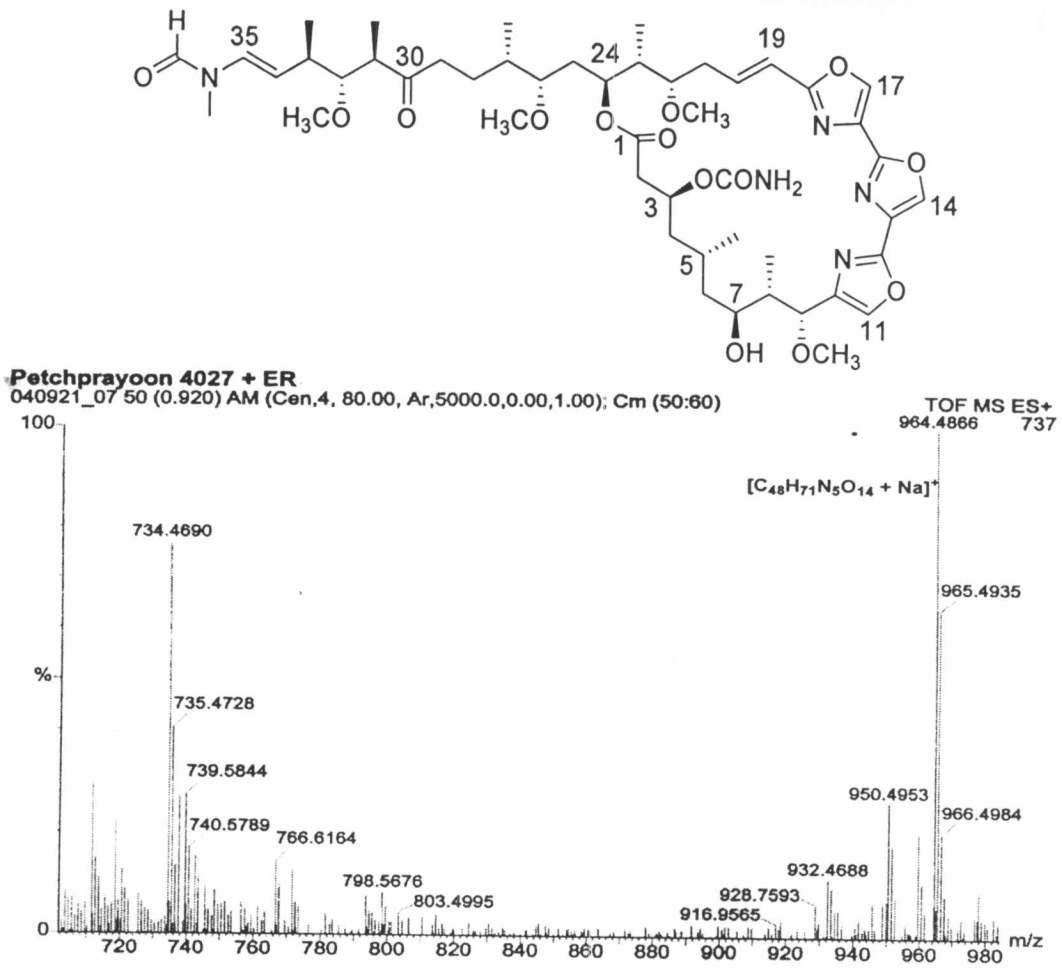

Figure 38 The ESI-TOF mass spectrum of kabiramide C.

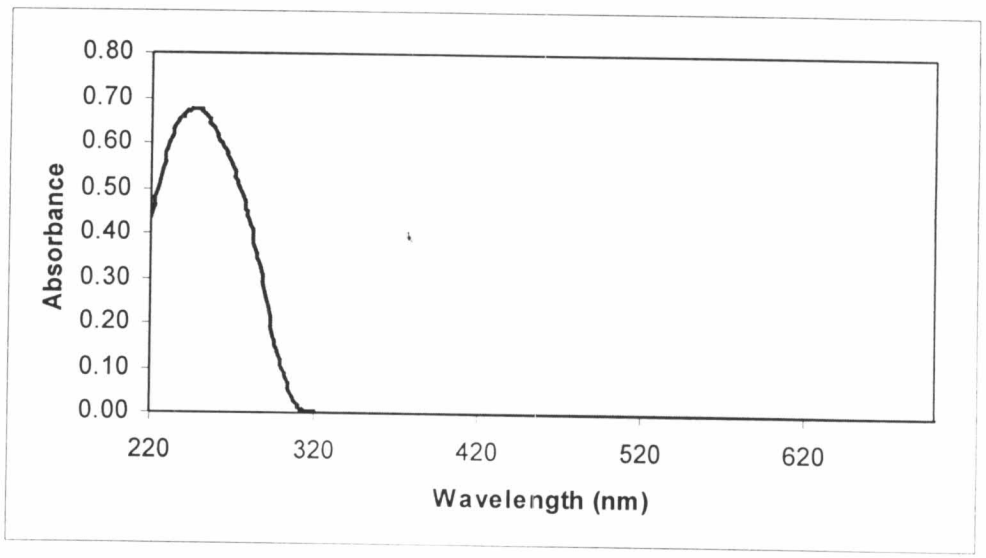

Figure 39 The UV spectrum of kabiramide C in MeOH.

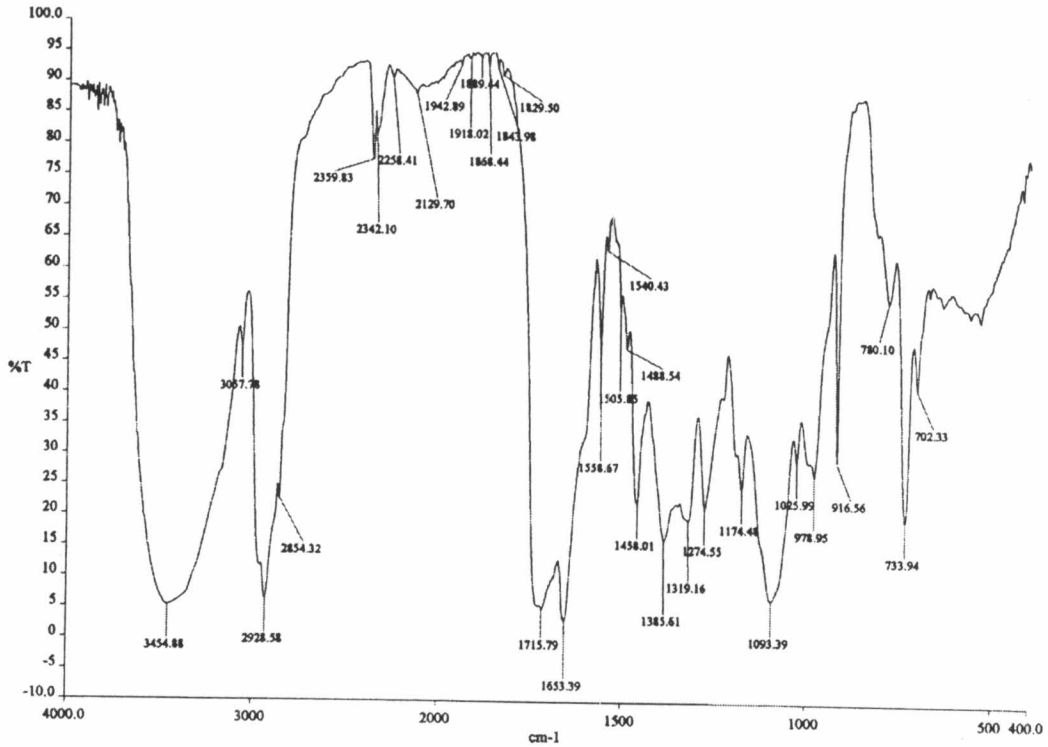

Figure 40 The IR spectrum of kabiramide C (film).

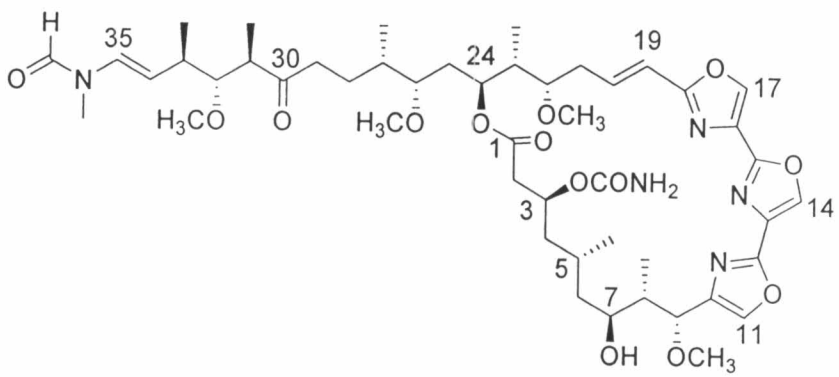

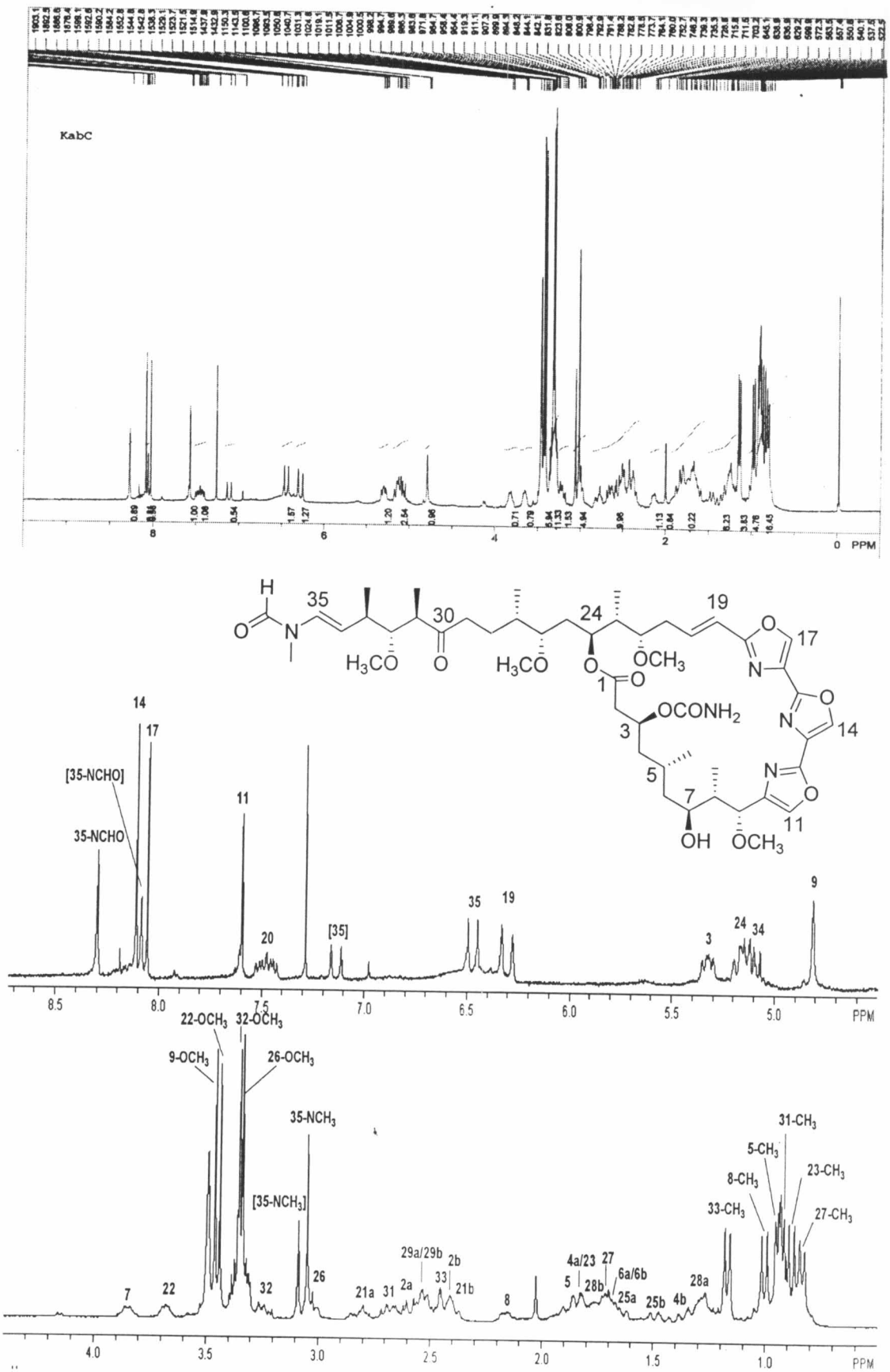

Figure 41 The 300 MHz ^{1}H NMR spectrum of kabiramide C in $CDCl_3$.

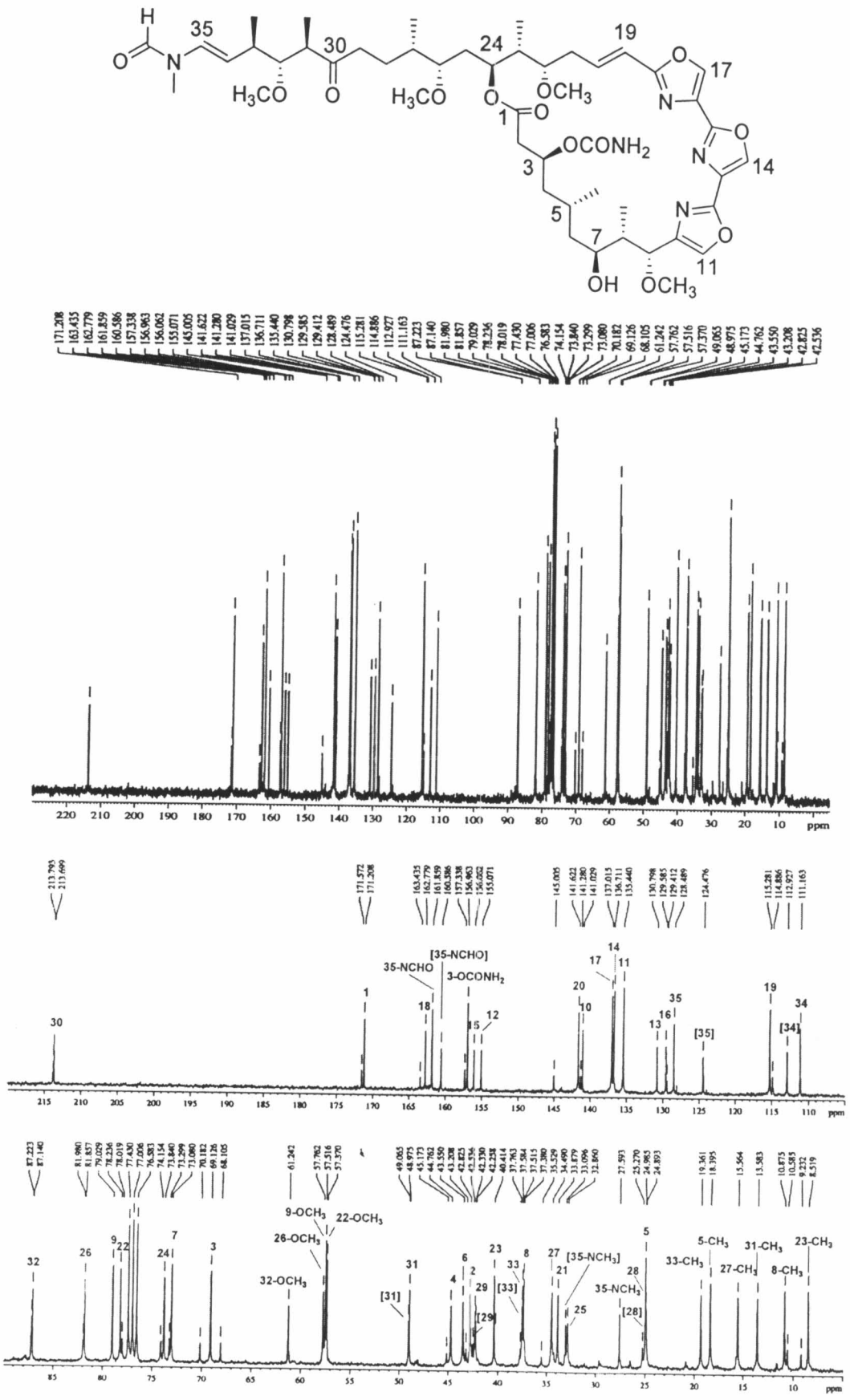

Figure 42 The 75 MHz ^{13}C NMR spectrum of kabiramide C in $CDCl_3$.

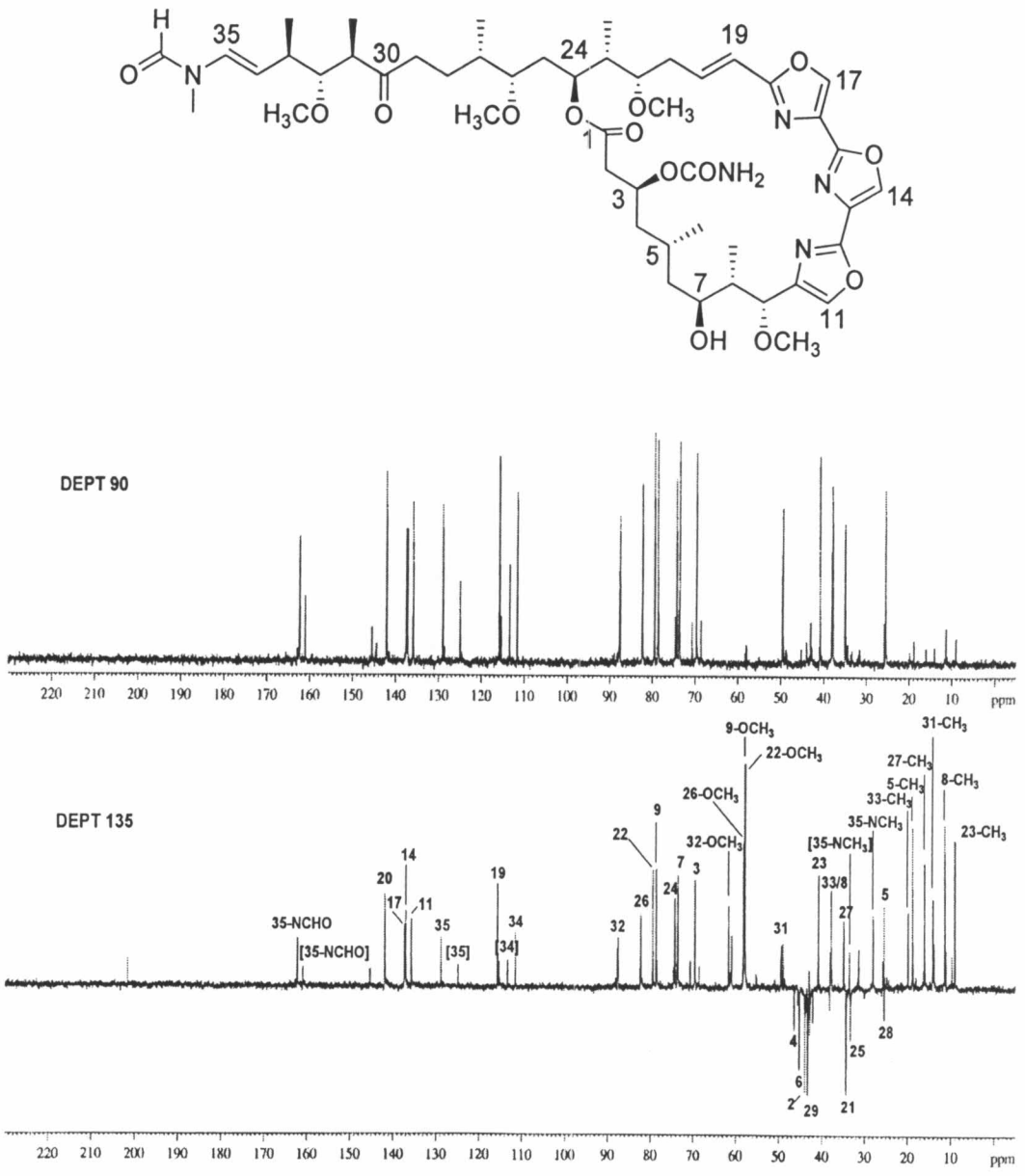

Figure 43 The 75 MHz DEPT90 and DEPT135 spectra of kabiramide C in $CDCl_3$.

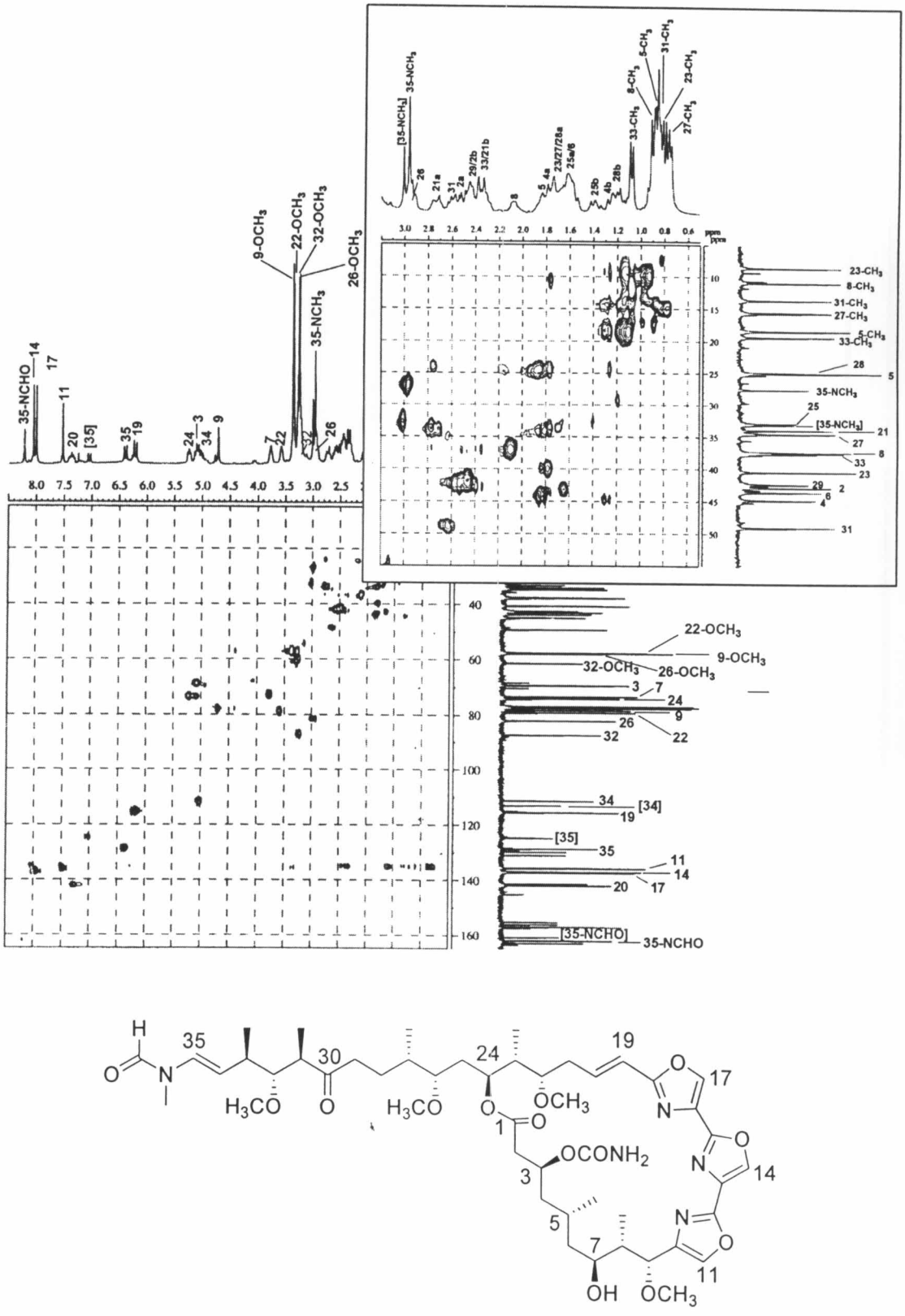

Figure 44 The 300 MHz HMQC spectrum of kabiramide C in $CDCl_3$.

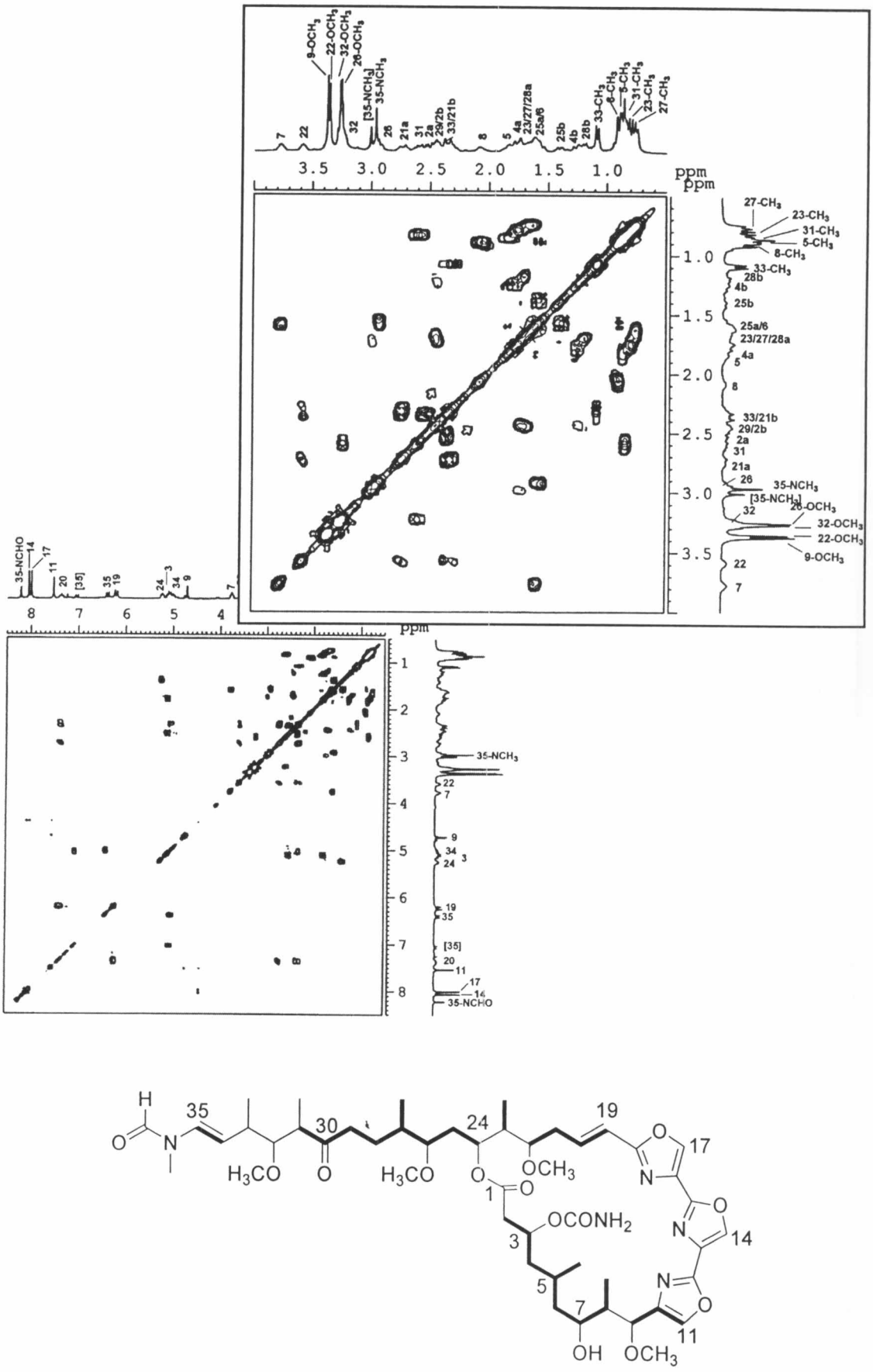

Figure 45 The 300 MHz H,H COSY spectrum of kabiramide C in $CDCl_3$.

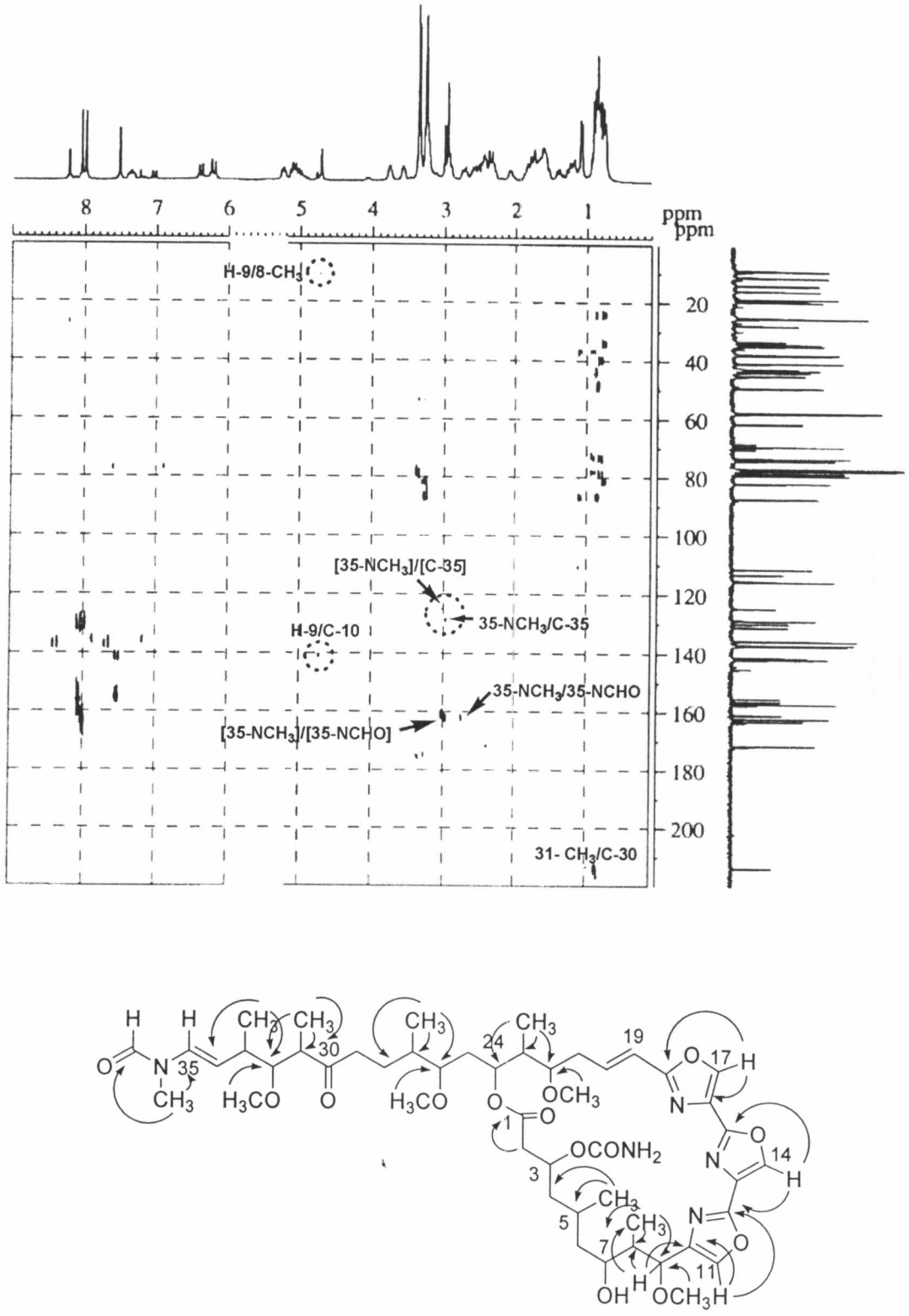

Figure 46 The 300 MHz HMBC spectrum ($^{n}J_{HC}$ = 8 Hz) of kabiramide C in $CDCl_3$.

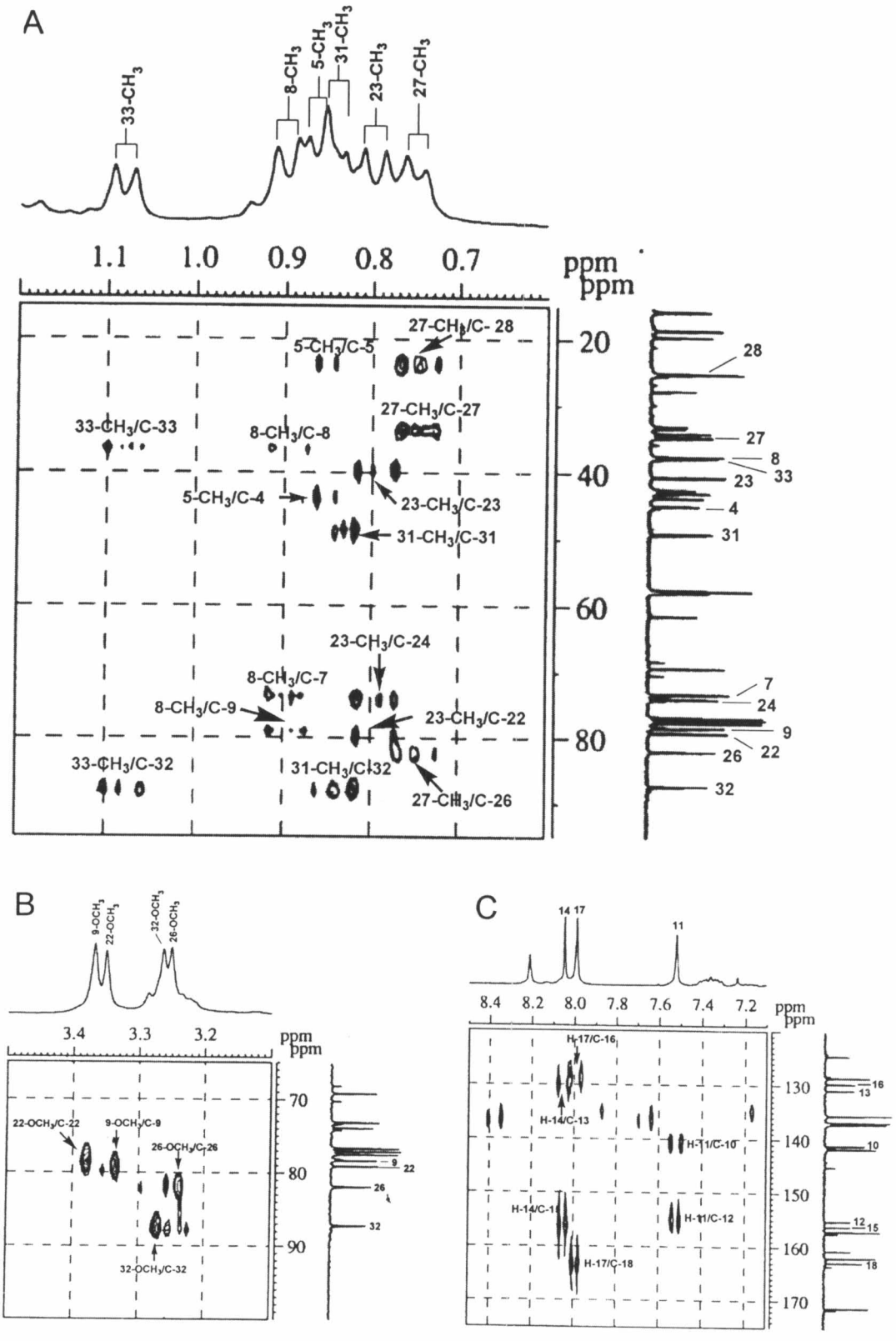

Figure 47 The 300 MHz HMBC spectrum (expanded) of kabiramide C in $CDCl_3$.

(A) F_2 axis (δ_H 0.6-1.2 ppm), F_1 axis (δ_C 15-95 ppm)

(B) F_2 axis (δ_H 0.6-1.2 ppm), F_1 axis (δ_C 15-95 ppm)

(C) F_2 axis (δ_H 0.6-1.2 ppm), F_1 axis (δ_C 15-95 ppm)

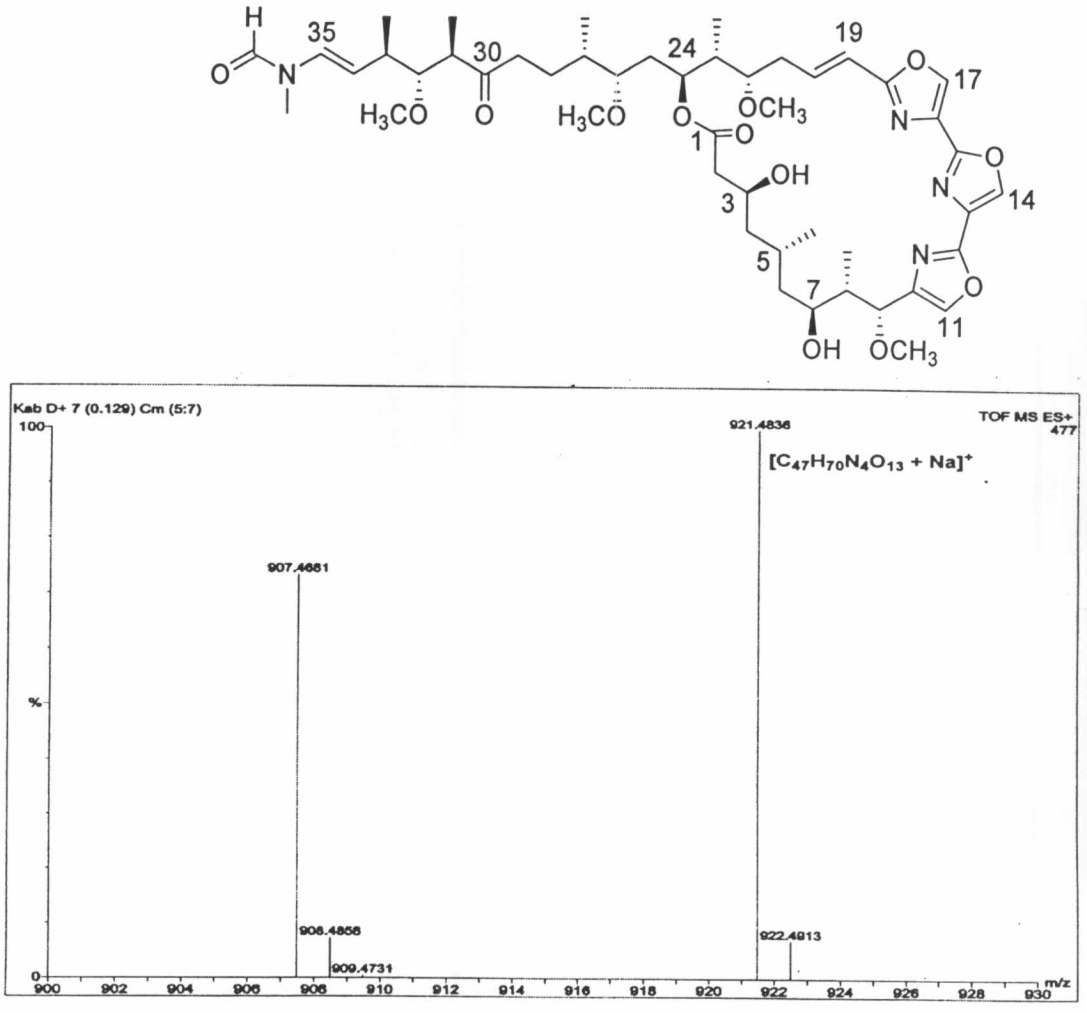

Figure 48 The ESI-TOF mass spectrum of kabiramide D.

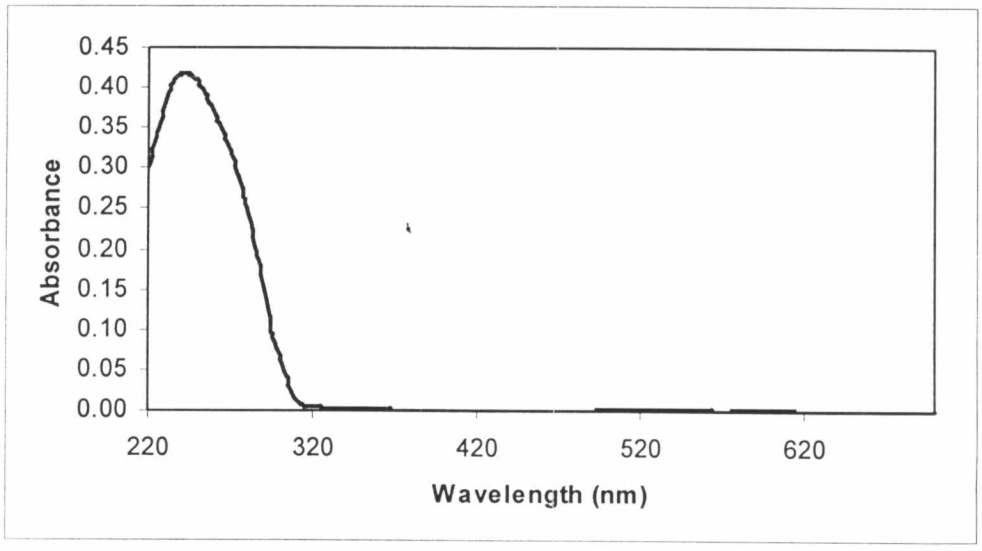

Figure 49 The UV spectrum of kabiramide D in MeOH.

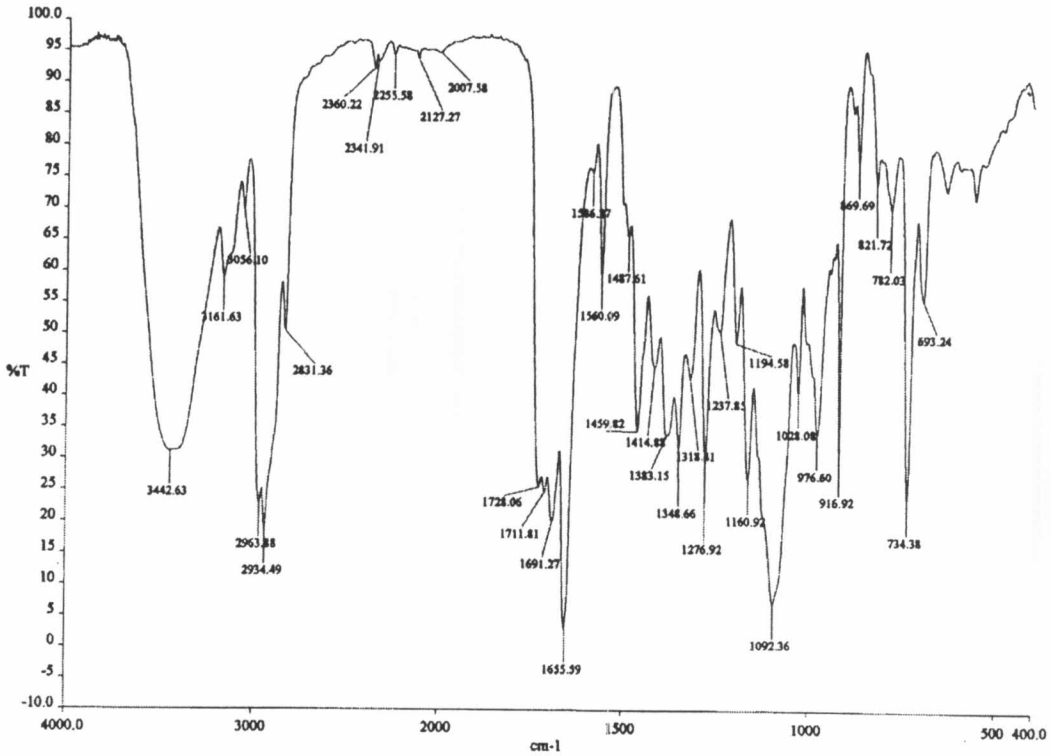

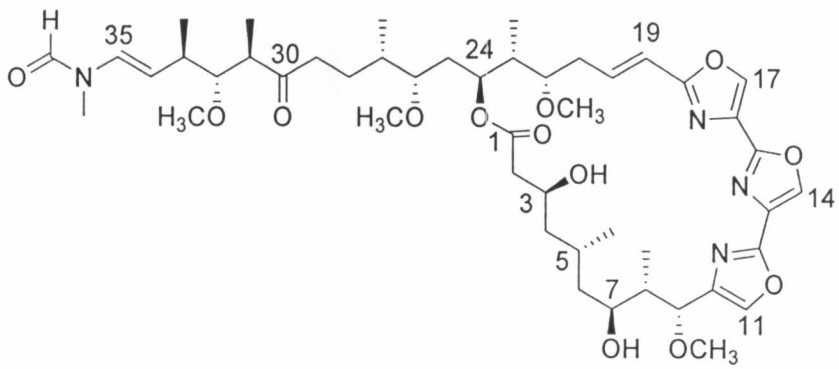

Figure 50 The IR spectrum of kabiramide D (film).

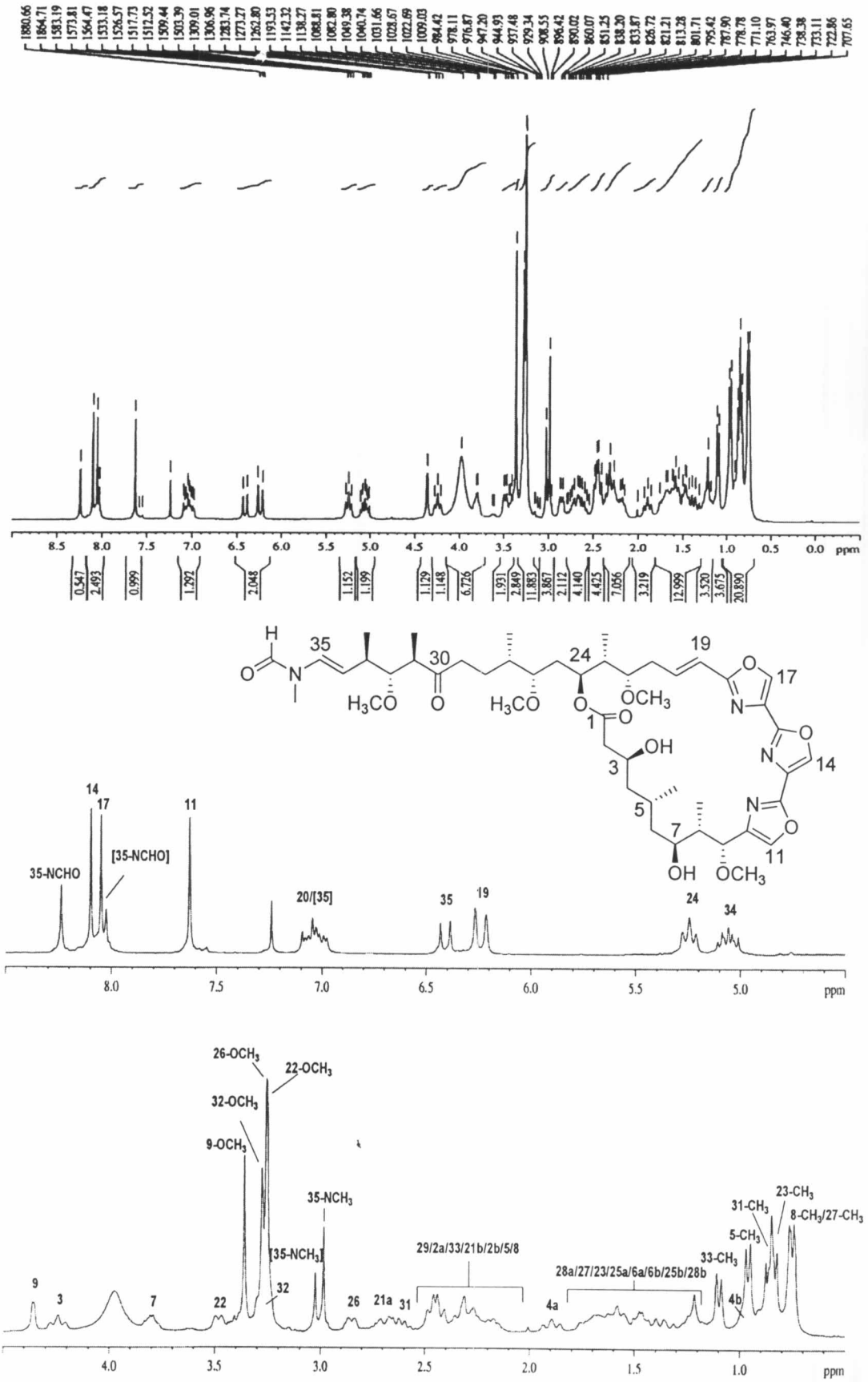

Figure 51 The 300 MHz ^{1}H NMR spectrum of kabiramide D in $CDCl_3$.

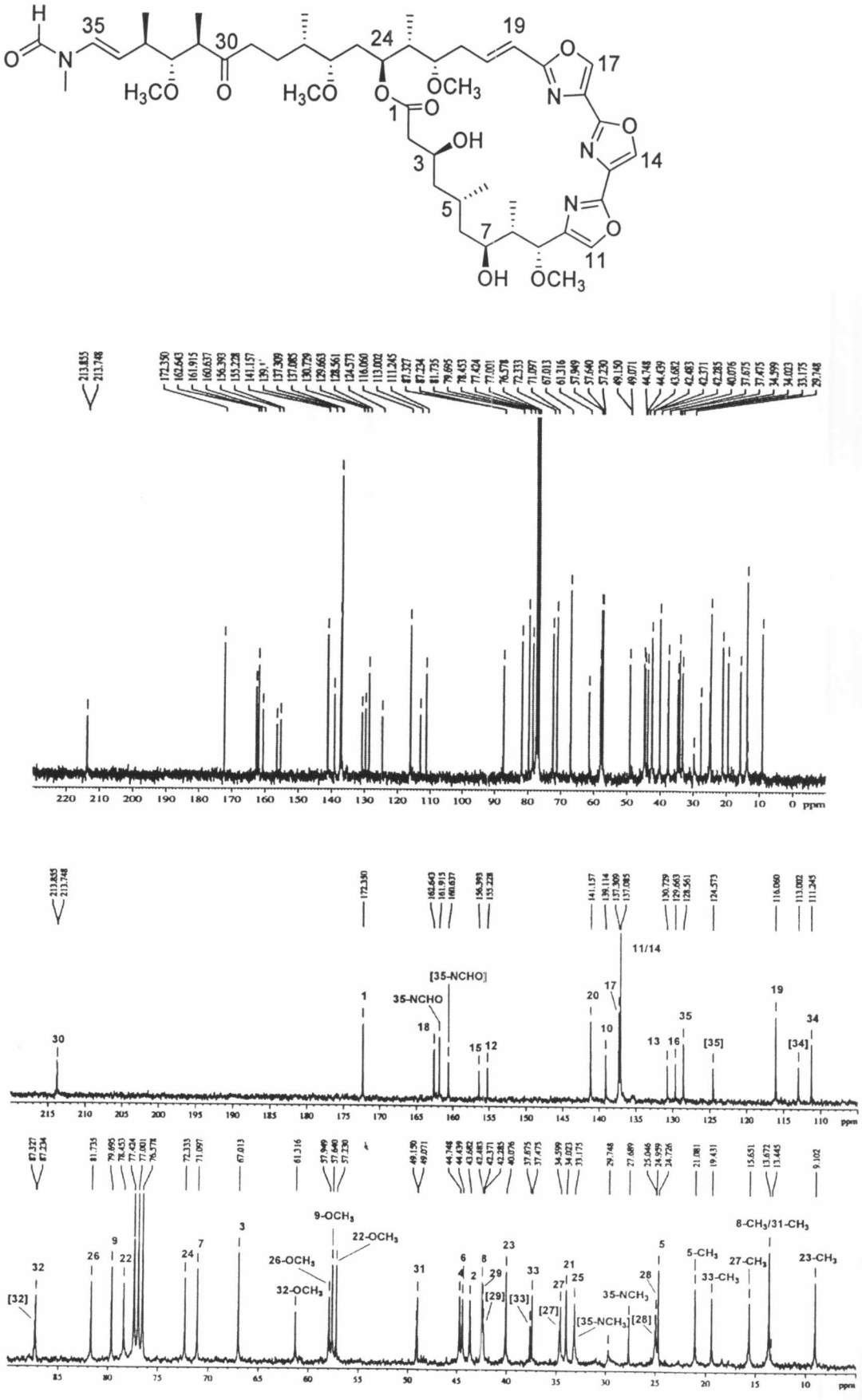

Figure 52 The 75 MHz ^{13}C NMR spectrum of kabiramide D in $CDCl_3$.

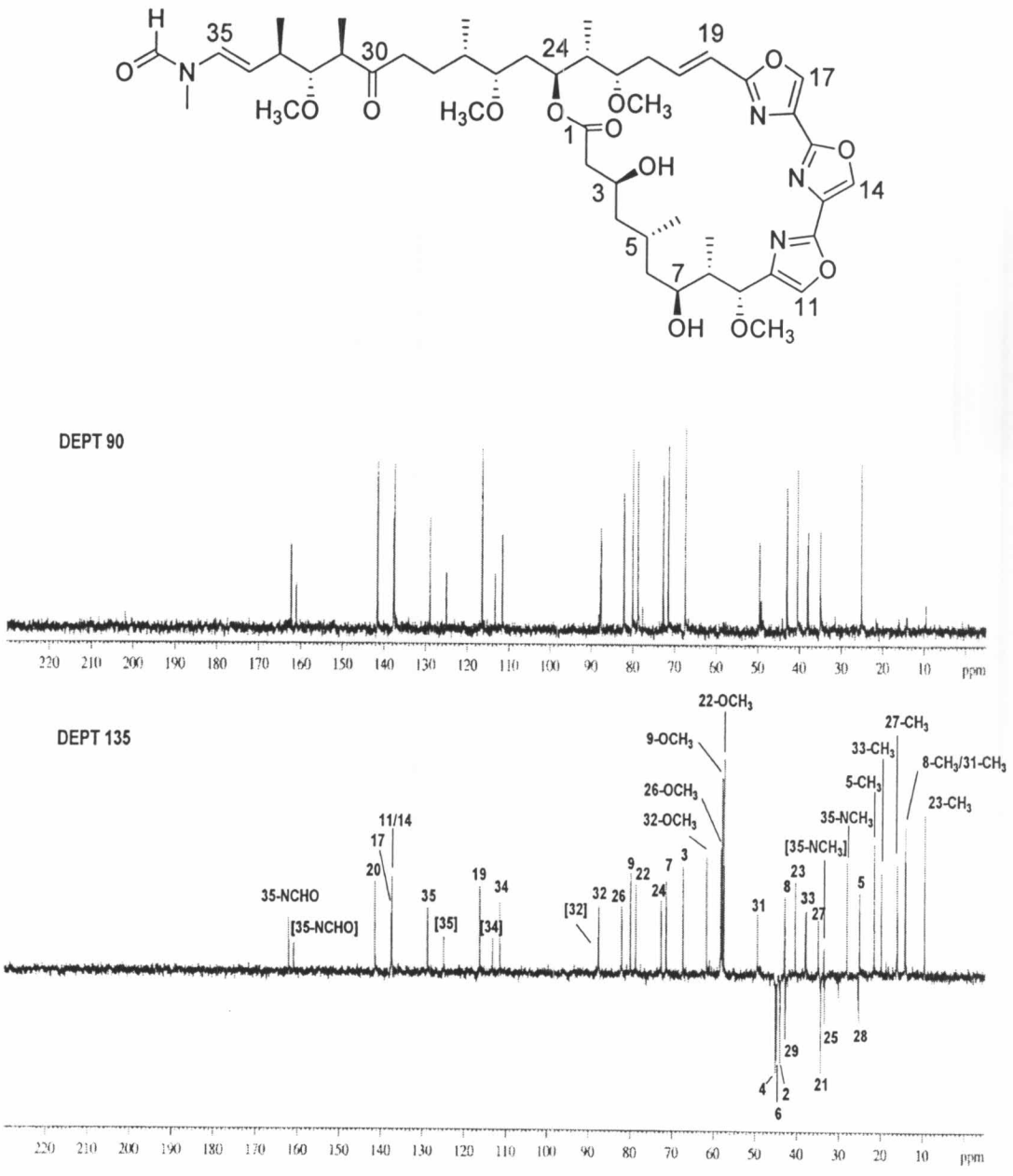

Figure 53 The 75 MHz DEPT90 and DEPT135 spectra of kabiramide D in $CDCl_3$.

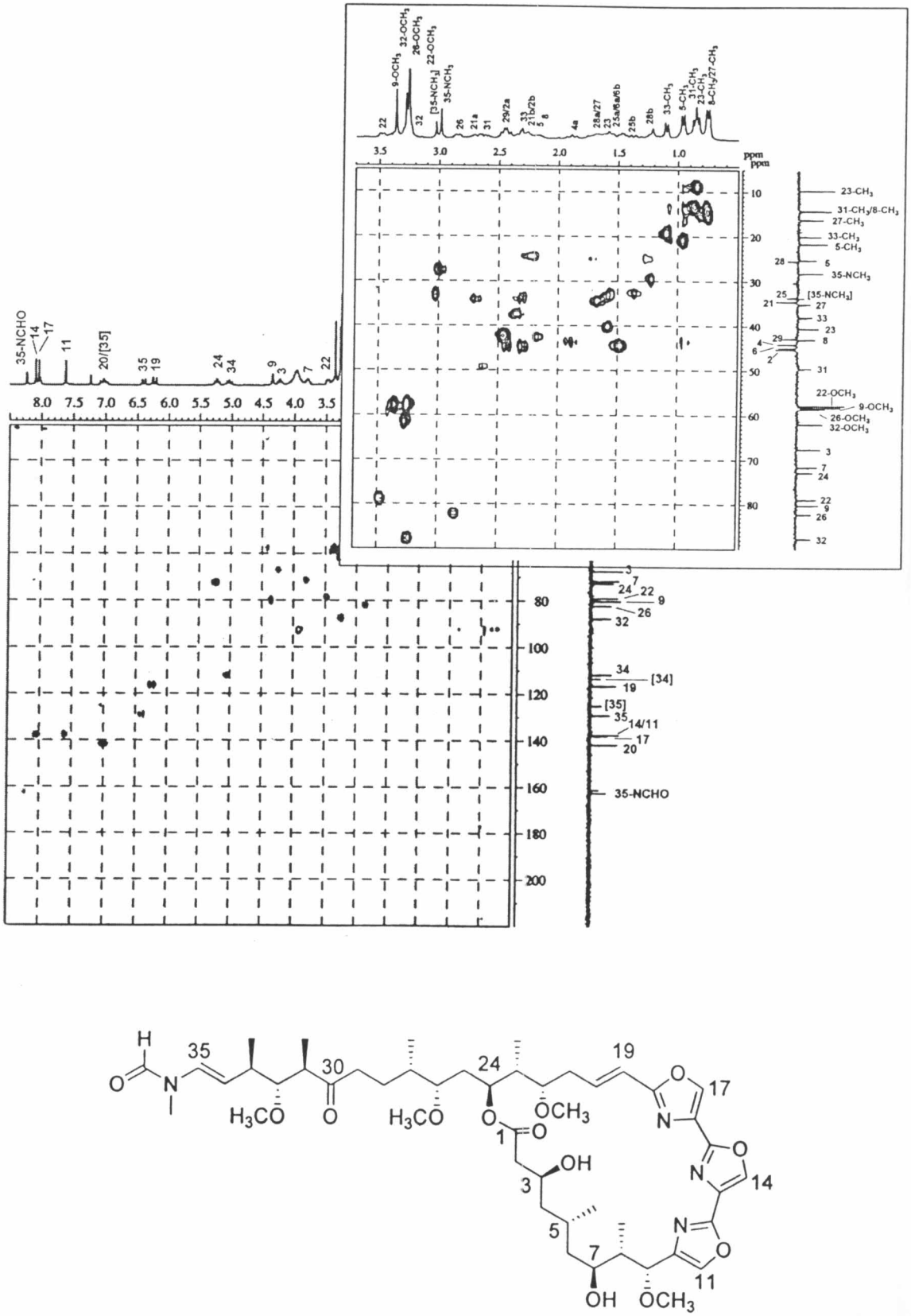

Figure 54 The 300 MHz HMQC spectrum of kabiramide D in $CDCl_3$.

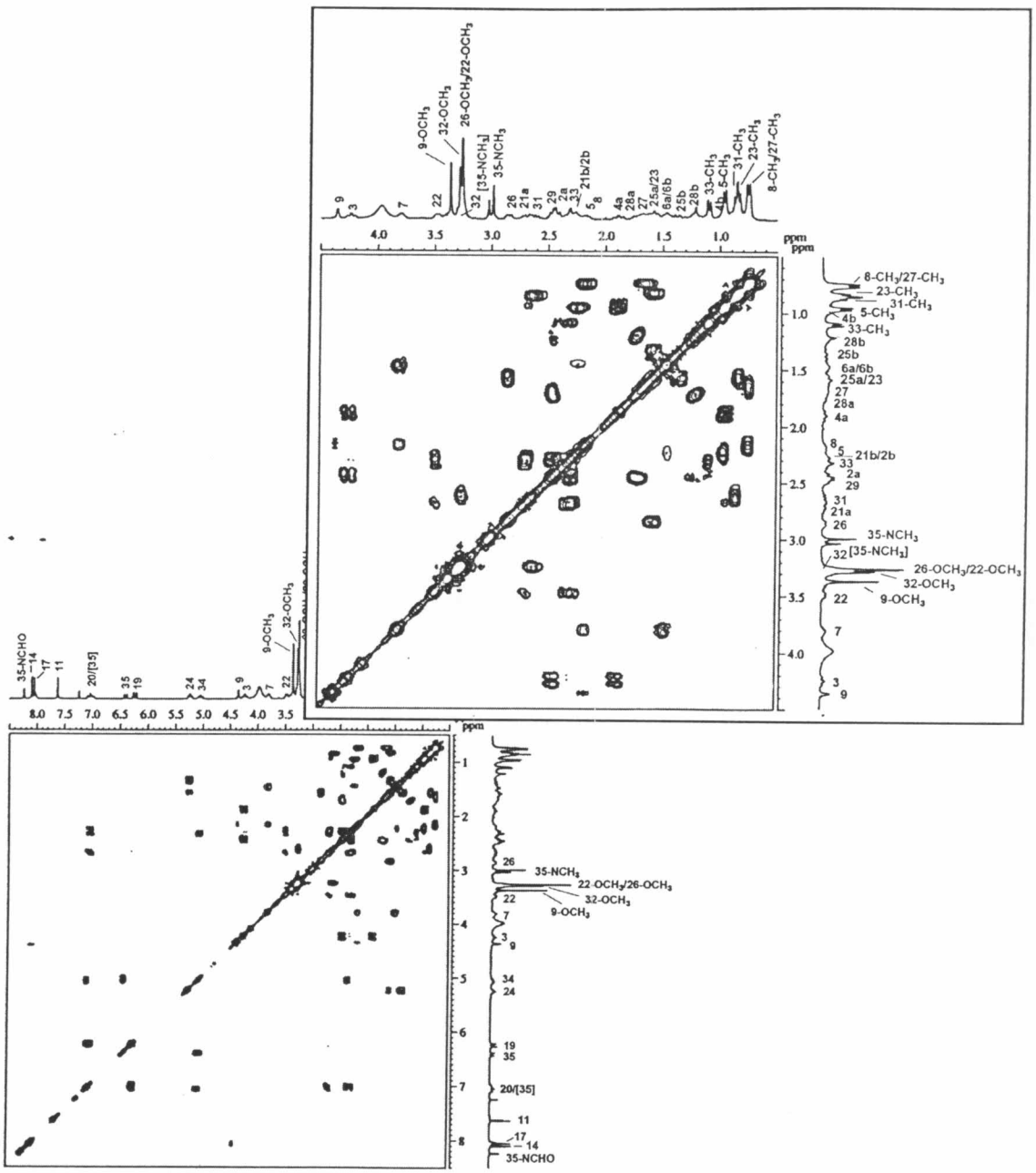

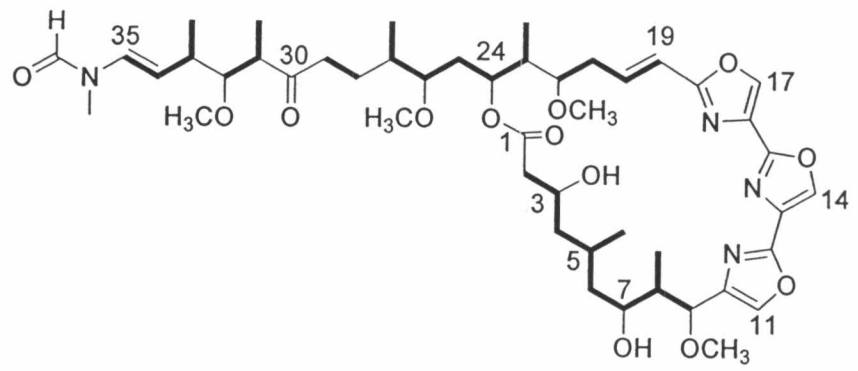

Figure 55 The 300 MHz H,H COSY spectrum of kabiramide D in $CDCl_3$.

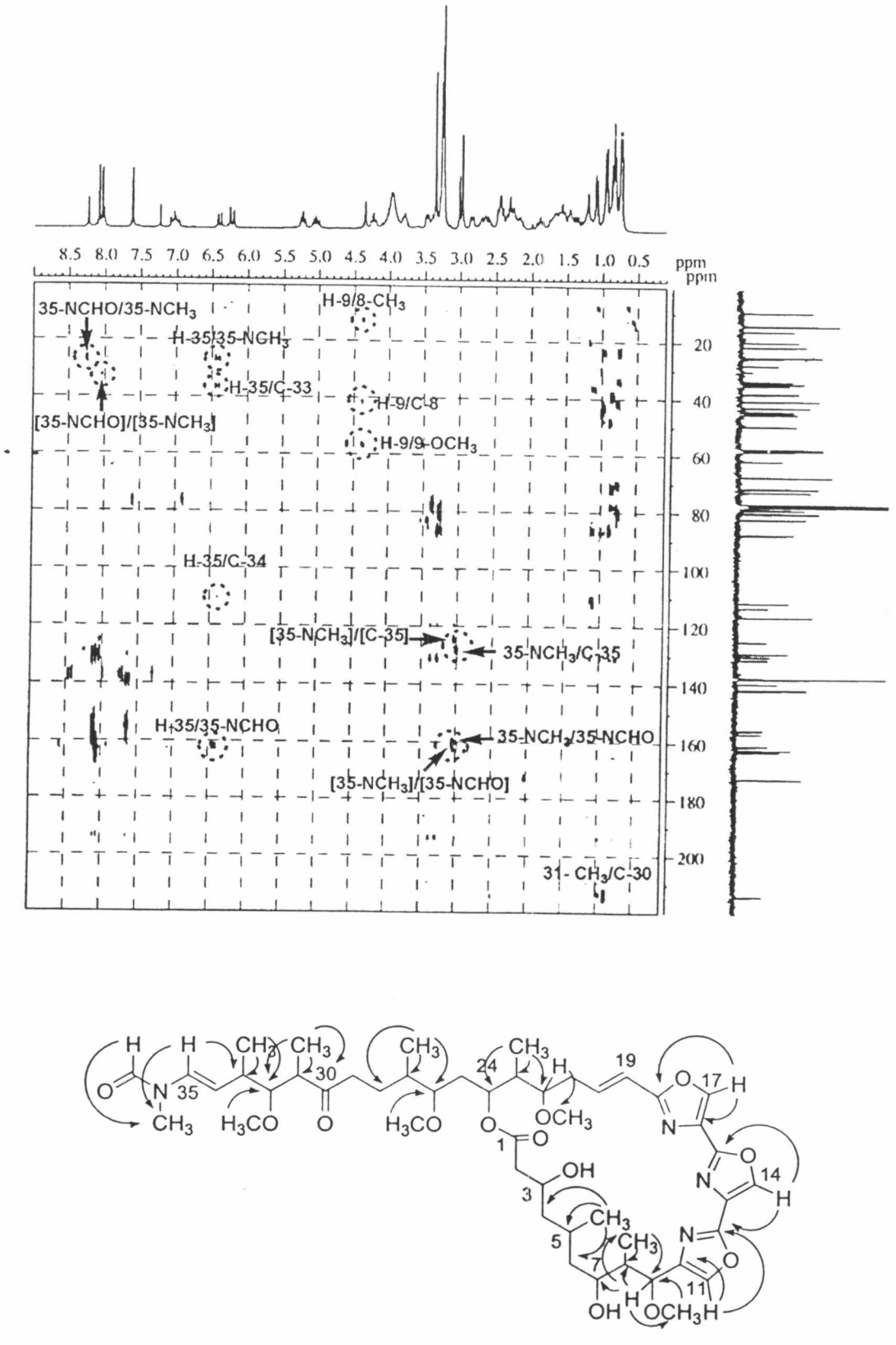

Figure 56 The 300 MHz HMBC spectrum ($^{n}J_{HC}$ = 8 Hz) of kabiramide D in $CDCl_3$.

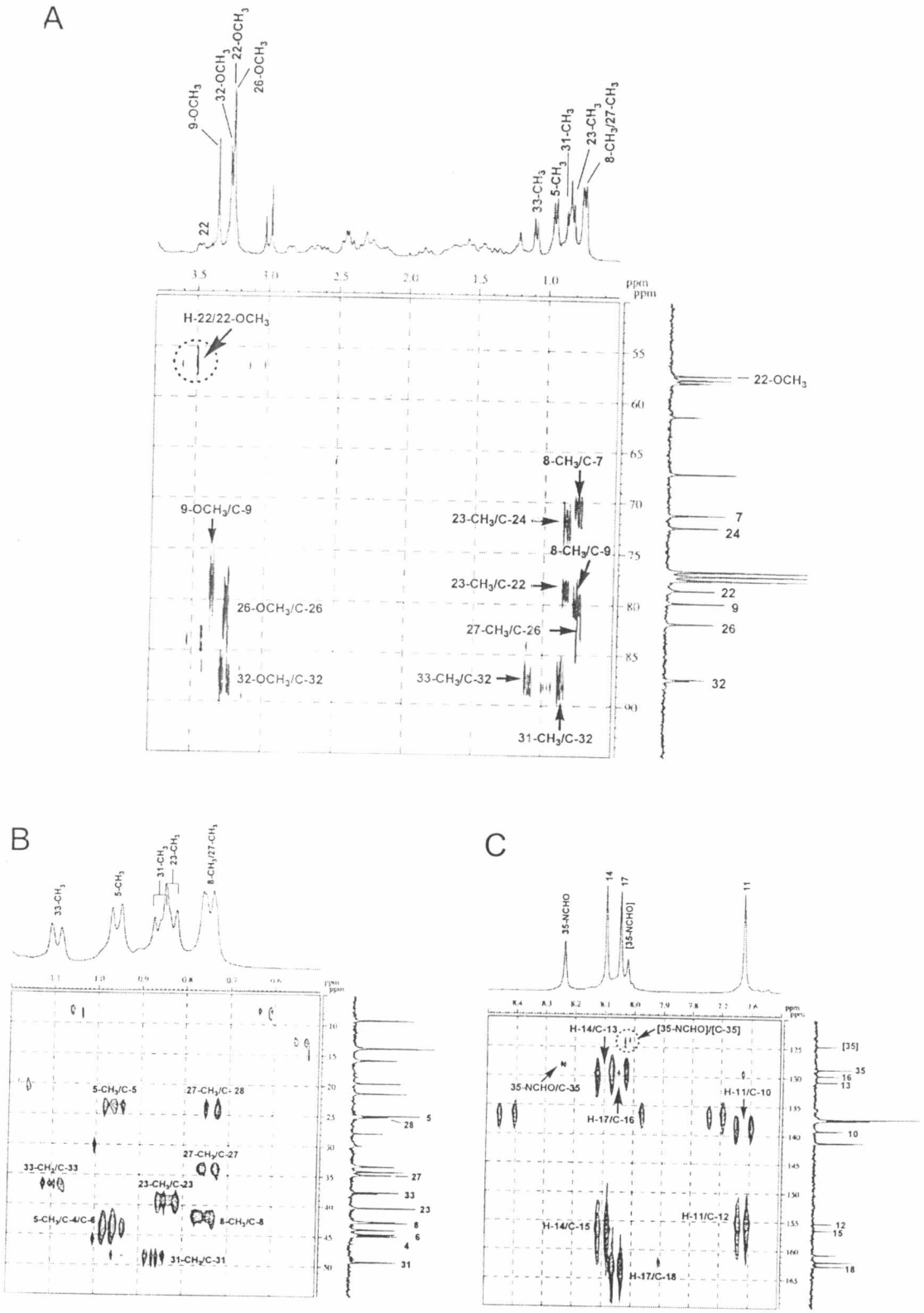

Figure 57 The 300 MHz HMBC spectrum ($^{n}J_{HC}$ = 8 Hz) of kabiramide D in $CDCl_3$.

(A) F_2 axis (δ_H 0.0-3.8 ppm), F_1 axis (δ_C 50-95 ppm)

(B) F_2 axis (δ_H 0.5-1.2 ppm), F_1 axis (δ_C 5-55 ppm)

(C) F_2 axis (δ_H 7.5-8.5 ppm), F_1 axis (δ_C 120-170 ppm)

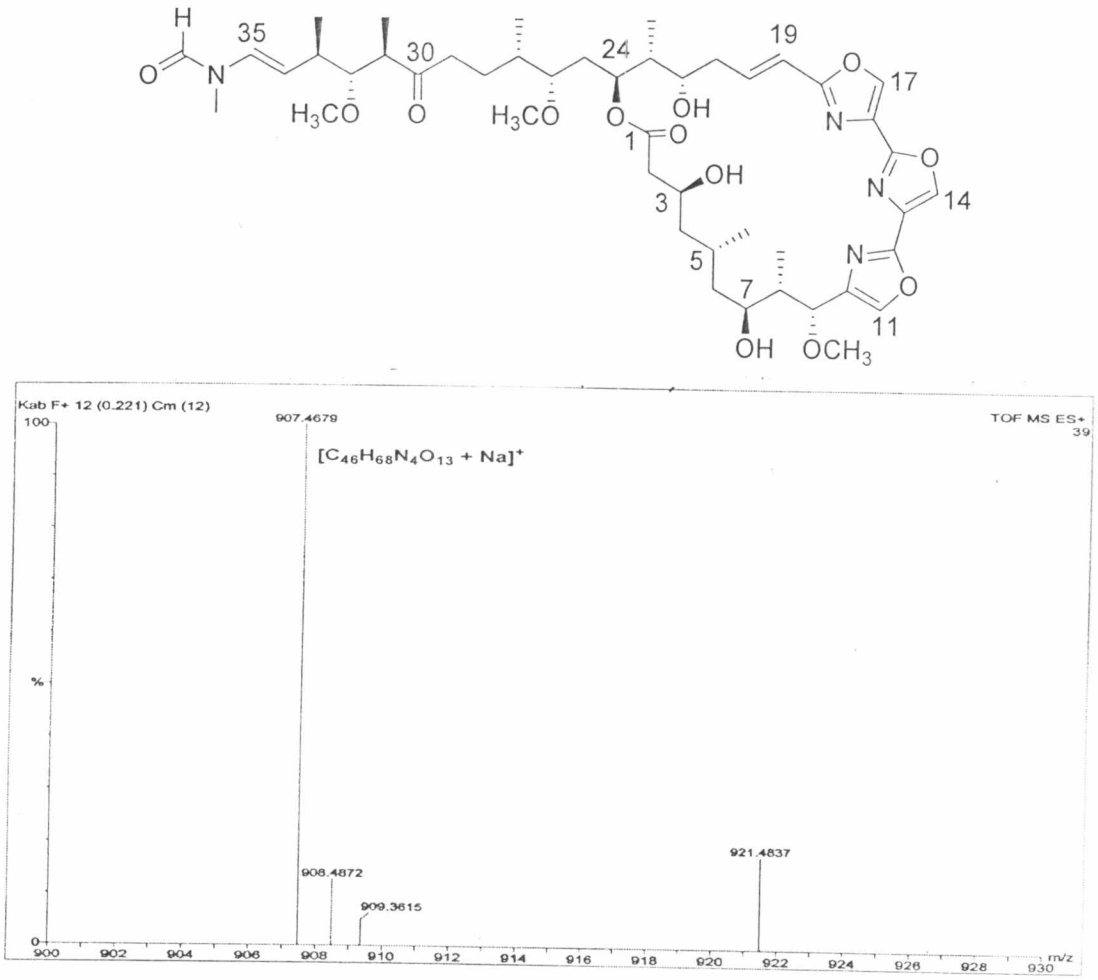

Figure 58 The ESI-TOF mass spectrum of kabiramide F.

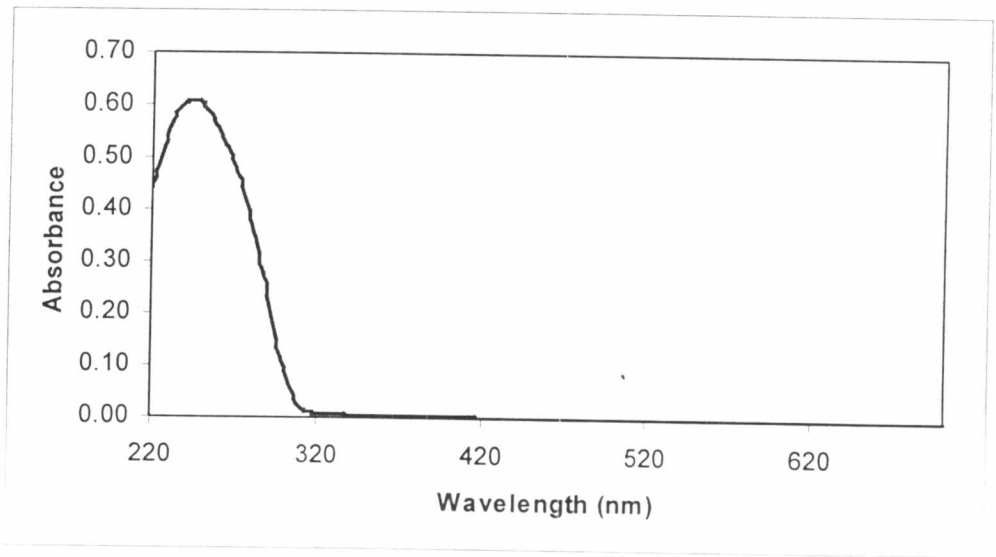

Figure 59 The UV spectrum of kabiramide F in MeOH.

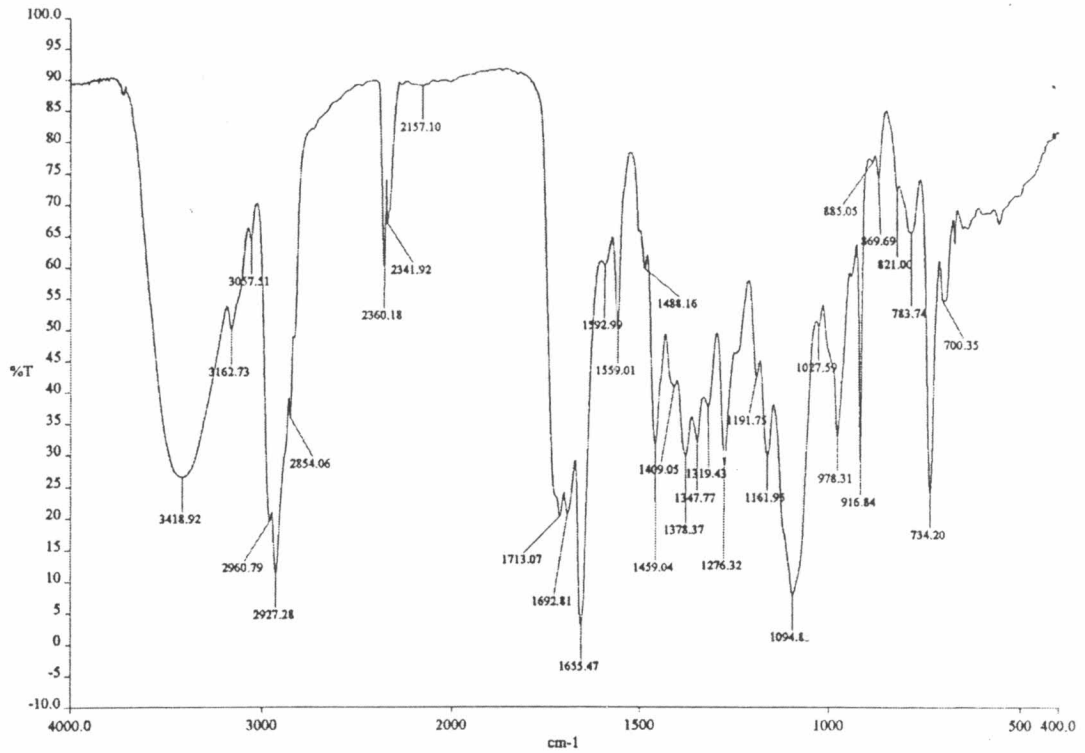

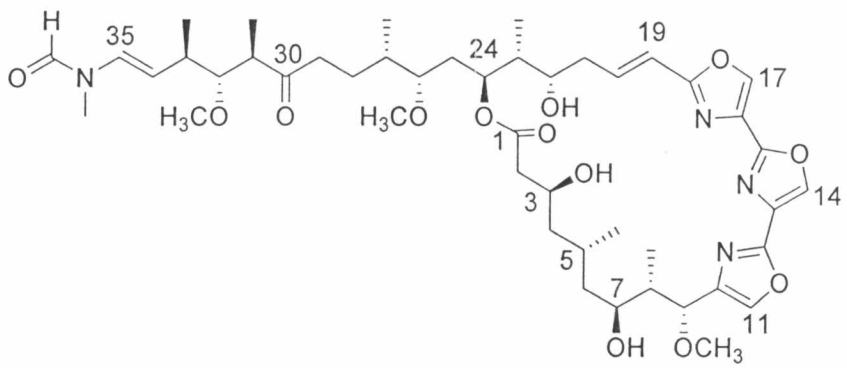

Figure 60 The IR spectrum of kabiramide F (film).

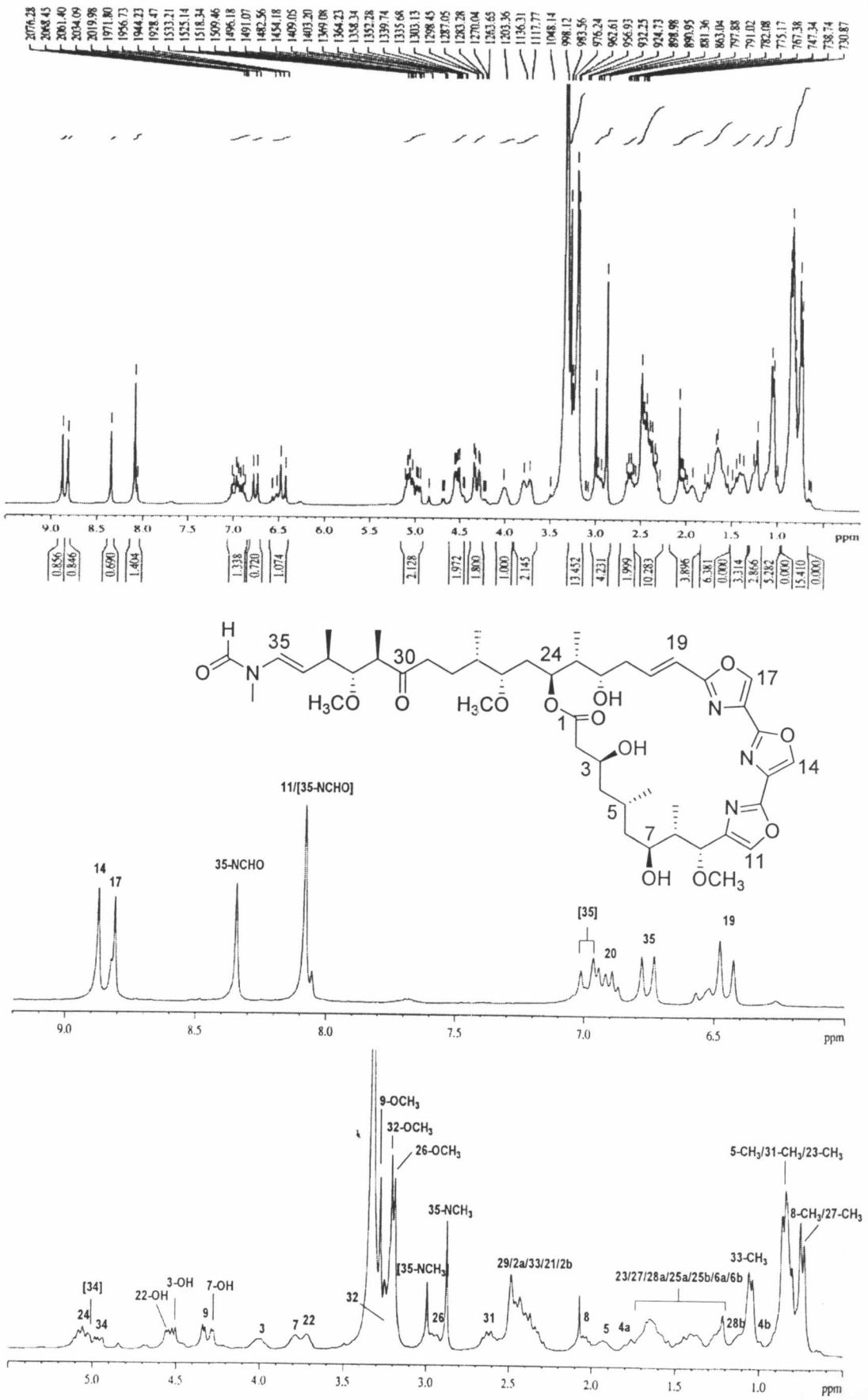

Figure 61 The 300 MHz ^{1}H NMR spectrum of kabiramide F in DMSO-d_6.

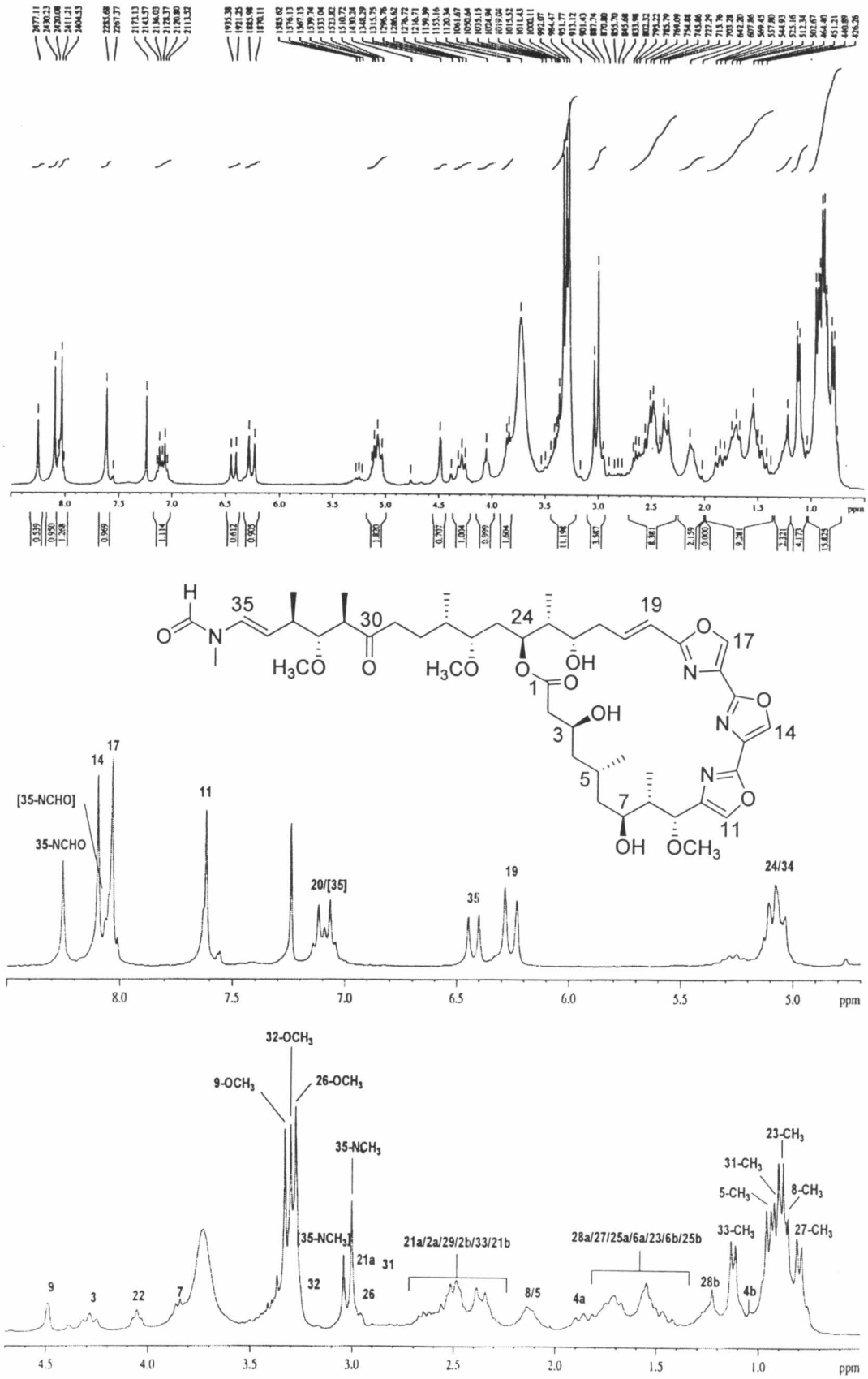

Figure 62 The 300 MHz ^{1}H NMR spectrum of kabiramide F in $CDCl_3$.

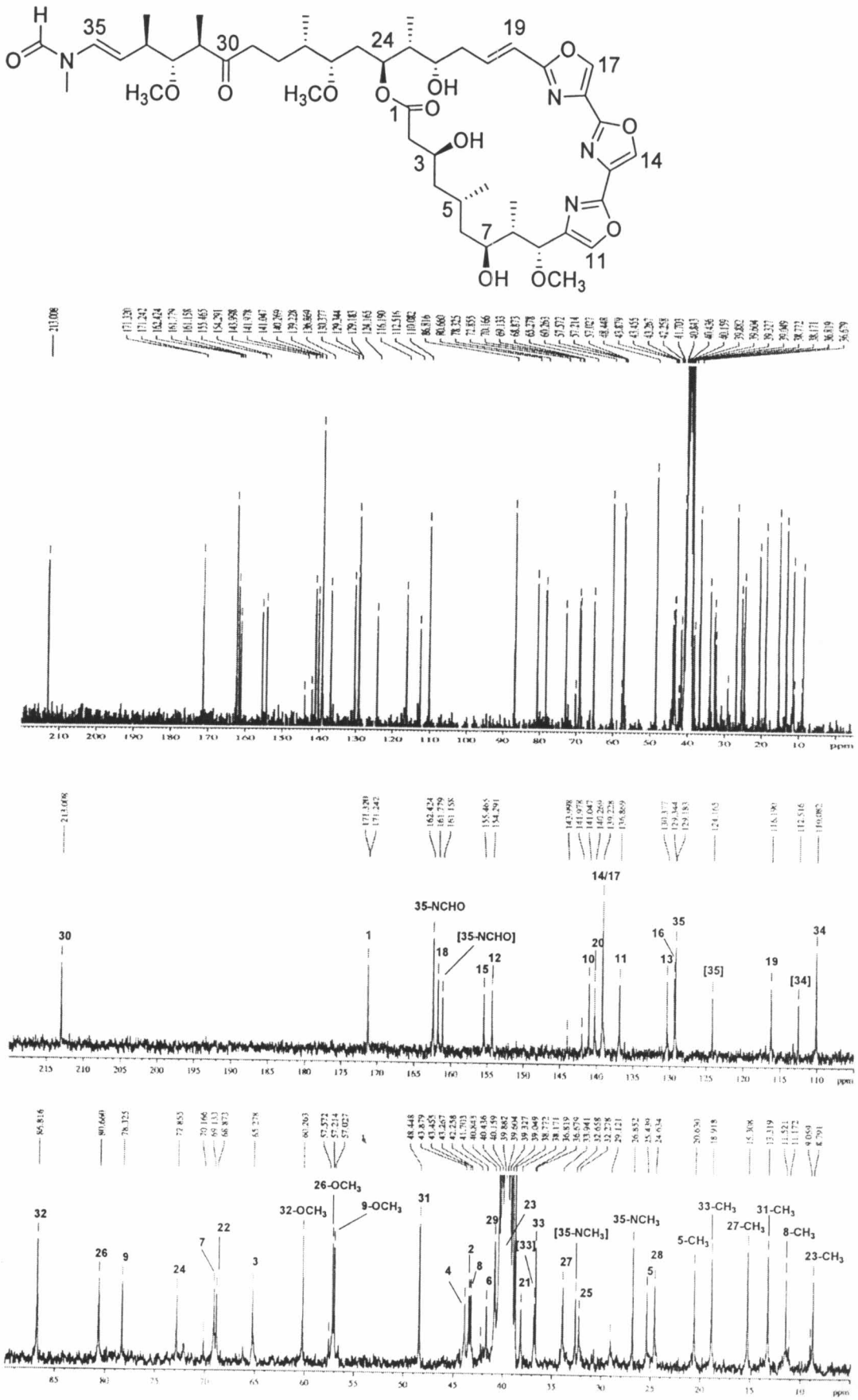

Figure 63 The 75 MHz ^{13}C NMR spectrum of kabiramide F in DMSO-d_6.

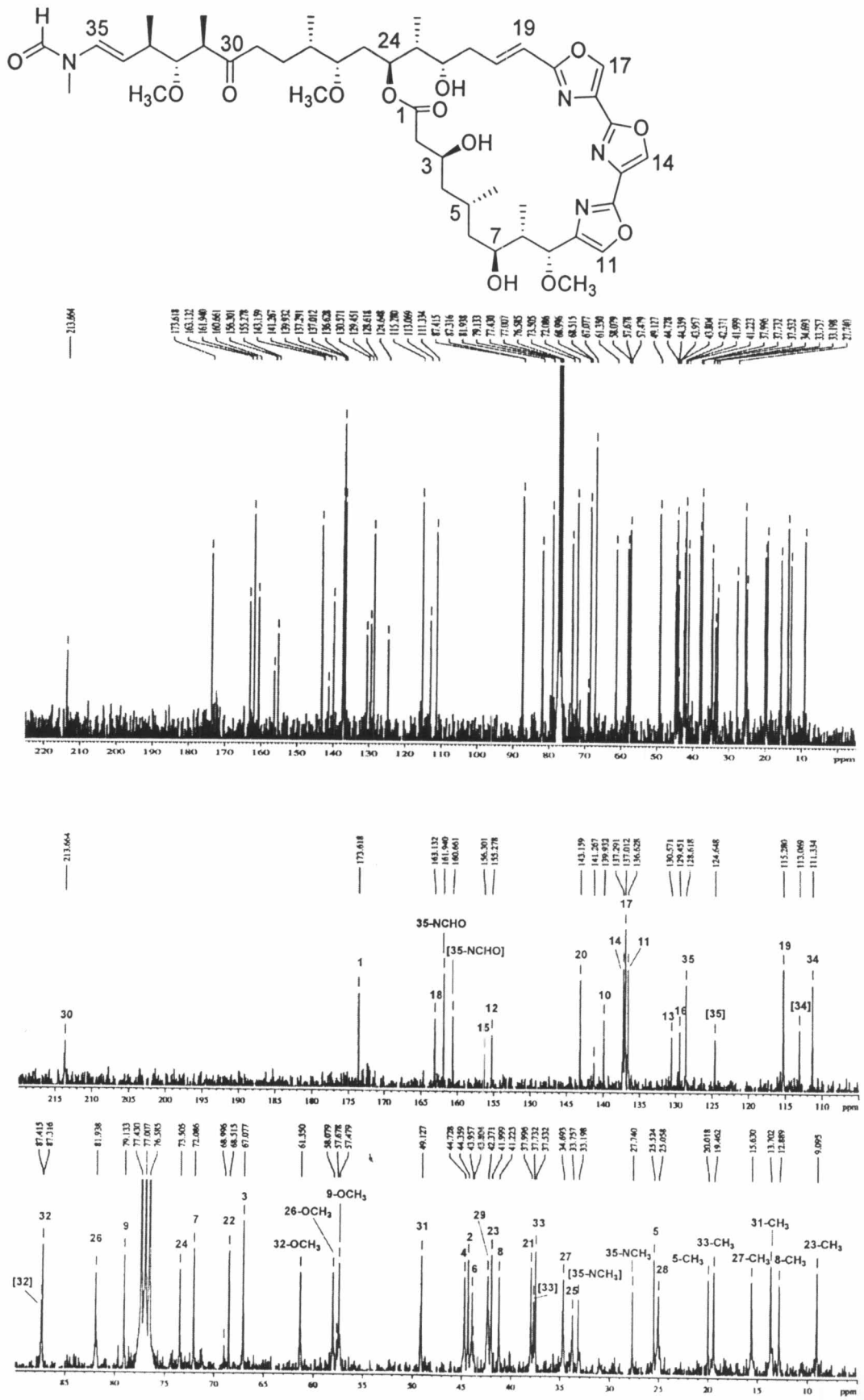

Figure 64 The 75 MHz ^{13}C NMR spectrum of kabiramide F in $CDCl_3$.

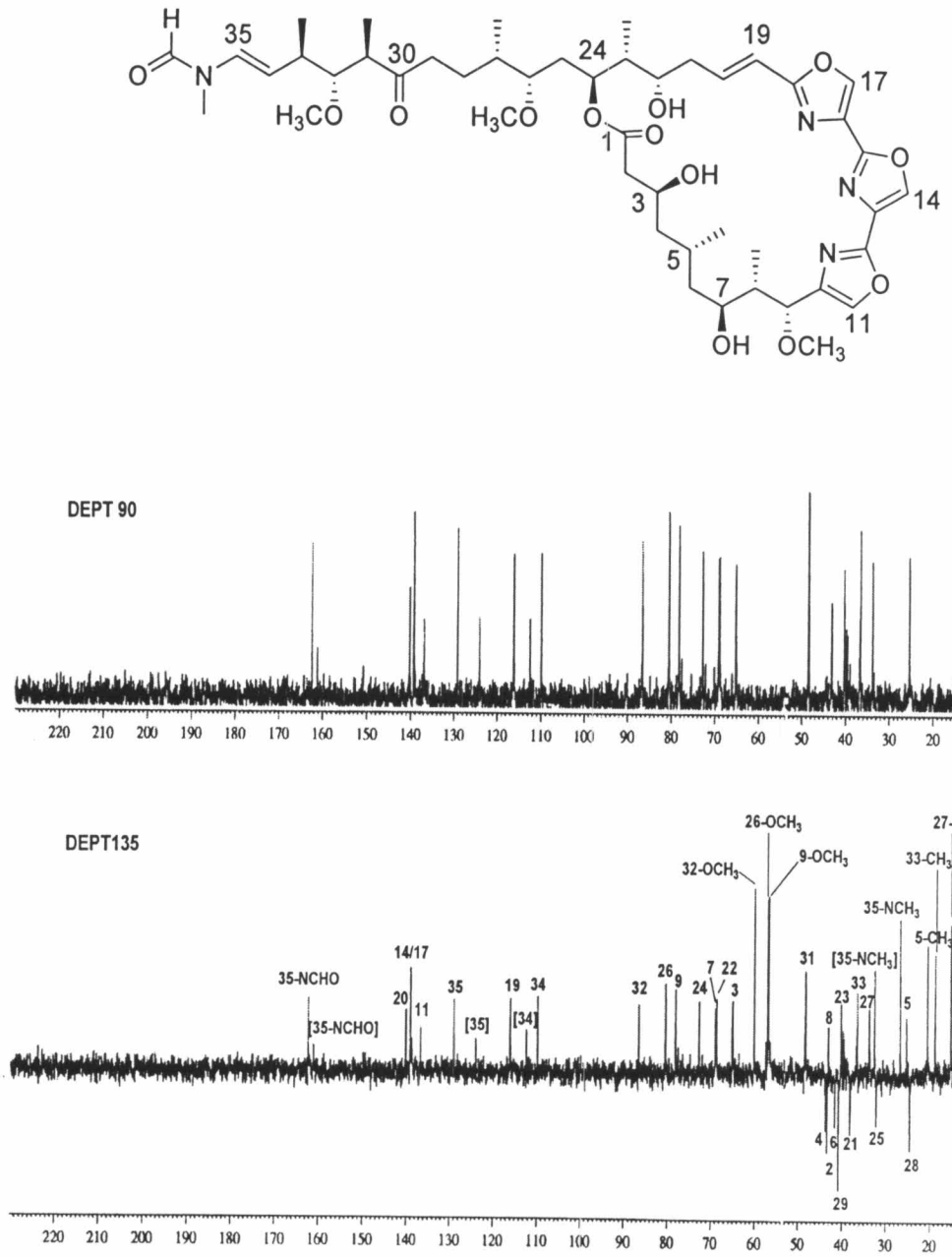

Figure 65 The 75 MHz DEPT90 and DEPT135 spectra of kabiramide F in DMSO-d_6.

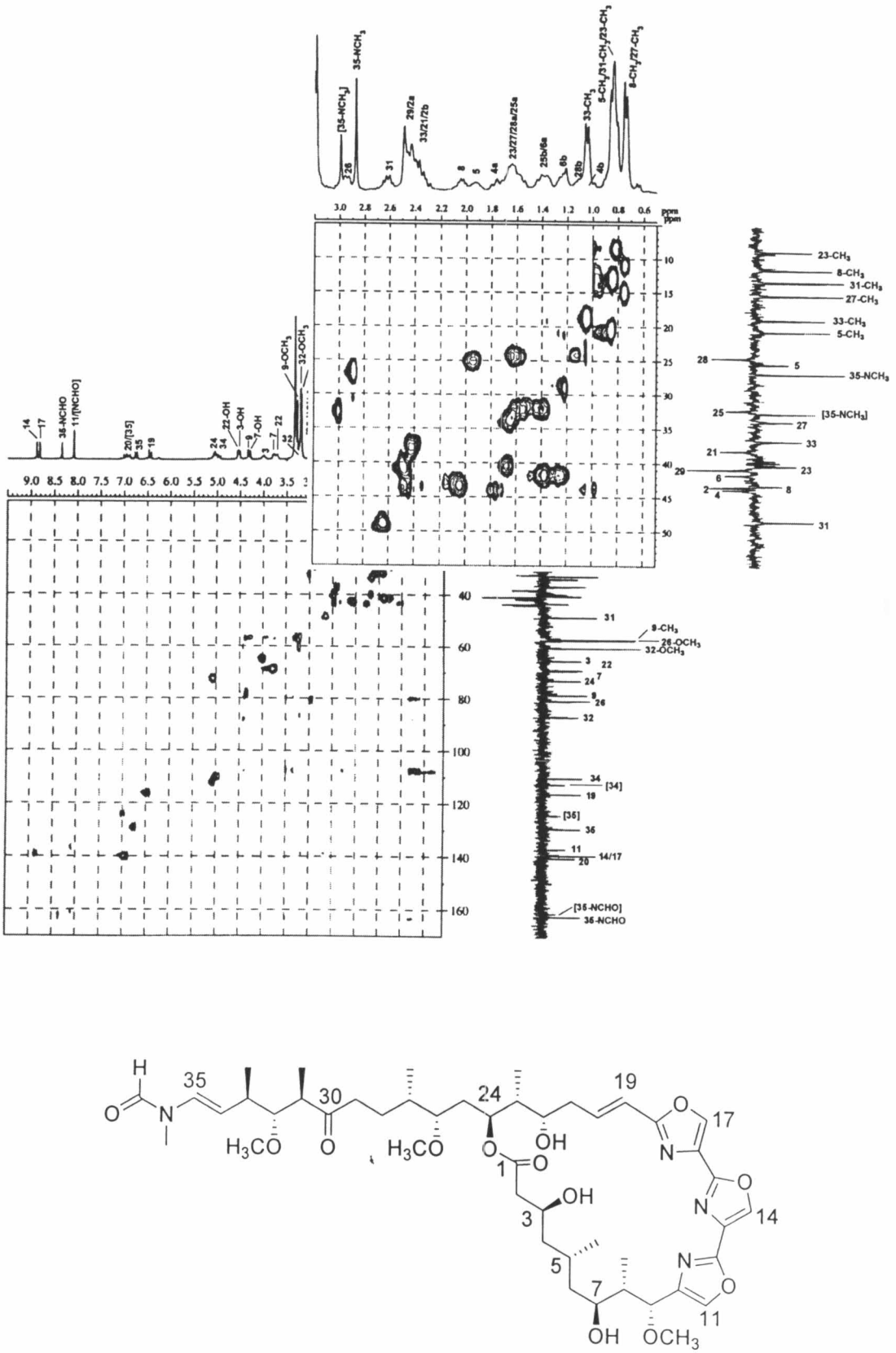

Figure 66 The 300 MHz HMQC spectrum of kabiramide F in DMSO-d_6.

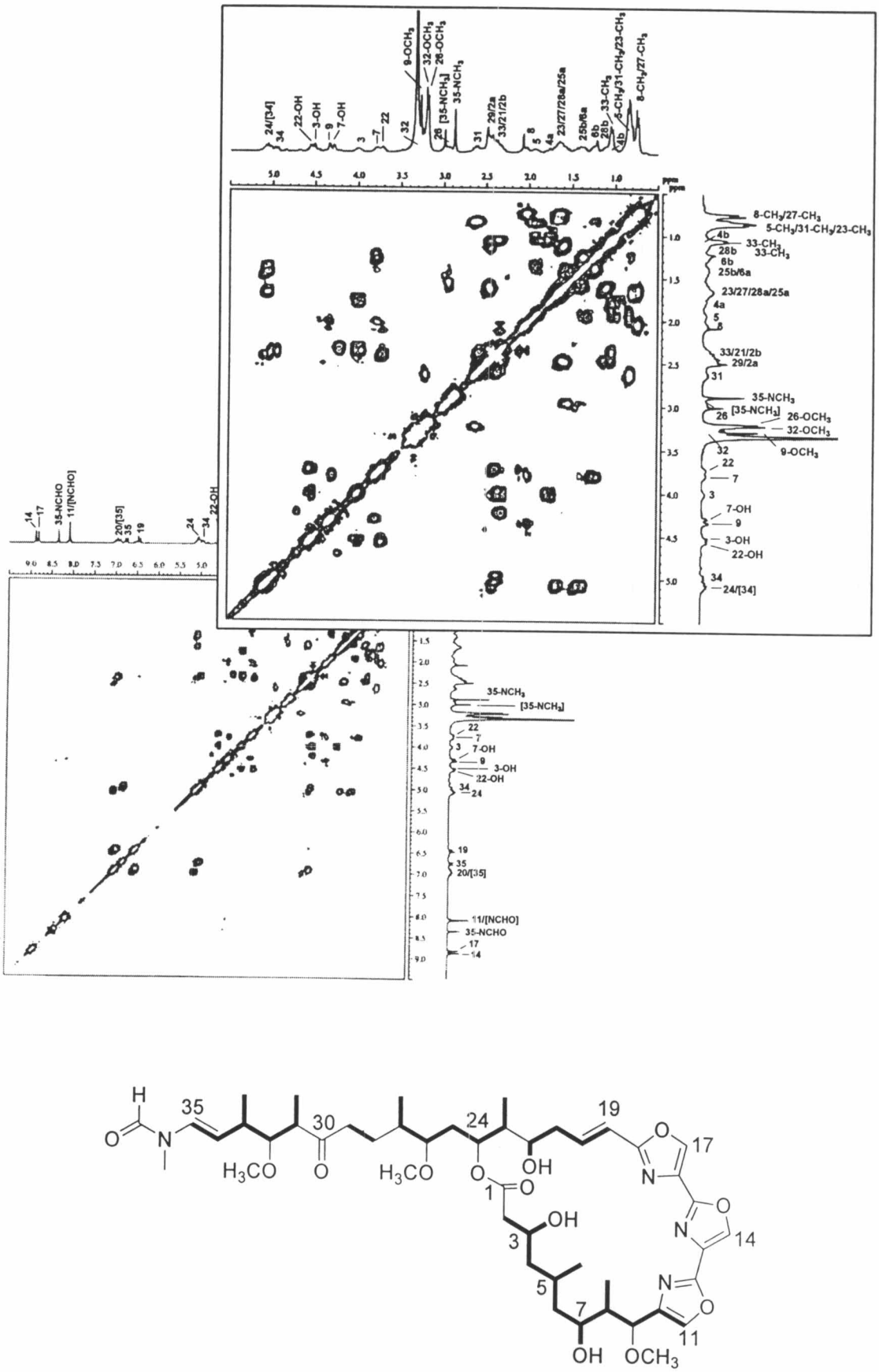

Figure 67 The 300 MHz H,H COSY spectrum of kabiramide F in DMSO-d_6.

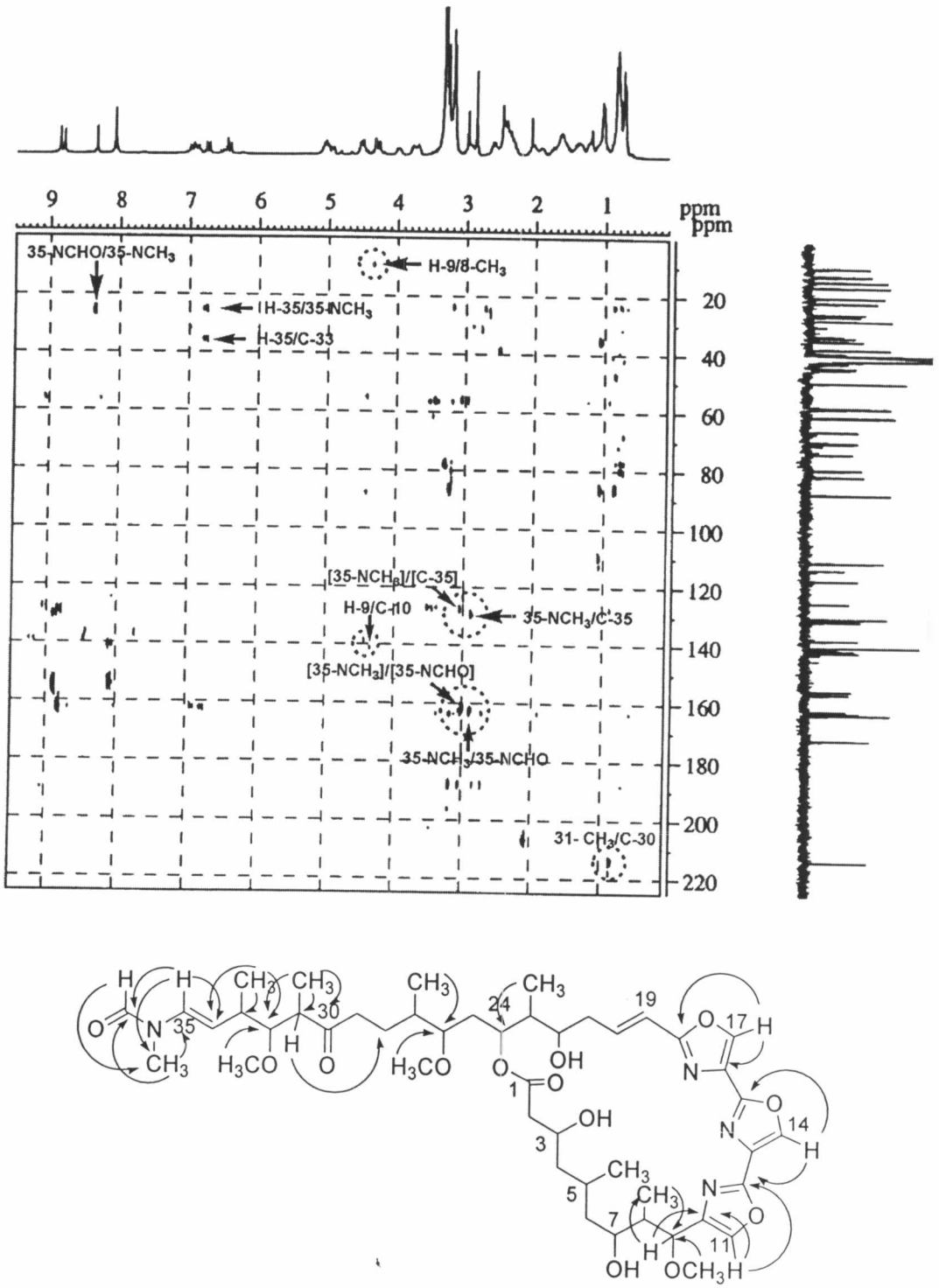

Figure 68 The 300 MHz HMBC spectrum ($^{n}J_{HC}$ = 8 Hz) of kabiramide F in DMSO-d_6.

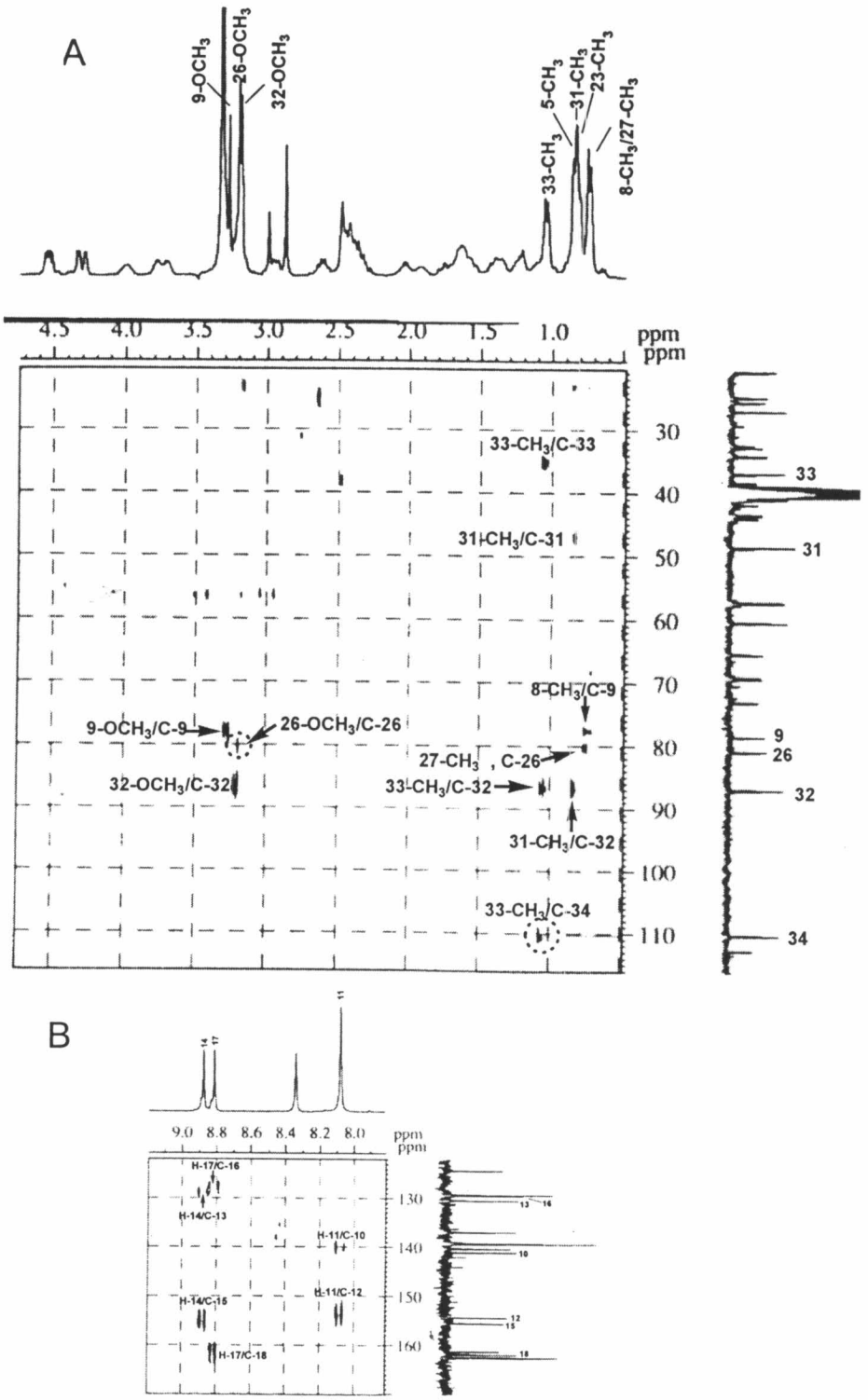

Figure 69 The 300 MHz HMBC spectrum (expanded) of kabiramide F in DMSO-d_6.

(A) F_2 axis (δ_H 0.5-4.2 ppm), F_1 axis (δ_C 20-115 ppm)

(B) F_2 axis (δ_H 7.8-9.2 ppm), F_1 axis (δ_C 120-170 ppm)

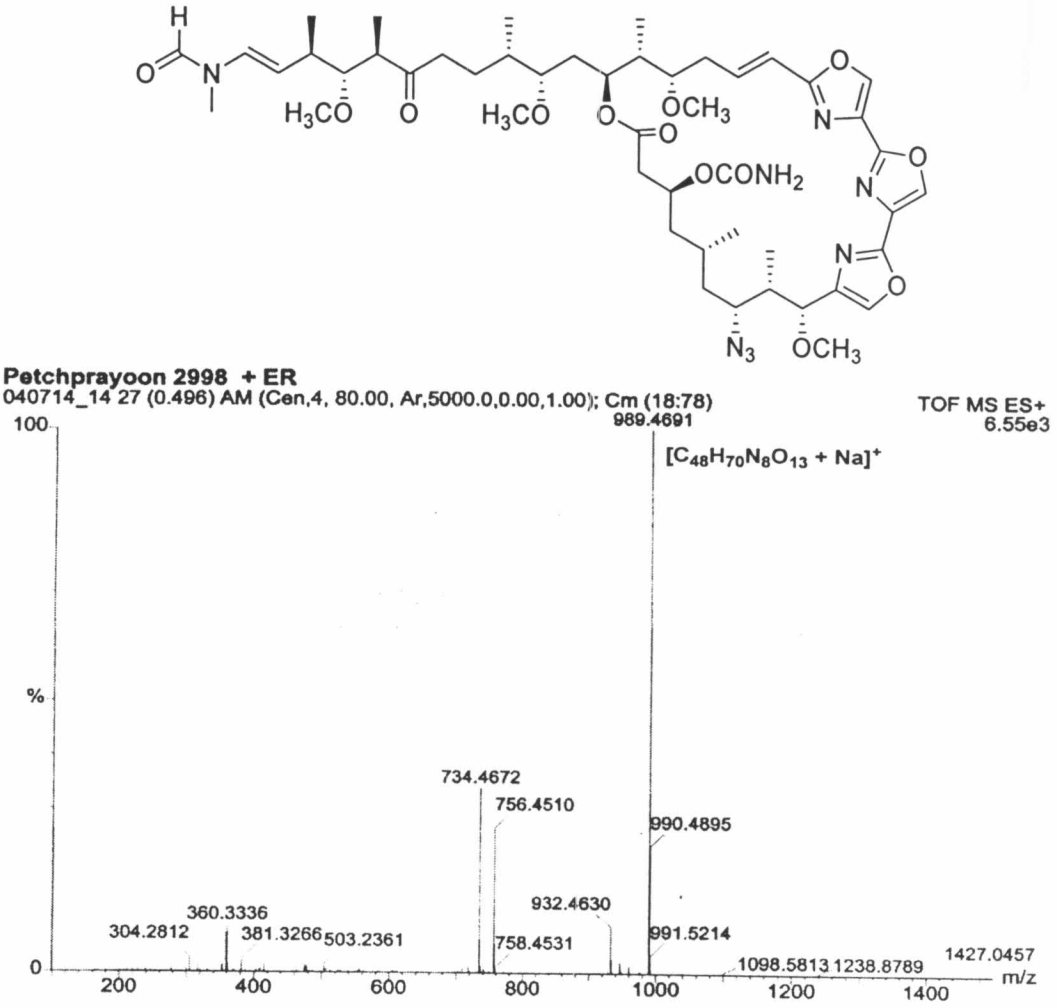

Figure 70 The ESI-TOF mass spectrum of 7-azidokabiramide C.

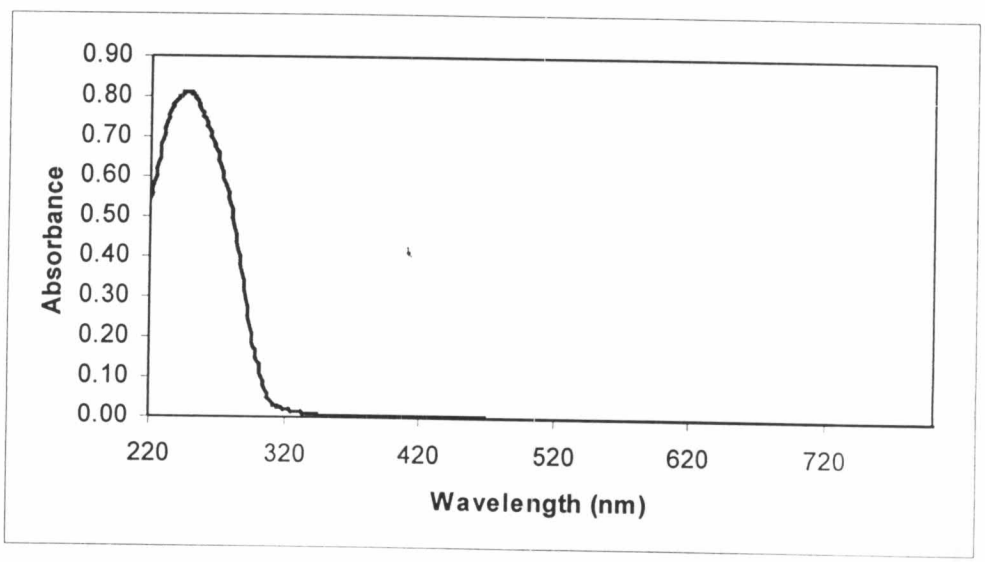

Figure 71 The UV spectrum of 7-azidokabiramide C in MeOH.

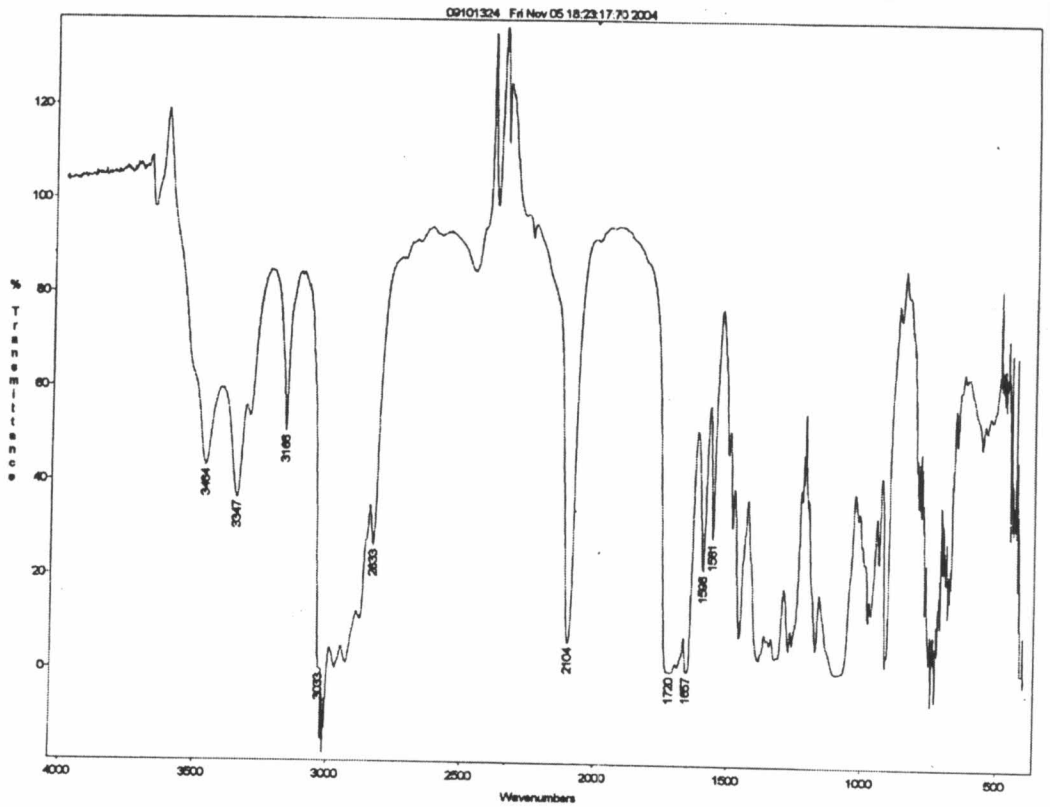

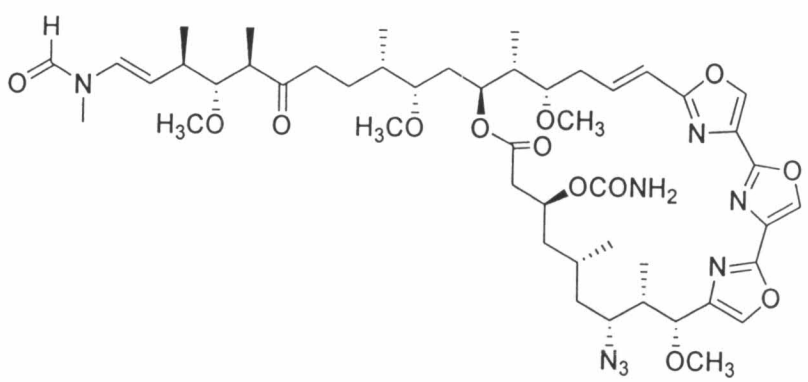

Figure 72 The IR spectrum of 7-azidokabiramide C ($CHCl_3$).

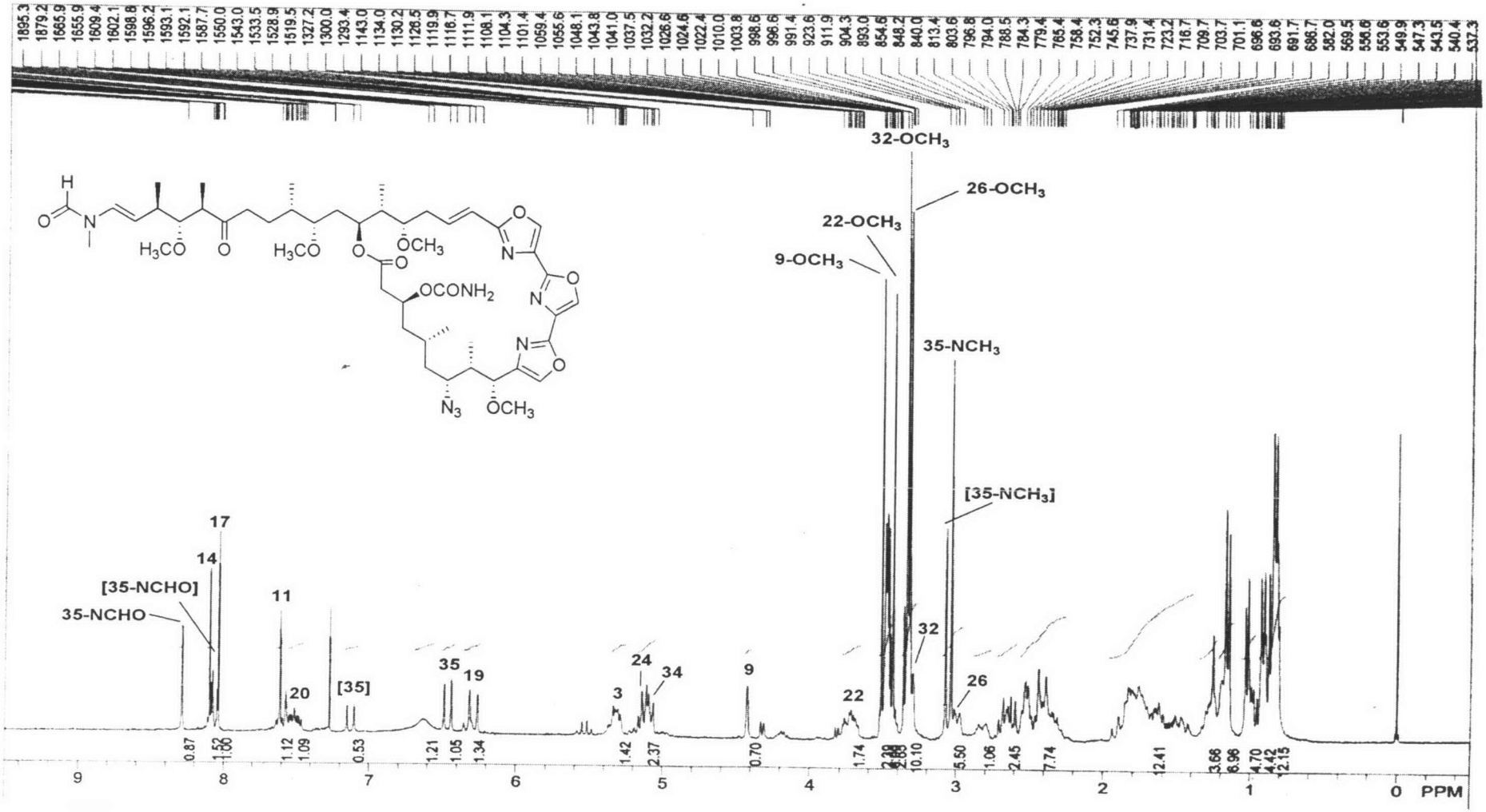

Figure 73 The 300 MHz ^{1}H NMR spectrum of 7-azidokabiramide C in $CDCl_3$.

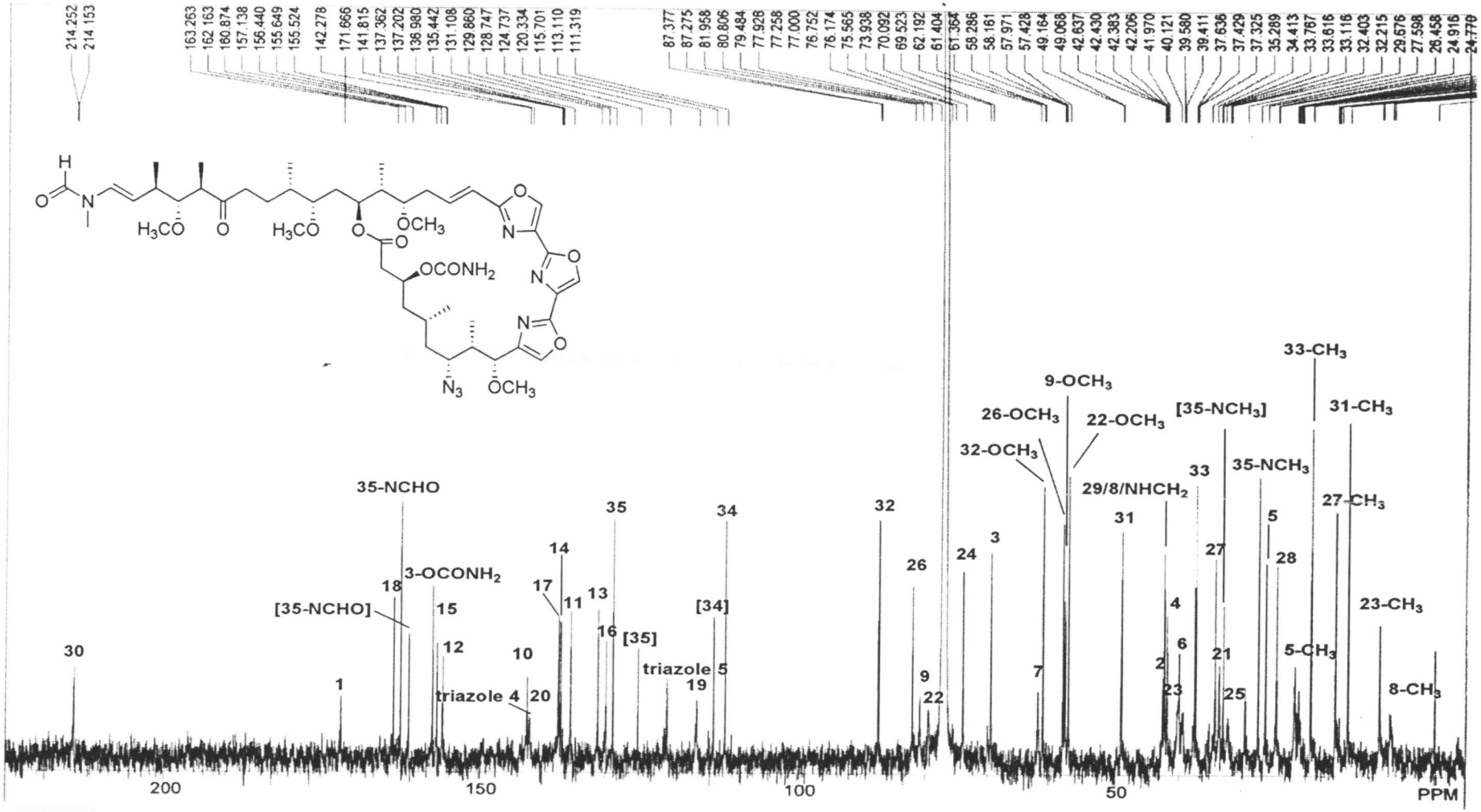

Figure 74 The 75 MHz ^{13}C NMR spectrum of 7-azidokabiramide C in $CDCl_3$.

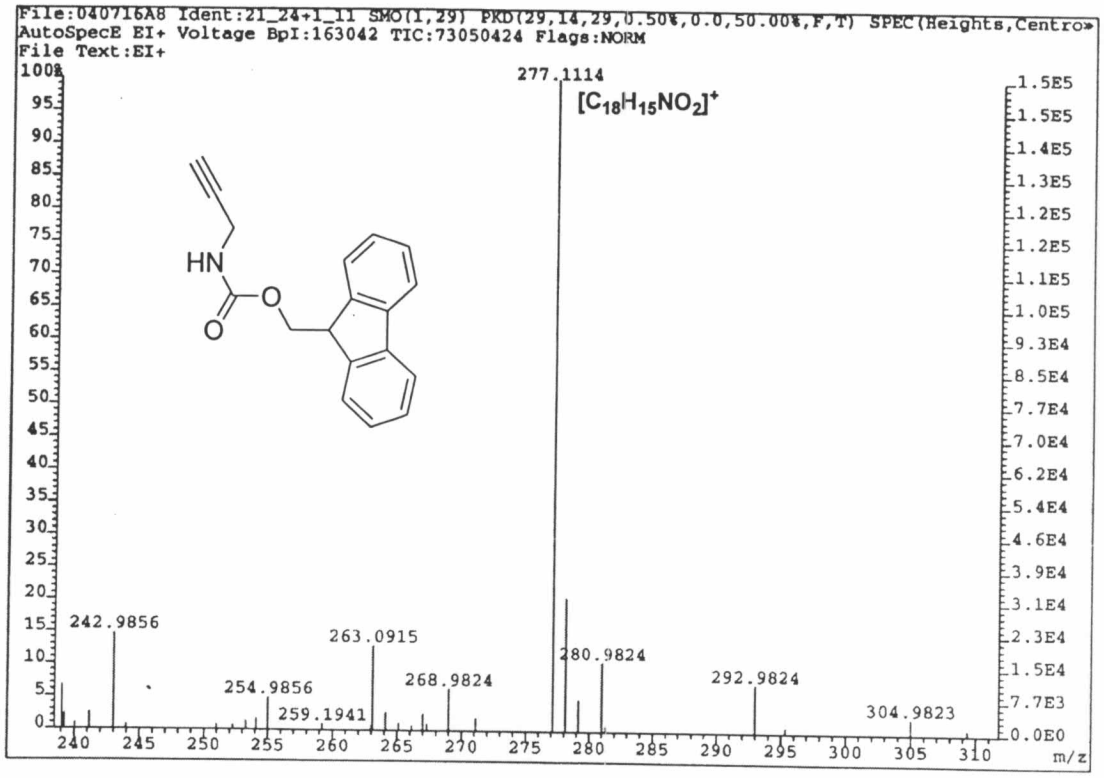

Figure 75 The EI mass spectrum of 3-(fluoren-9-yl-methoxycarbonyl)aminopropyne.

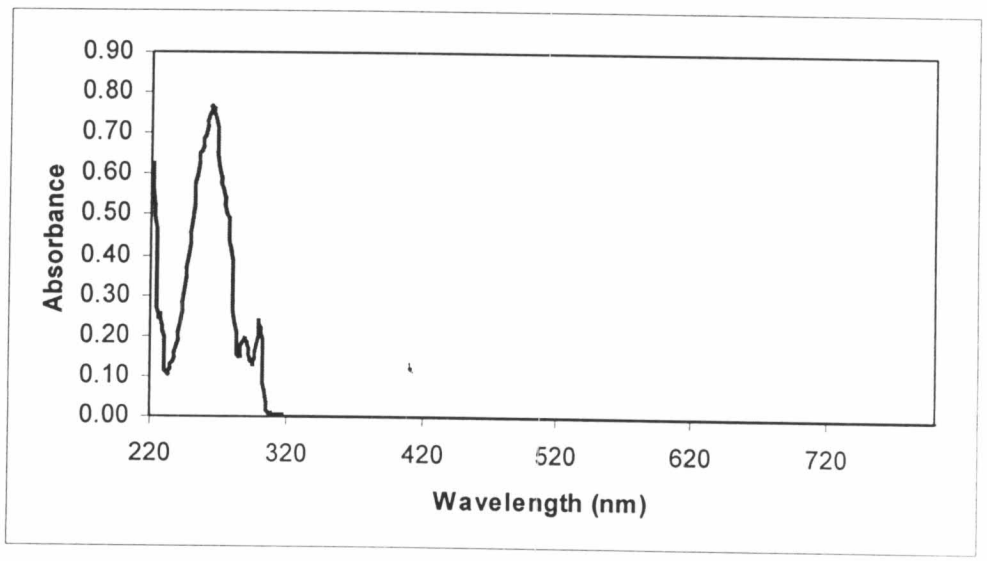

Figure 76 The UV spectrum of 3-(fluoren-9-yl-methoxycarbonyl)aminopropyne in MeOH.

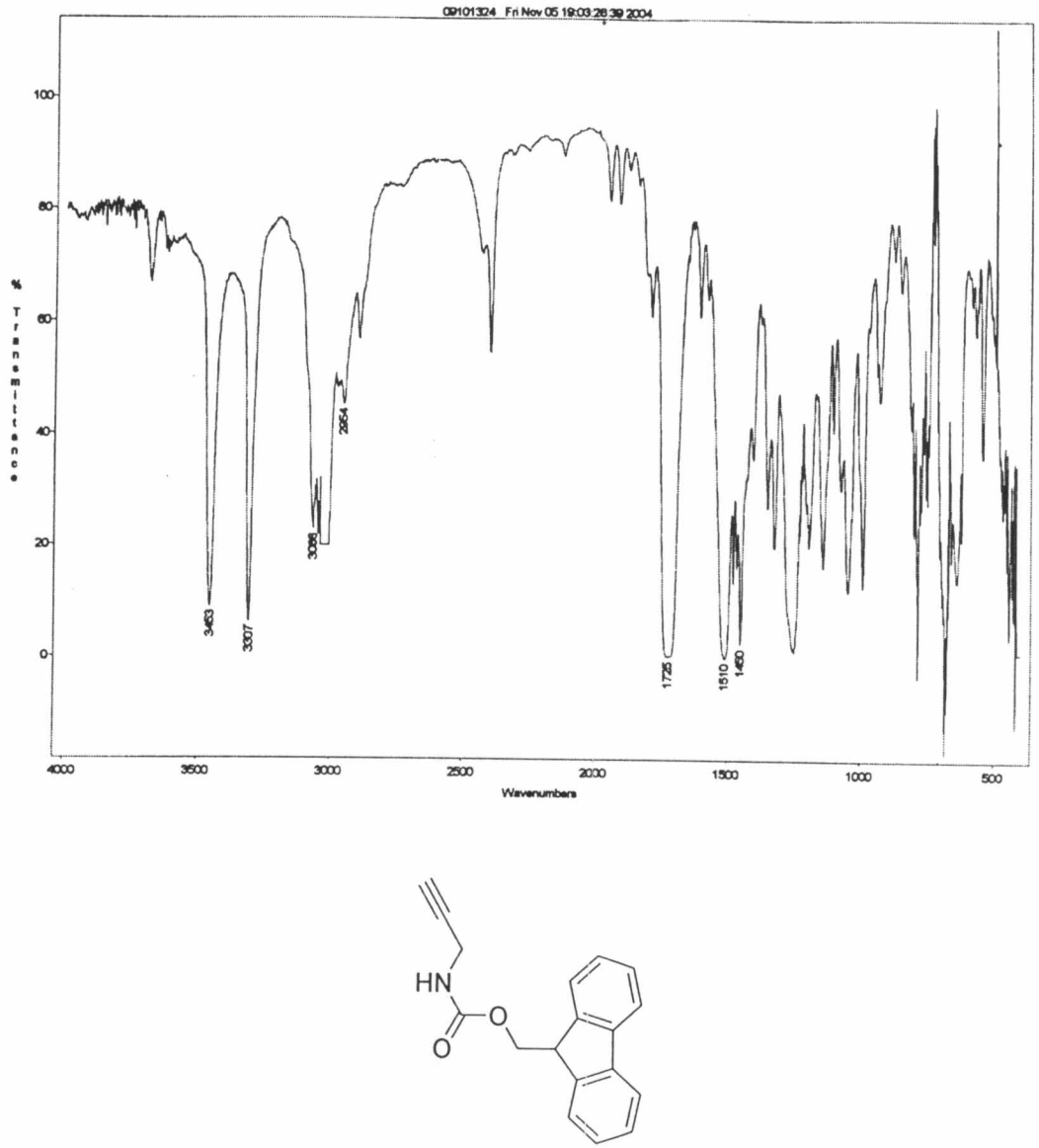

Figure 77 The IR spectrum of 3-(fluoren-9-yl-methoxycarbonyl)aminopropyne ($CHCl_3$).

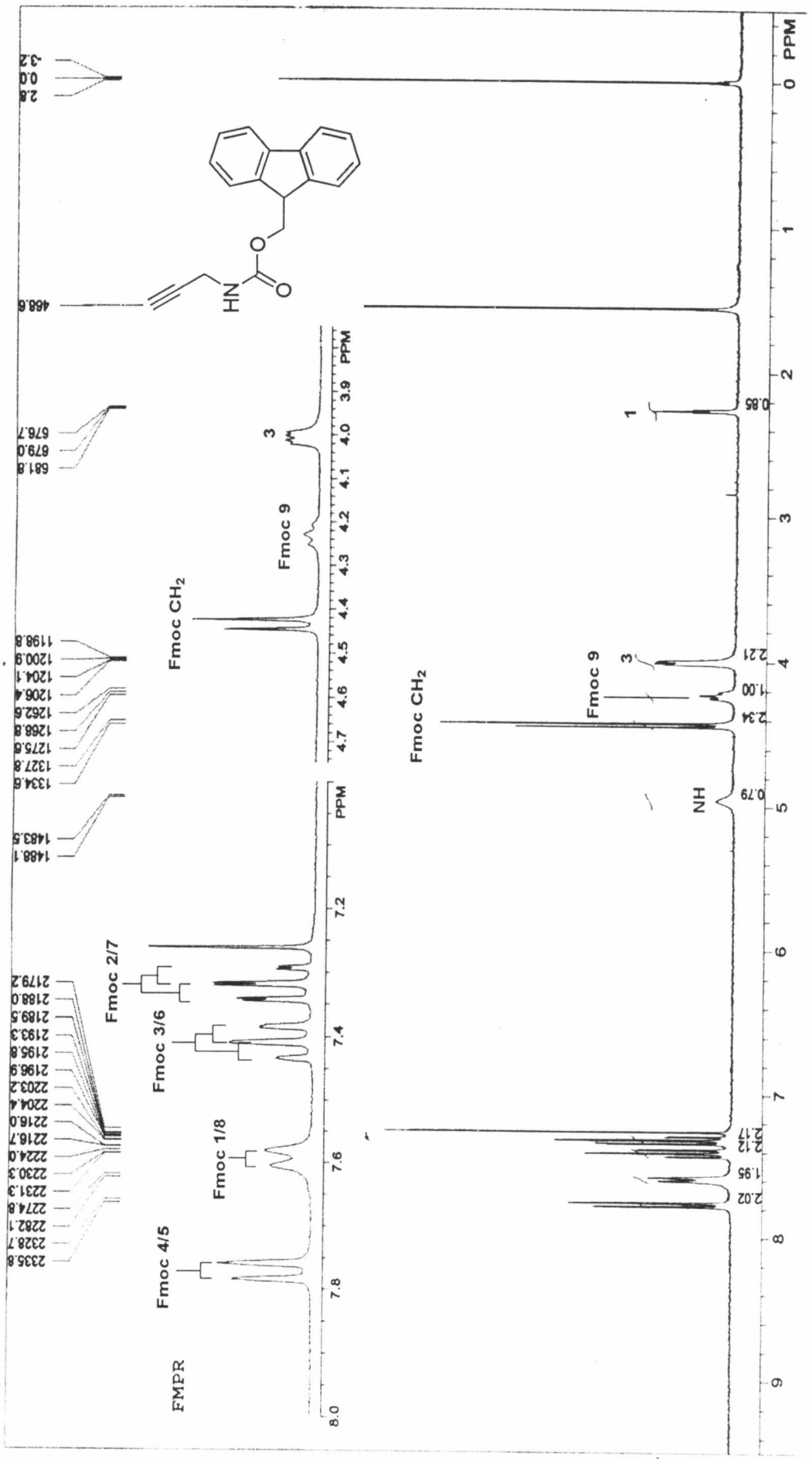

Figure 78 The 300 MHz ^{1}H NMR spectrum of 3-(fluoren-9-yl-methoxycarbonyl)aminopropyne in $CDCl_3$.

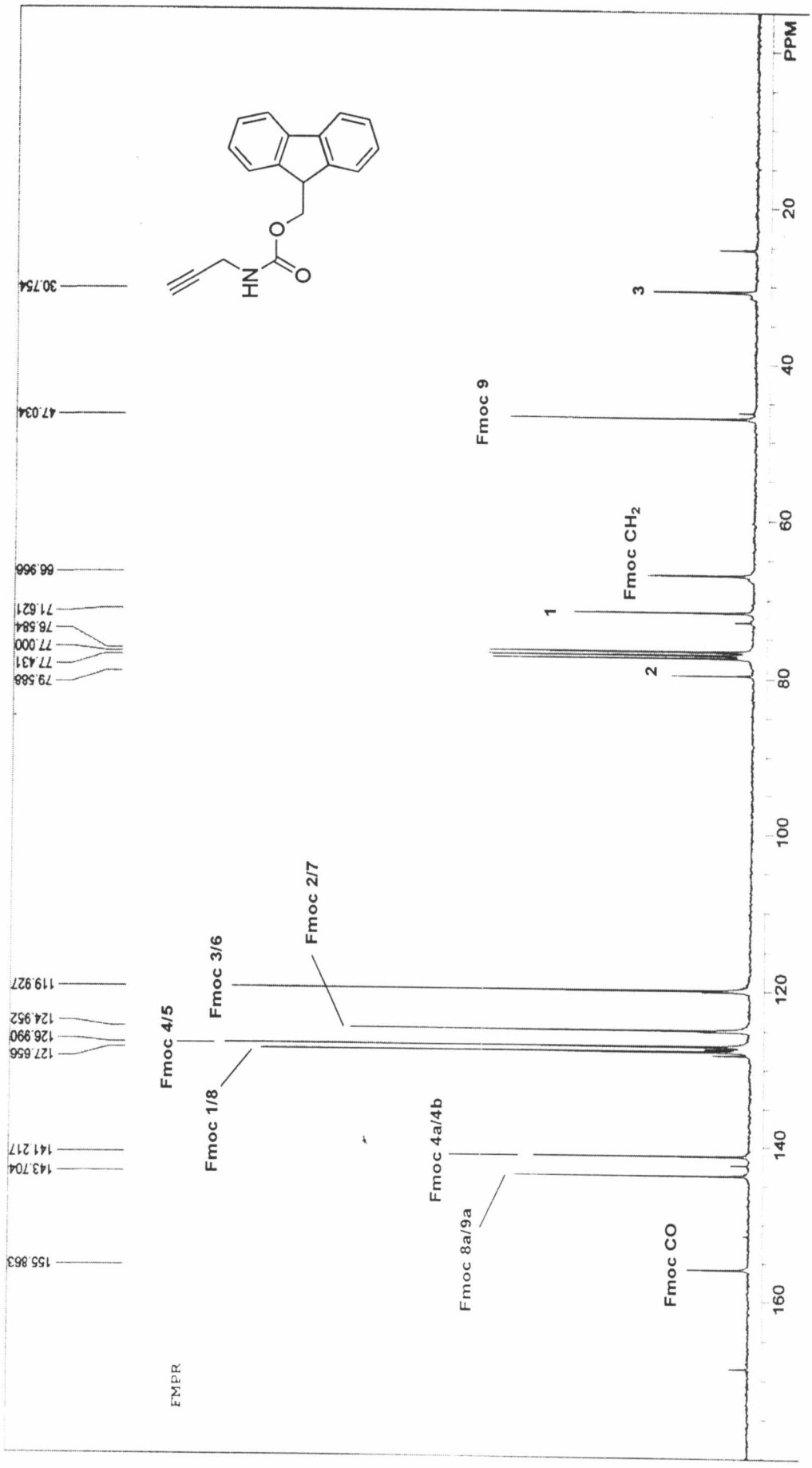

Figure 79 The 75 MHz ^{13}C NMR spectrum of 3-(fluoren-9-yl-methoxycarbonyl)aminopropyne in $CDCl_3$.

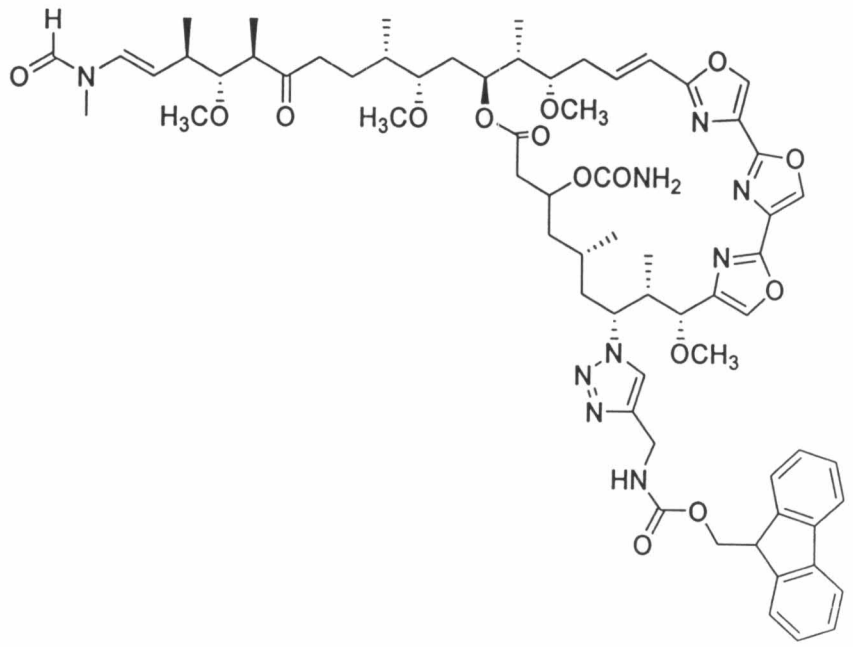

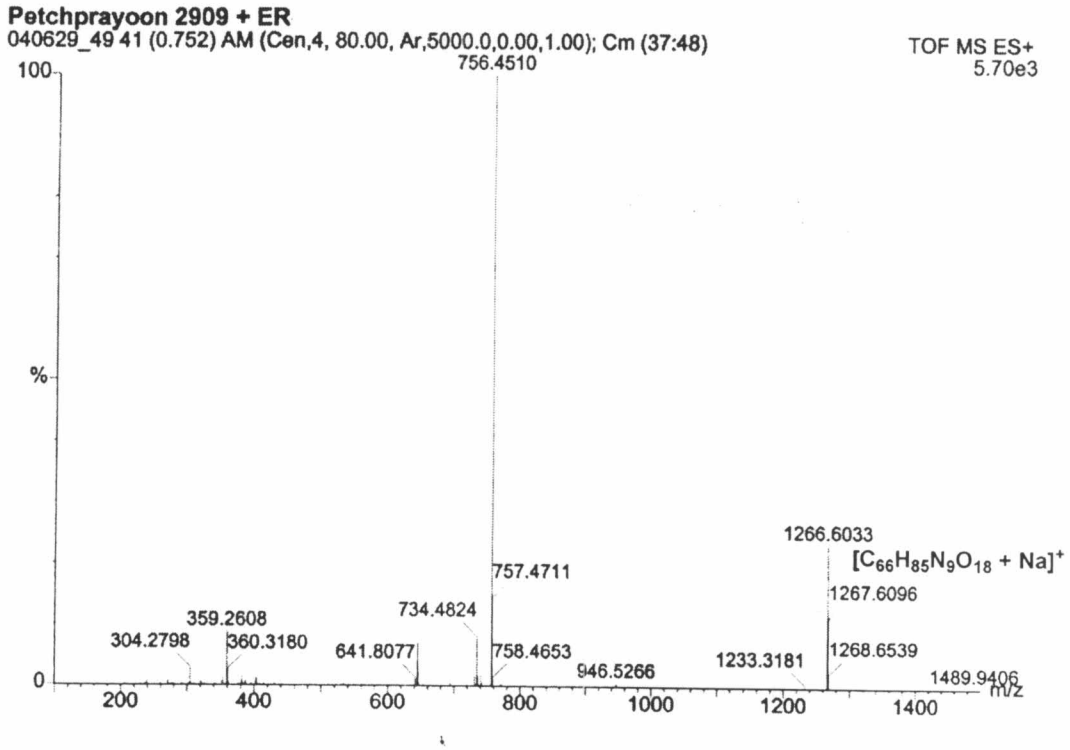

Figure 80 The ESI-TOF mass spectrum of 7-[4-*N*-(9*H*-fluoren-9-yl-methoxycarbonyl) aminomethyl-1,2,3-triazol-1-yl]kabiramide C.

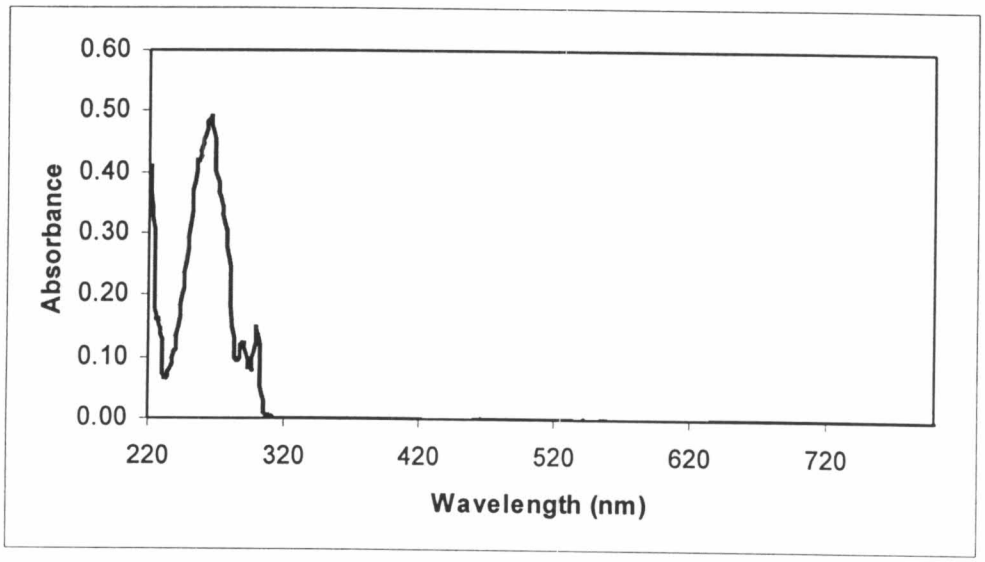

Figure 81 The UV spectrum of 7-[4-*N*-(9*H*-fluoren-9-yl-methoxycarbonyl)aminomethyl-1,2,3-triazol-1-yl]kabiramide C in MeOH.

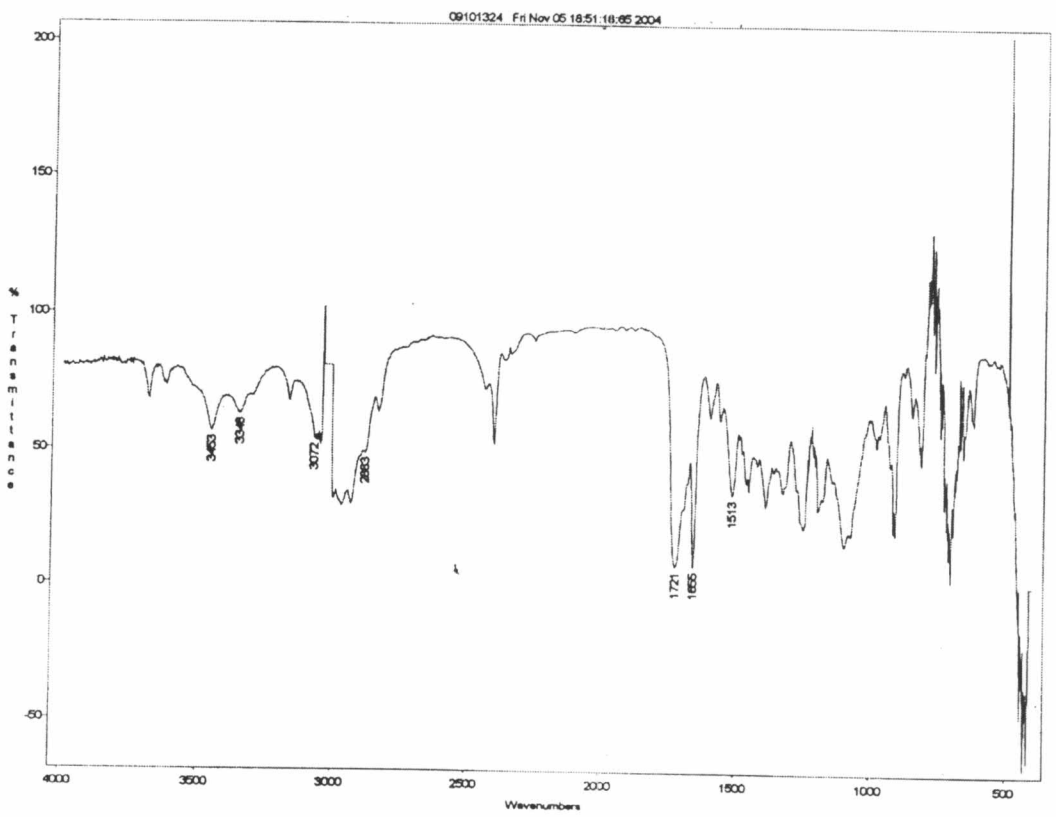

Figure 82 The IR spectrum of 7-[4-*N*-(9*H*-fluoren-9-yl-methoxycarbonyl)aminomethyl-1,2,3-triazol-1-yl]kabiramide C ($CHCl_3$).

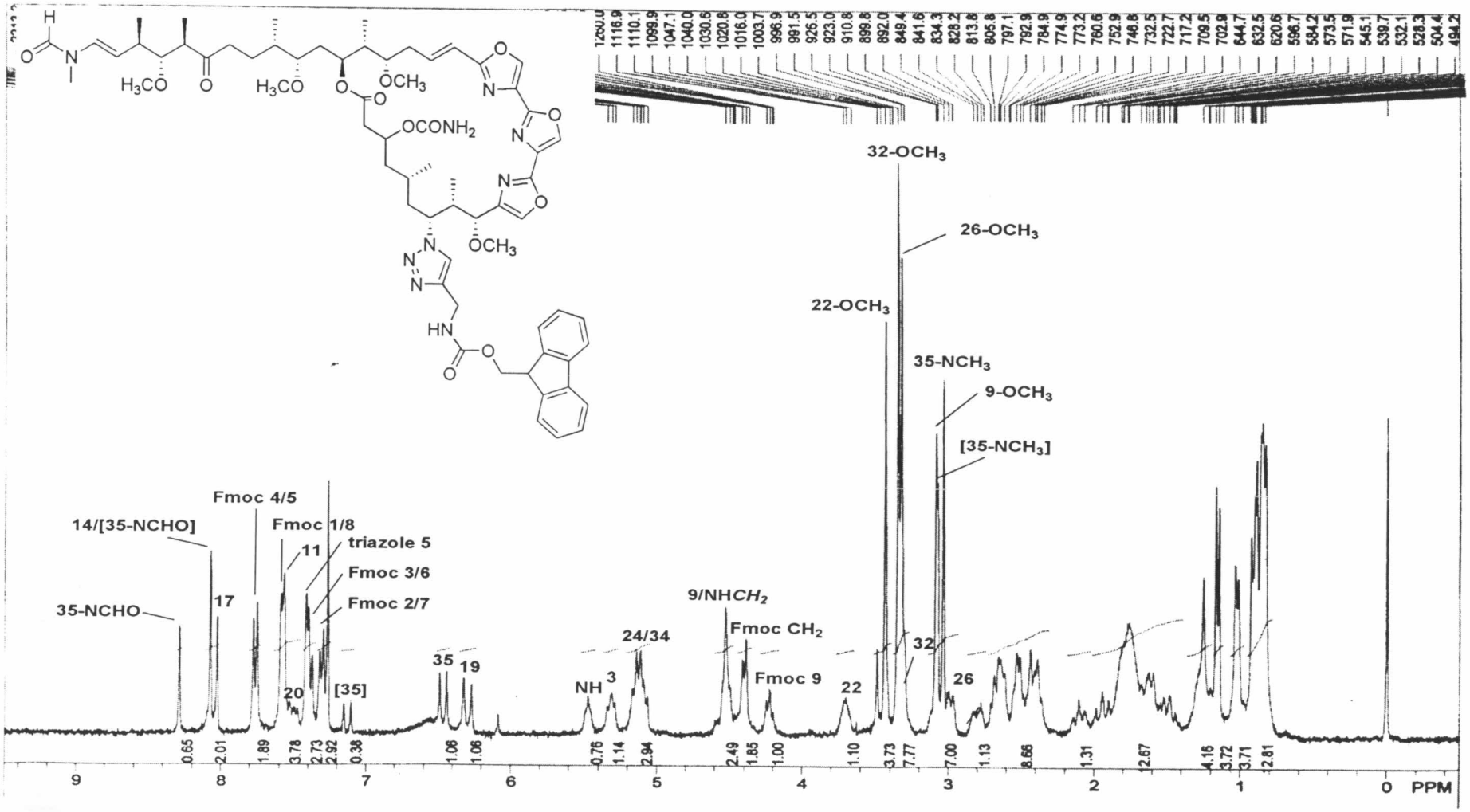

Figure 83 The 300 MHz ^{1}H NMR spectrum of 7-[4-*N*-(9*H*-fluoren-9-yl-methoxycarbonyl)aminomethyl-1,2,3-triazol-1-yl]kabiramide C in $CDCl_3$.

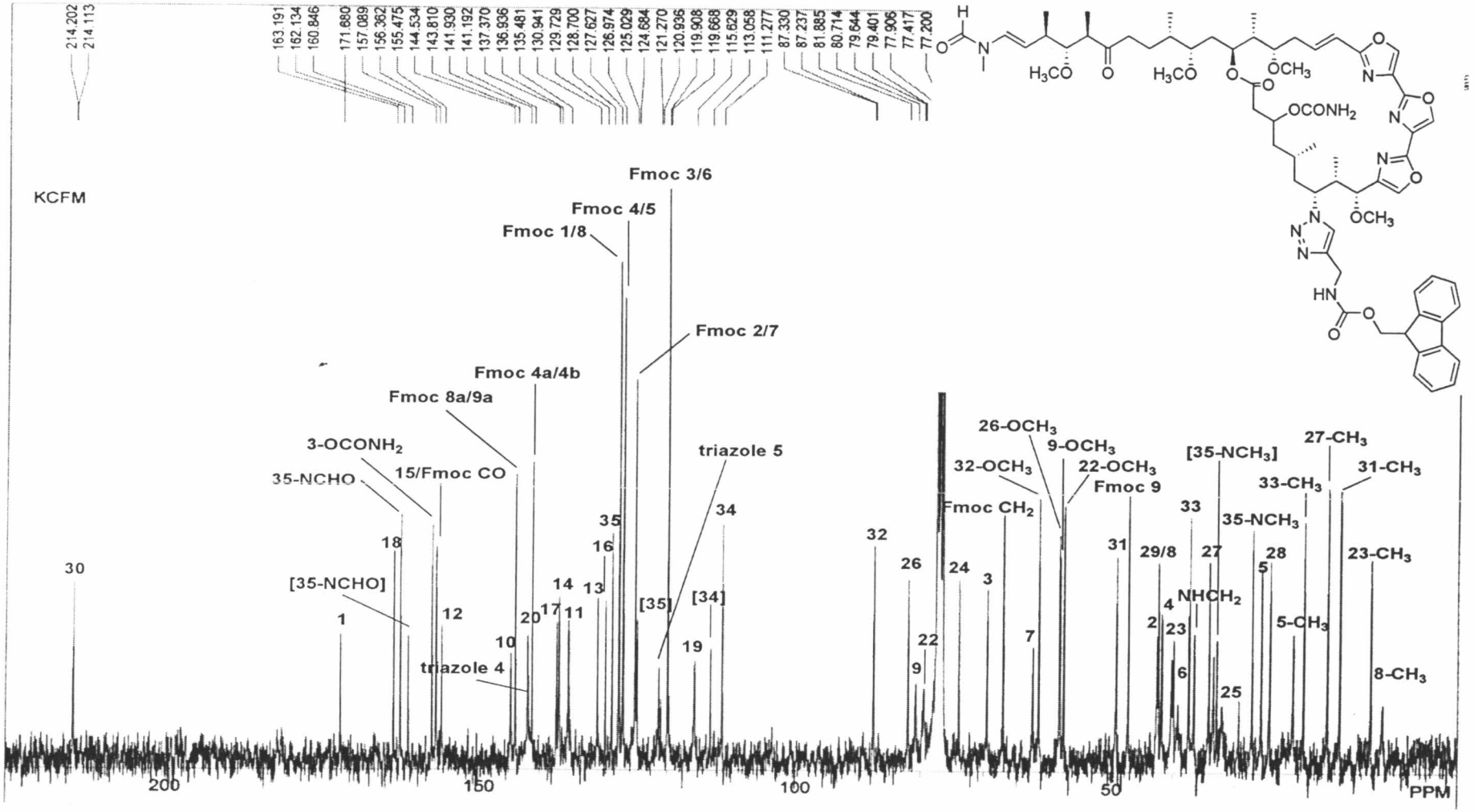

Figure 84 The 75 MHz ^{13}C NMR spectrum of 7-[4-*N*-(9*H*-fluoren-9-yl-methoxycarbonyl)aminomethyl-1,2,3-triazol-1-yl]kabiramide C in $CDCl_3$.

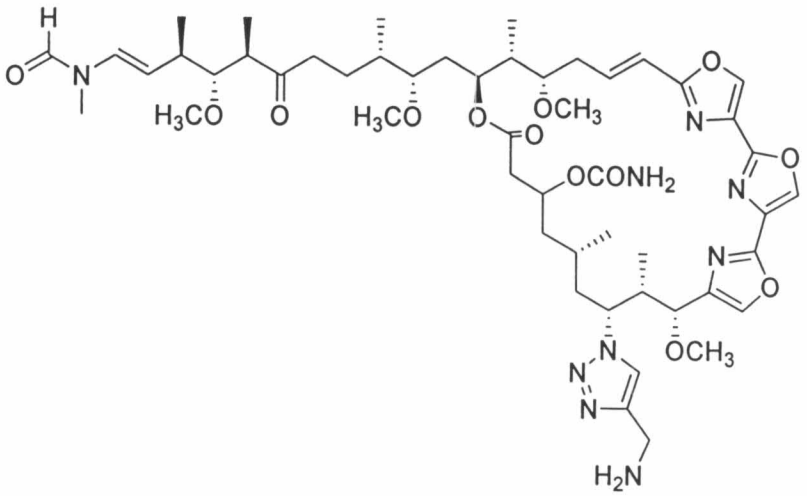

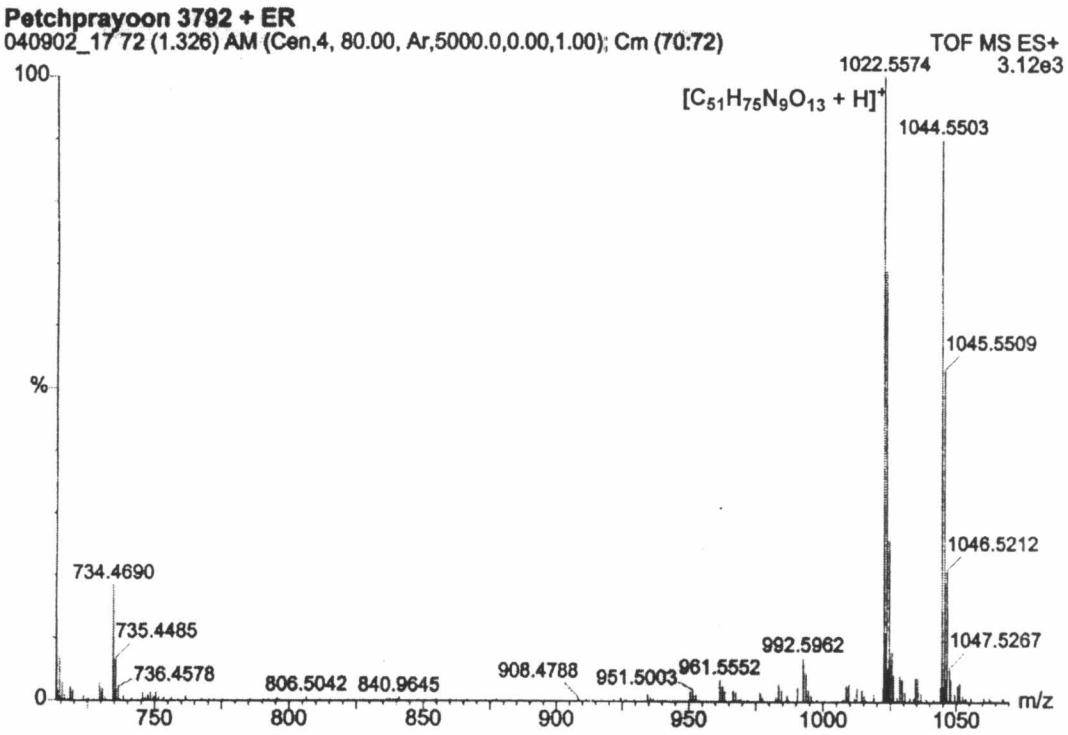

Figure 85 The ESI-TOF mass spectrum of 7-(4-aminomethyl-1*H*-1,2,3-triazol-1-yl) kabiramide C.

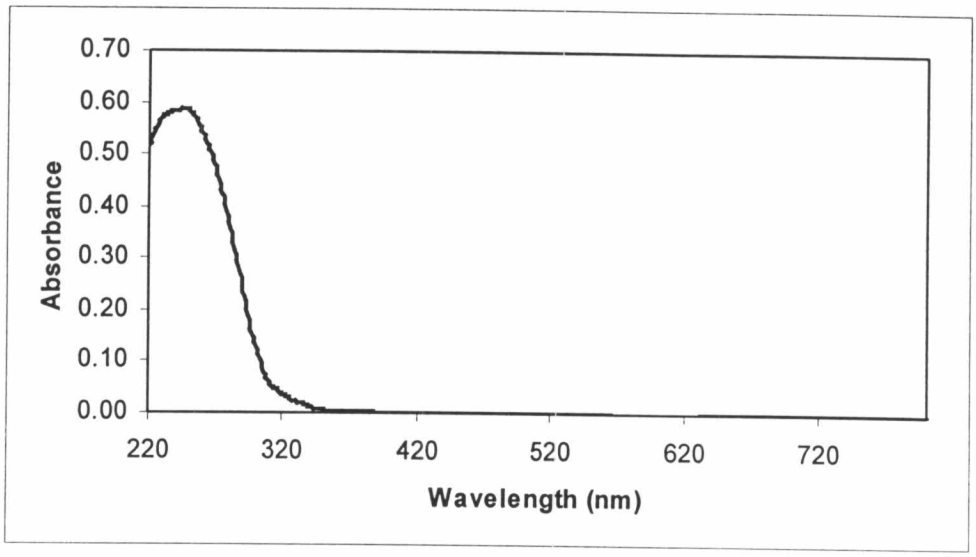

Figure 86 The UV spectrum of 7-(4-aminomethyl-1*H*-1,2,3-triazol-1-yl)kabiramide C in MeOH.

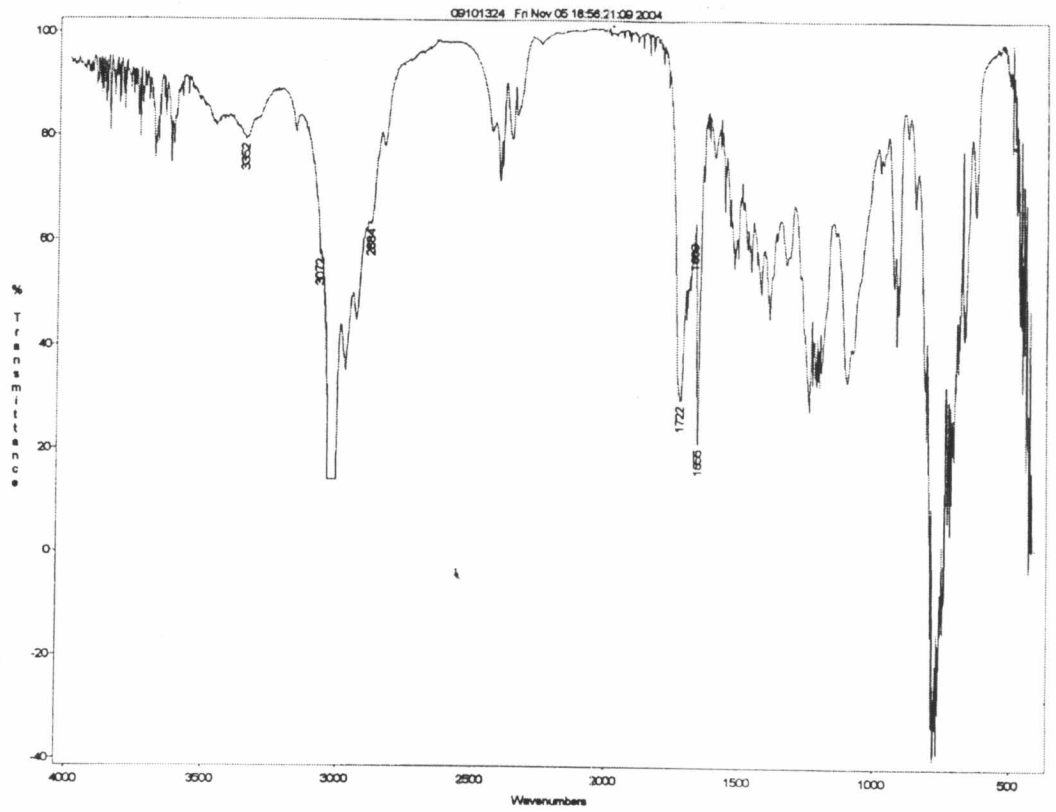

Figure 87 The IR spectrum of 7-4-aminomethyl-1*H*-1,2,3-triazol-1-yl)kabiramide C ($CHCl_3$).

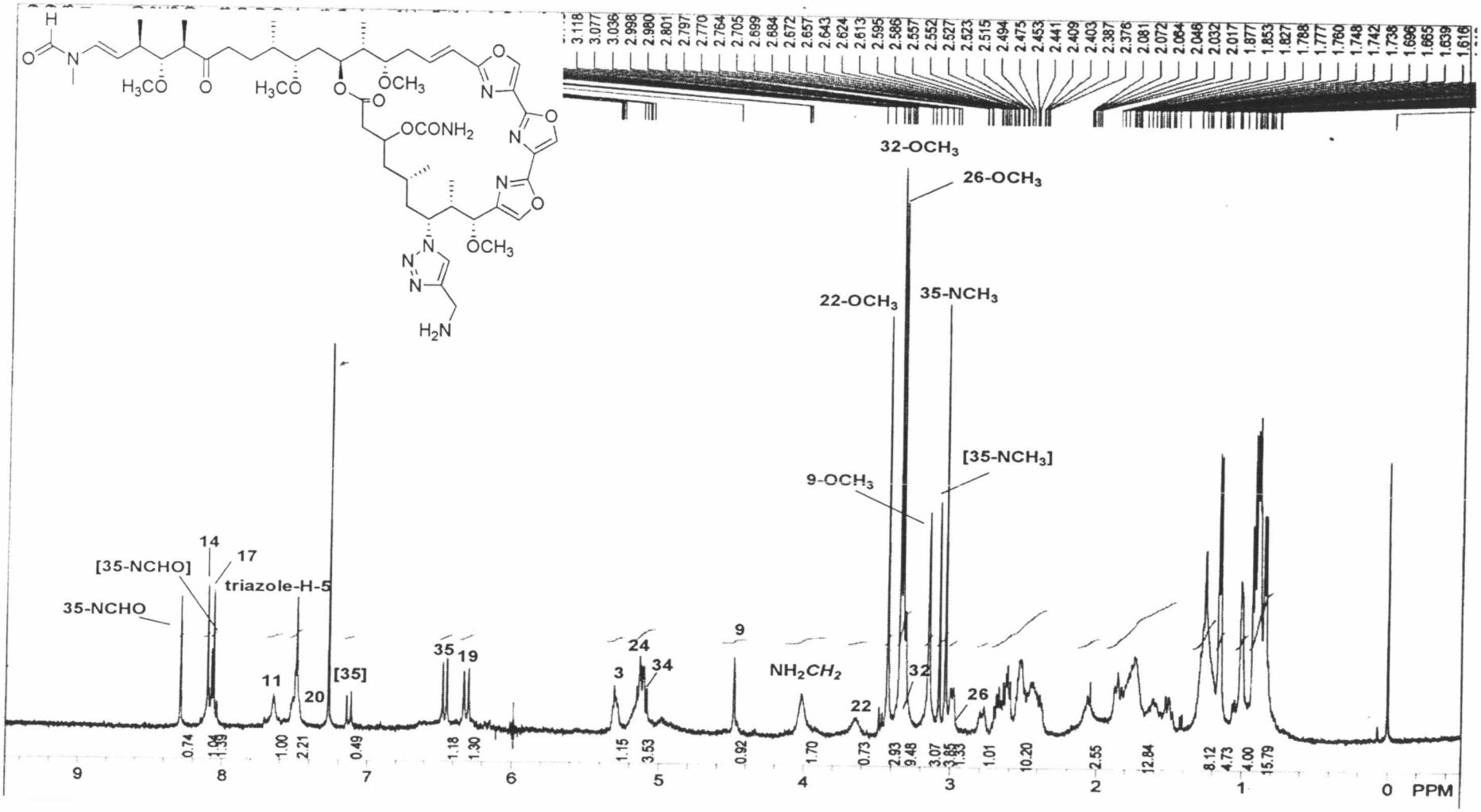

Figure 88 The 500 MHz ^{1}H NMR spectrum of 7-(4-aminomethyl-1*H*-1,2,3-triazol-1-yl)kabiramide C in $CDCl_3$.

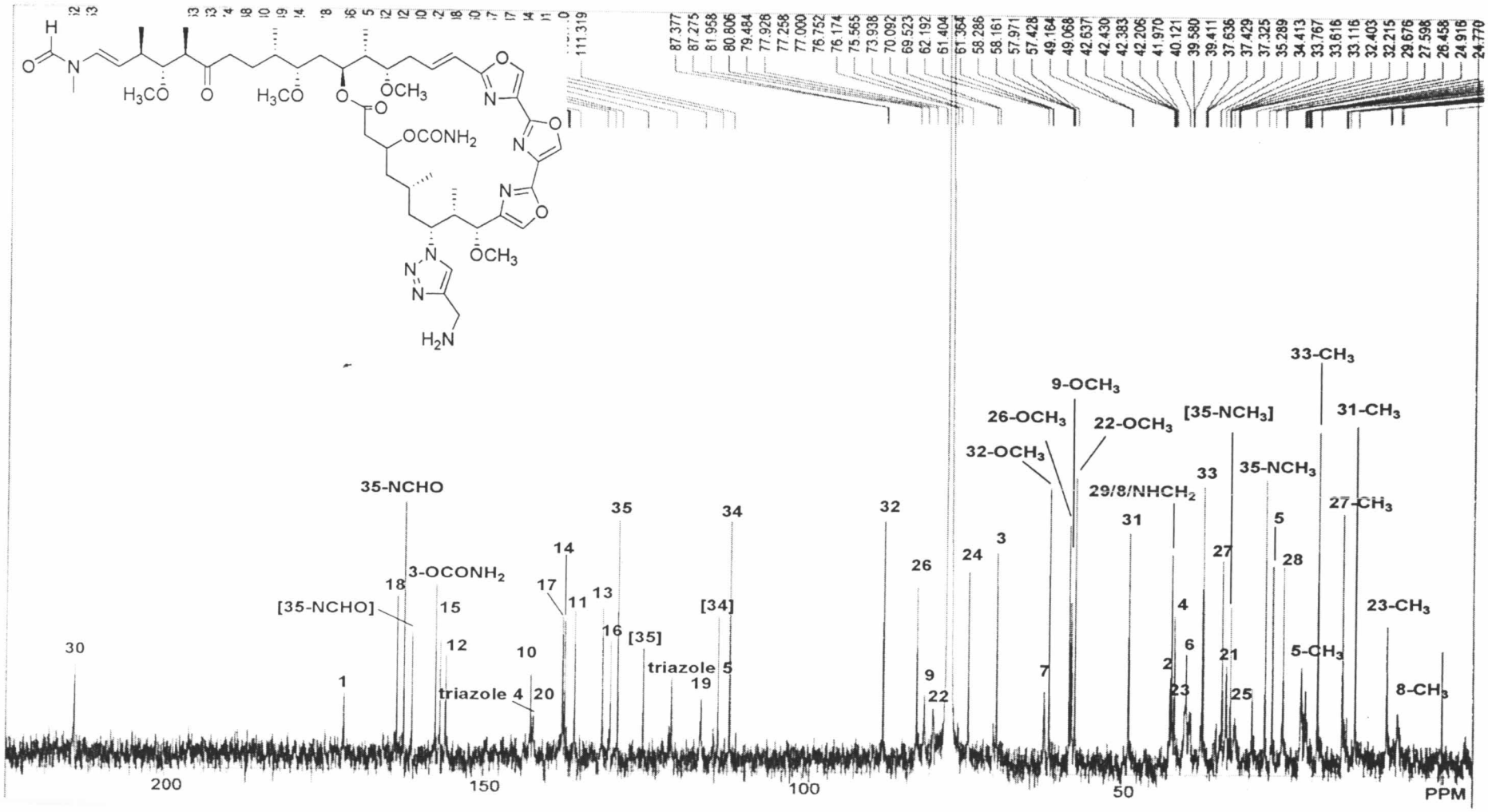

Figure 89 The 125 MHz ^{13}C NMR spectrum of 7-(4-aminomethyl-1*H*-1,2,3-triazol-1-yl)kabiramide C in $CDCl_3$.

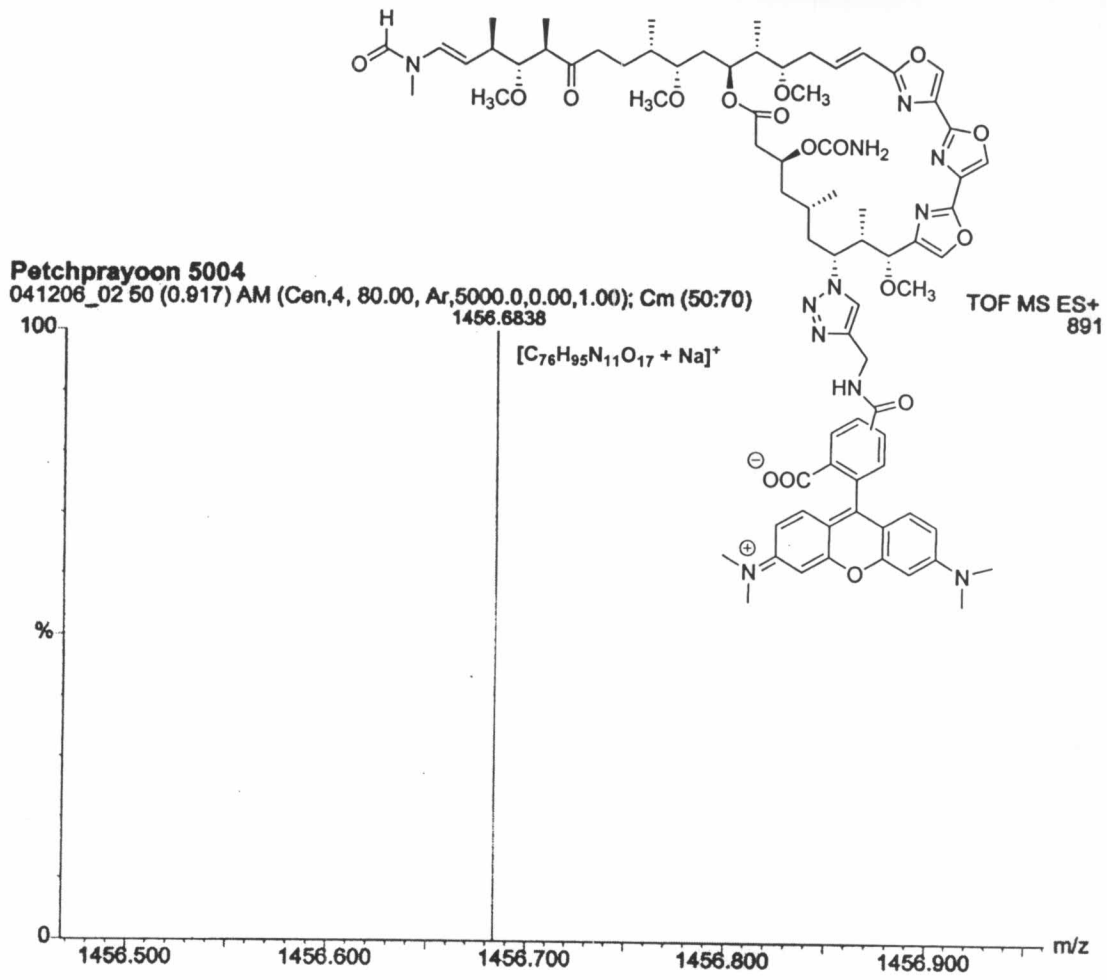

Figure 90 The ESI-TOF mass spectrum of TMR-KabC.

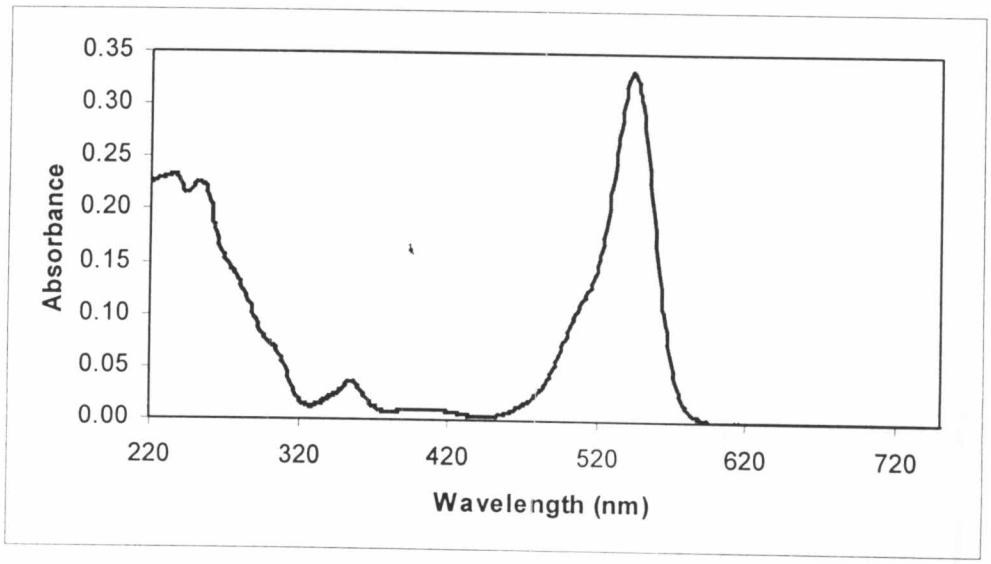

Figure 91 The UV spectrum of TMR-KabC in MeOH.

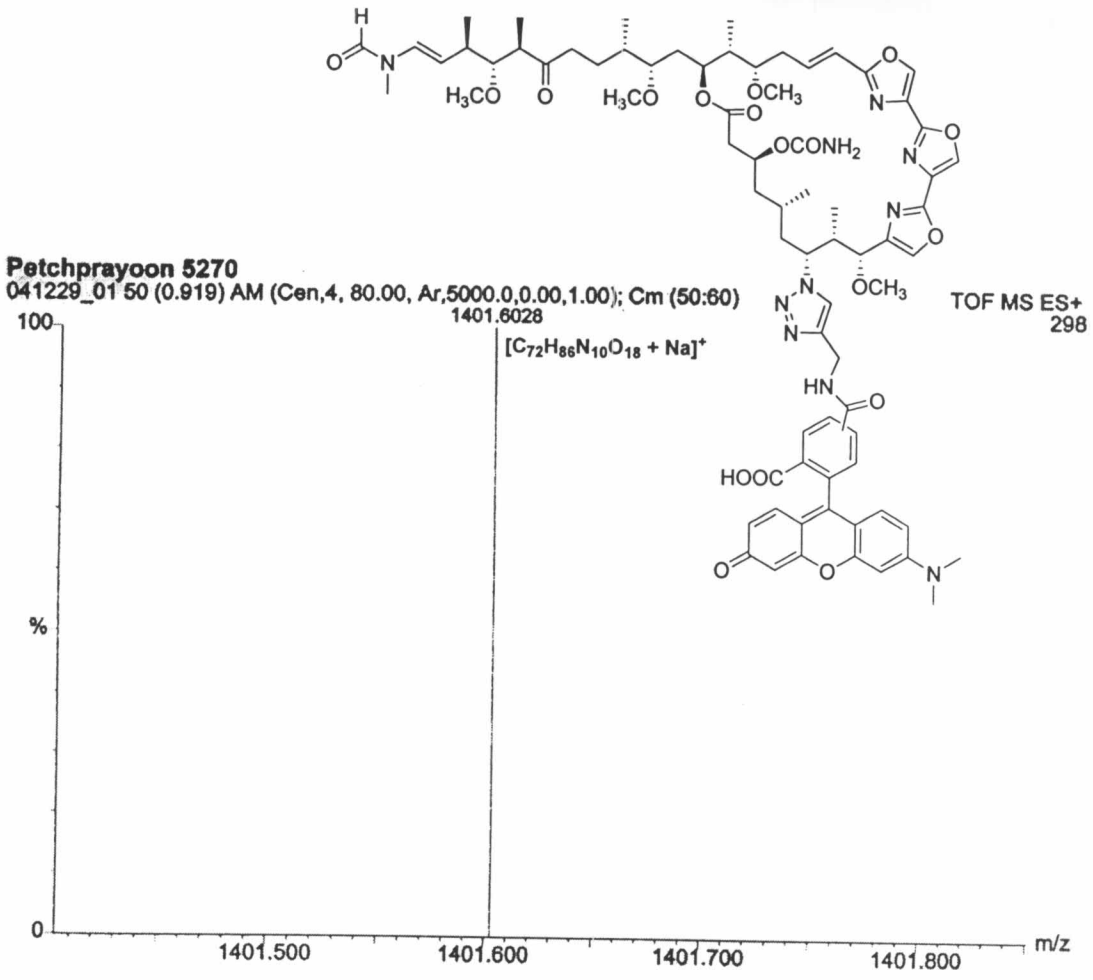

Figure 92 The ESI-TOF mass spectrum of RG-KabC.

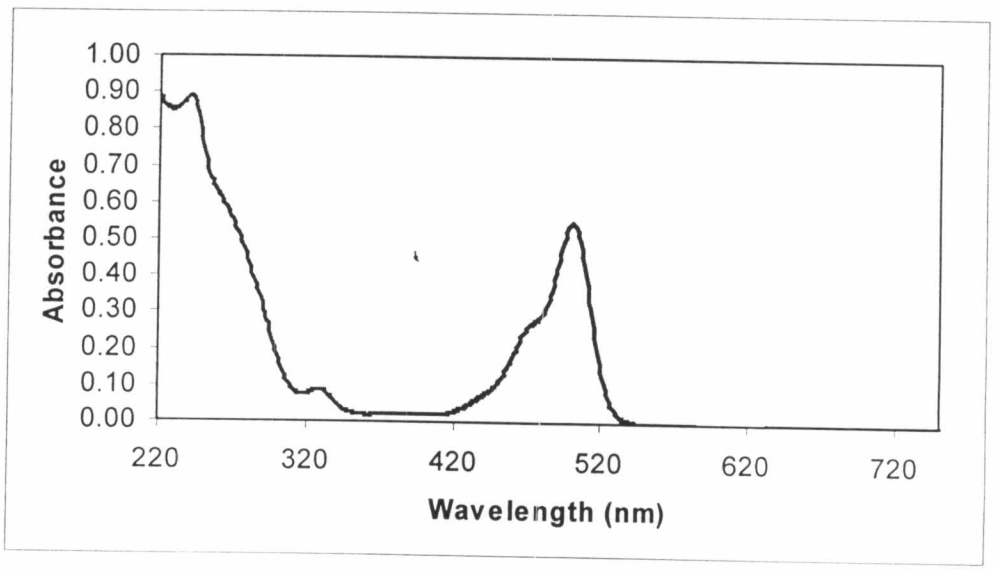

Figure 93 The UV spectrum of RG-KabC in MeOH.

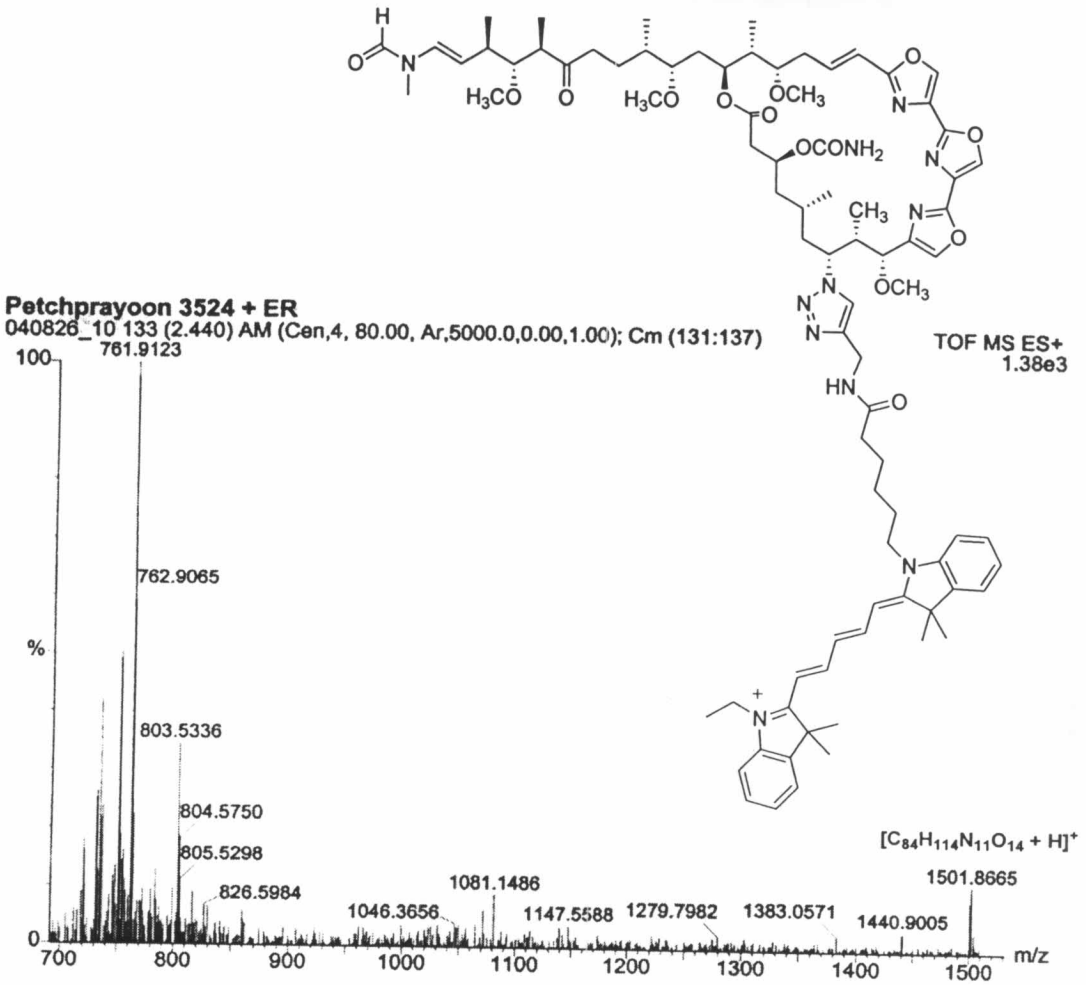

Figure 94 The ESI-TOF mass spectrum of IC5-KabC.

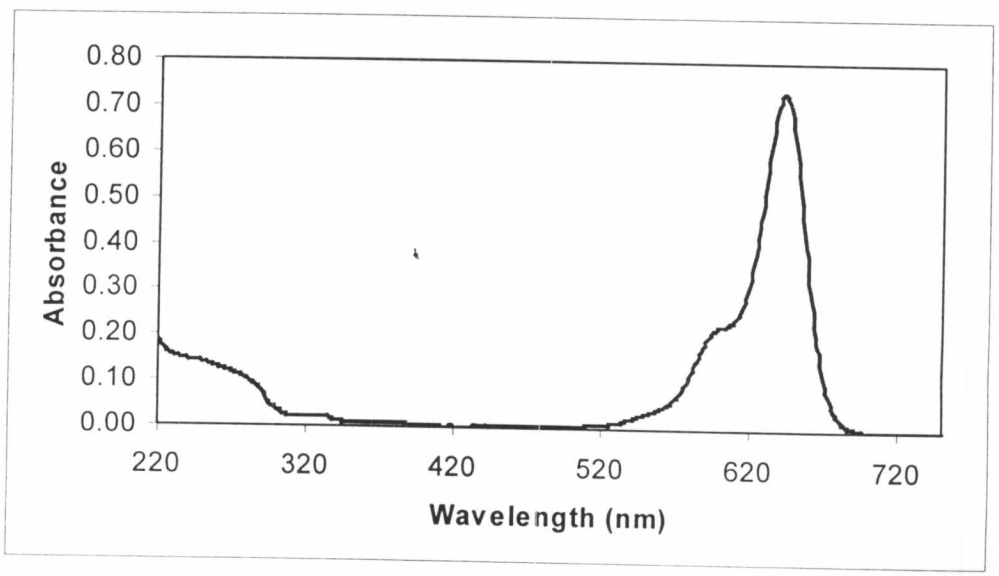

Figure 95 The UV spectrum of IC5-KabC in MeOH.

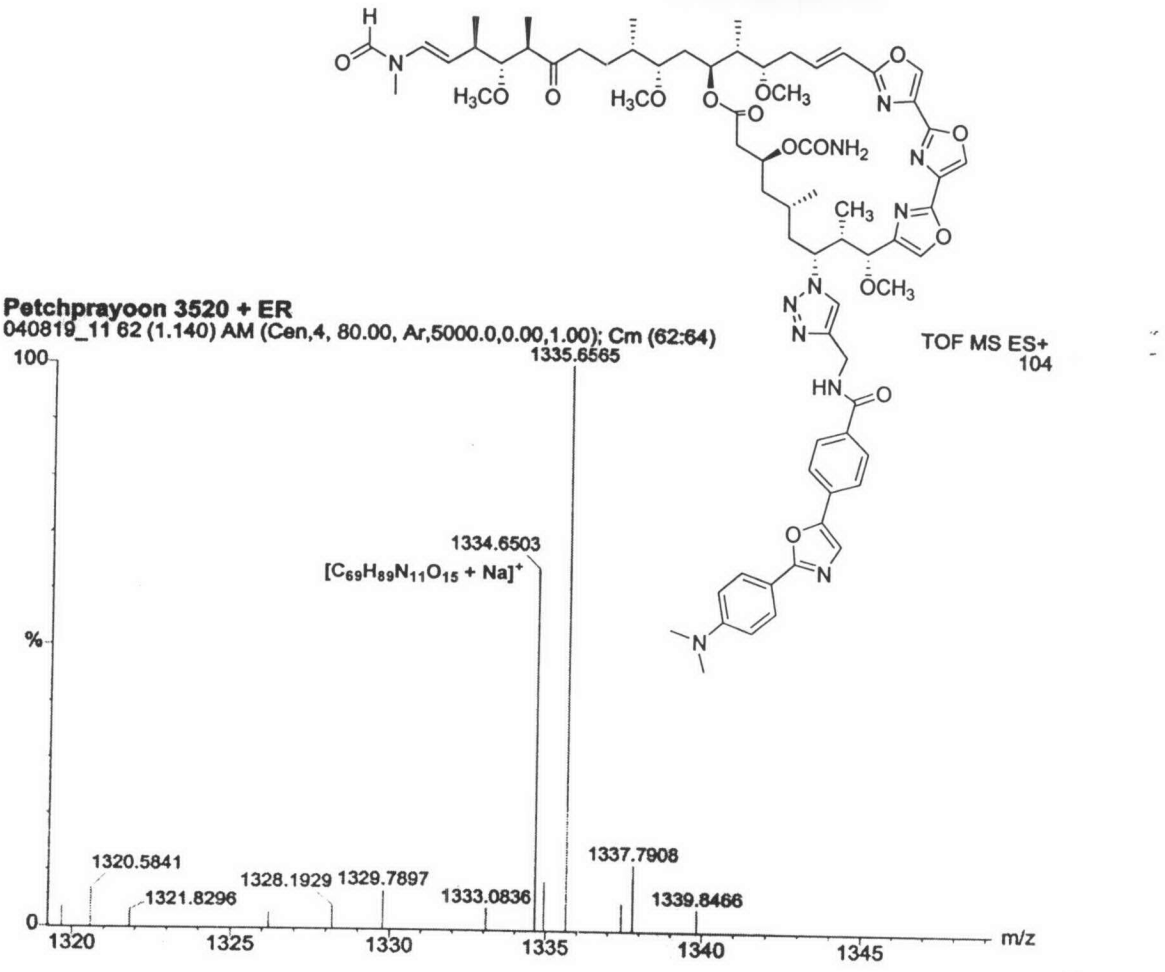

Figure 96 The ESI-TOF mass spectrum of DAP-KabC.

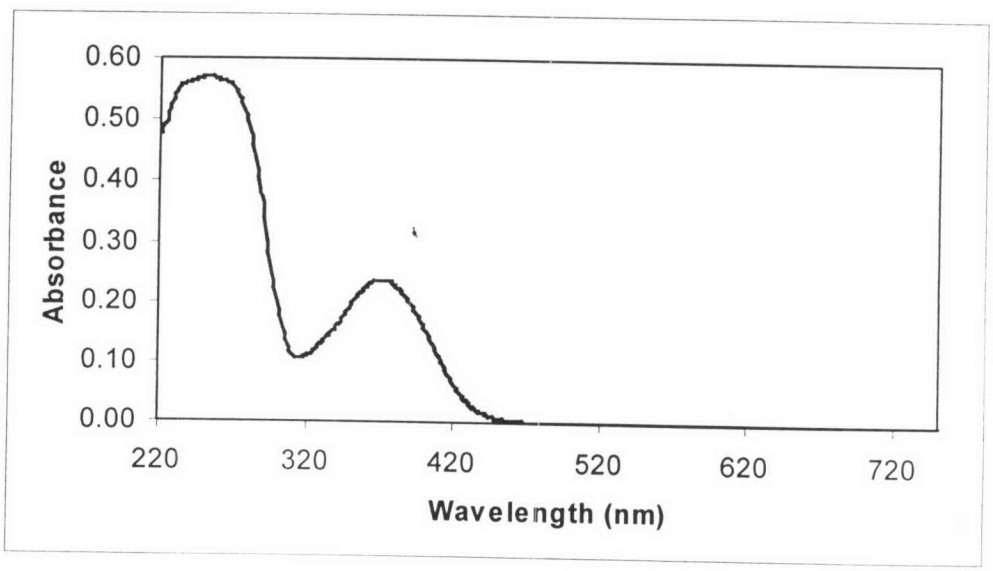

Figure 97 The UV spectrum of DAP-KabC in MeOH.

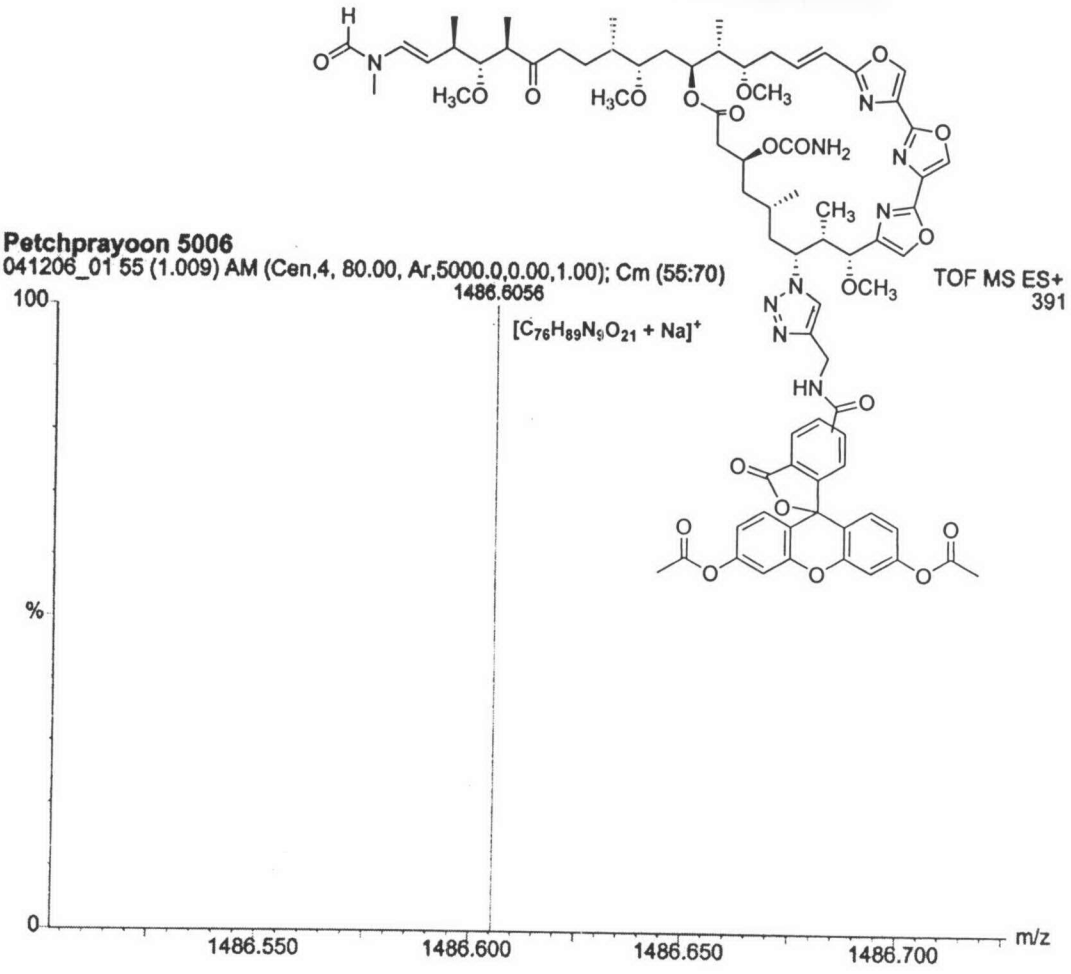

Figure 98 The ESI-TOF mass spectrum of FDE-KabC.

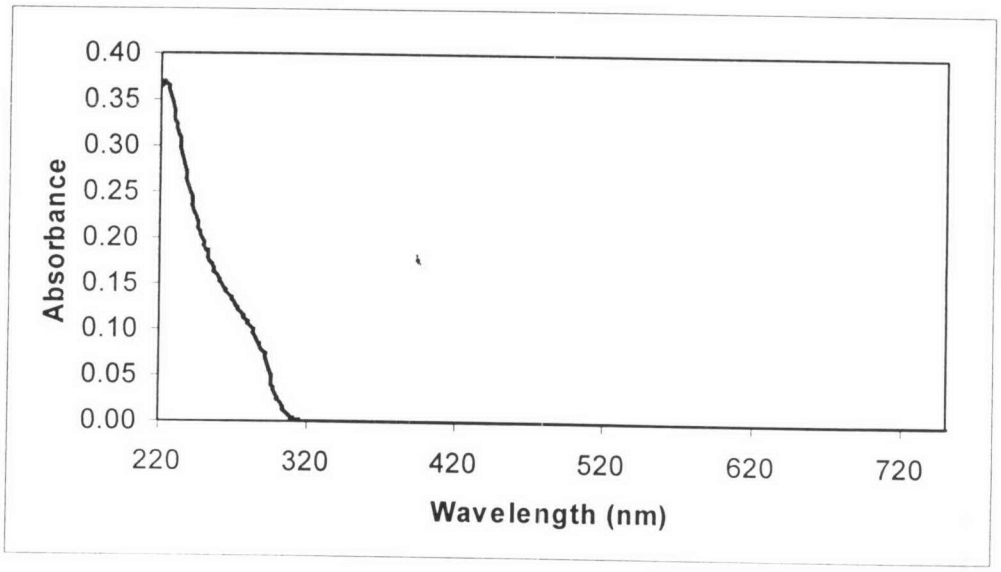

Figure 99 The UV spectrum of FDE-KabC in MeOH.

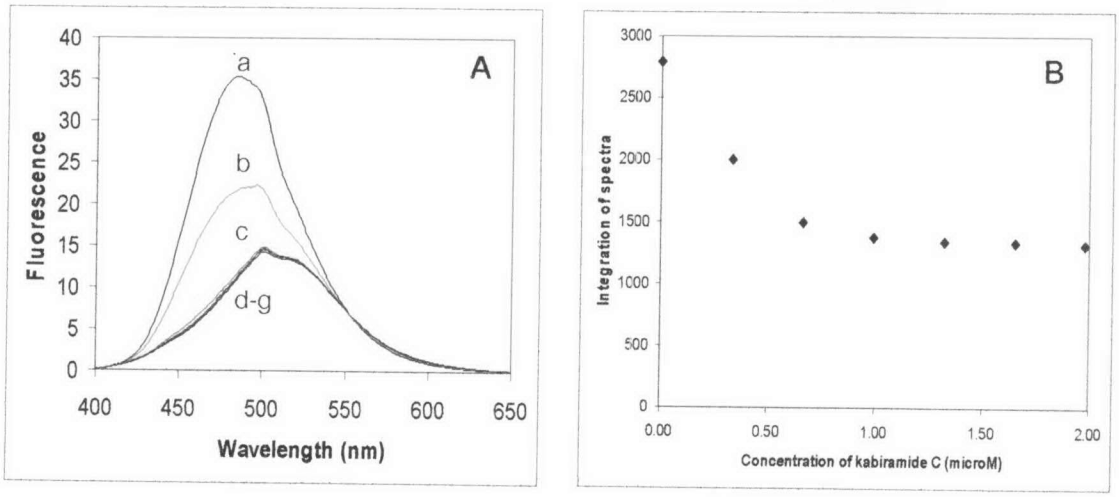

Figure 100 Spectroscopic and actin-binding property of kabiramide C [23].

(A) Stoichiometric binding of prodan-G-actin in G-buffer with 23 at final concentration: (a) 0 μM, (b) 0.33 μM, (c) 0.66 μM, (d) 0.99 μM, (e), 1.32 μM, (f) 1.64 μM, (g) 1.96 μM.

(B) Plot of the integrated intensity in (A) against concentration of 23.

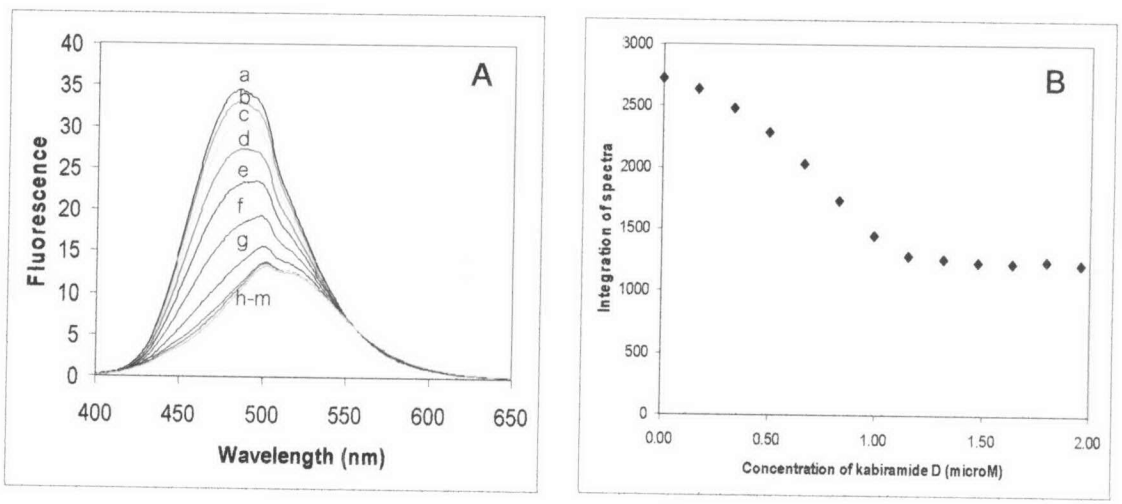

Figure 101 Spectroscopic and actin-binding property of kabiramide D [24].

(A) Stoichiometric binding of prodan-G-actin in G-buffer with 24 at final concentration: (a) 0 μM, (b) 0.17 μM, (c) 0.33 μM, (d) 0.50 μM, (e) 0.66 μM, (f) 0.83 μM, (g) 0.99 μM, (h) 1.15 μM, (i) 1.32 μM, (j) 1.48 μM, (k), 1.64 μM, (l) 1.80 μM, (m) and 1.96 μM.

(B) Plot of the integrated intensity in (A) against concentration of 24.

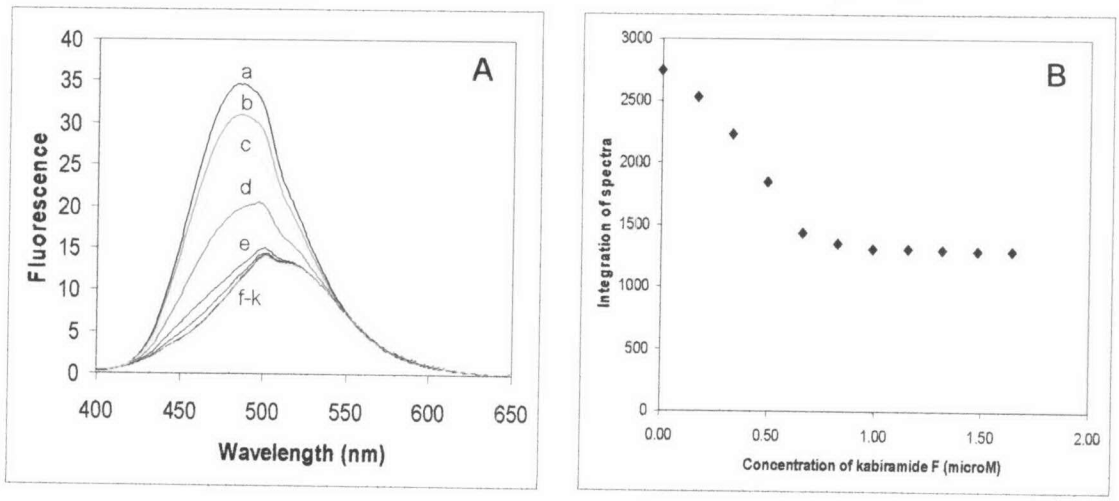

Figure 102 Spectroscopic and actin-binding property of kabiramide F [55].

(A) Stoichiometric binding of prodan-G-actin in G-buffer with 55 at final concentration: (a) 0 μM, (b) 0.17 μM, (c) 0.33 μM, (d) 0.50 μM, (e) 0.66 μM, (f) 0.83 μM, (g) 0.99 μM, (h) 1.15 μM, (i) 1.32 μM, (j) 1.48 μM, (k) 1.64 μM.

(B) Plot of the integrated intensity in (A) against concentration of 55.

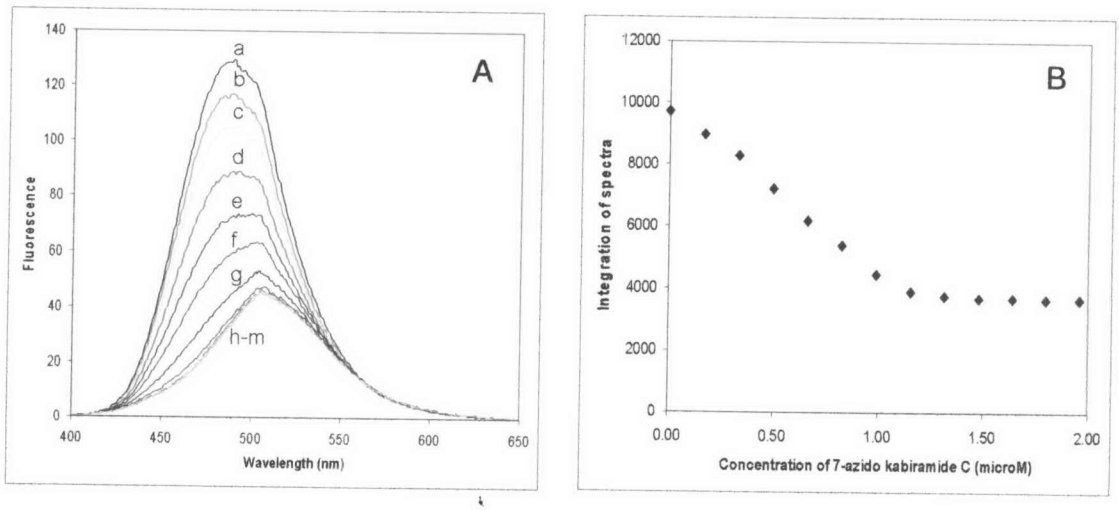

Figure 103 Spectroscopic and actin-binding property of 7-azidokabiramide C [56].

(A) Stoichiometric binding of prodan-G-actin in G-buffer with 56 at final concentration: (a) 0 μM, (b) 0.17 μM, (c) 0.33 μM, (d) 0.50 μM, (e), 0.66 μM, (f) 0.83 μM, (g) 0.99 μM, (h) 1.15 μM, (i) 1.32 μM, (j) 1.48 μM (k) 1.64 μM, (l) 1.80 μM, (m) and 1.96 μM.

(B) Plot of the integrated intensity in (A) against concentration of 56.

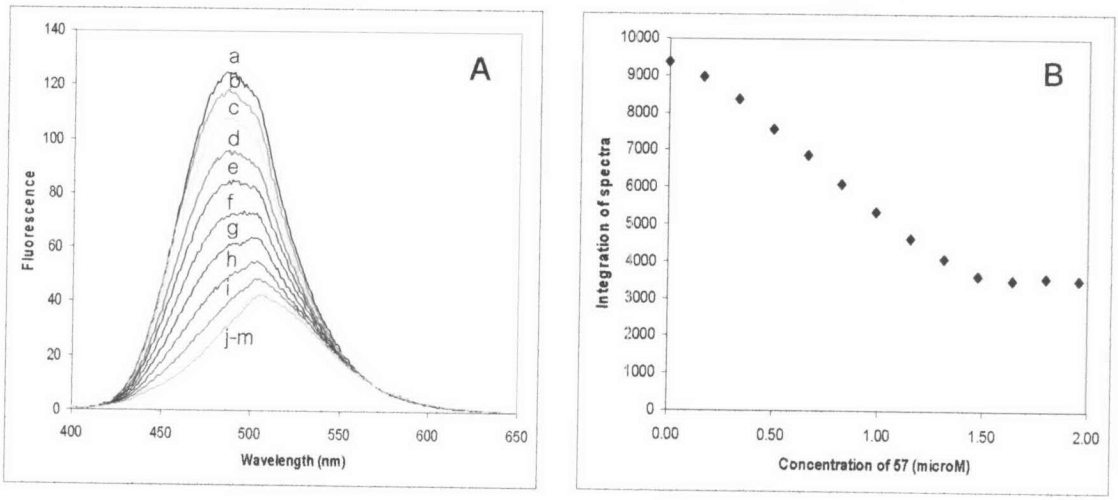

Figure 104 Spectroscopic and actin-binding property of 7-[4-*N*-(9*H*-fluoren-9-yl-methoxycarbonyl)aminomethyl-1,2,3-triazol-1-yl]kabiramide C [57].

(A) Stoichiometric binding of prodan-G-actin in G-buffer with 57 at final concentration: (a) 0 μM, (b) 0.17 μM, (c) 0.33 μM, (d) 0.50 μM, (e), 0.66 μM, (f) 0.83 μM, (g) 0.99 μM, (h) 1.15 μM, (i) 1.32 μM, (j) 1.48 μM (k) 1.64 μM, (l) 1.80 μM, (m) and 1.96 μM.

(B) Plot of the integrated intensity in (A) against concentration of 57.

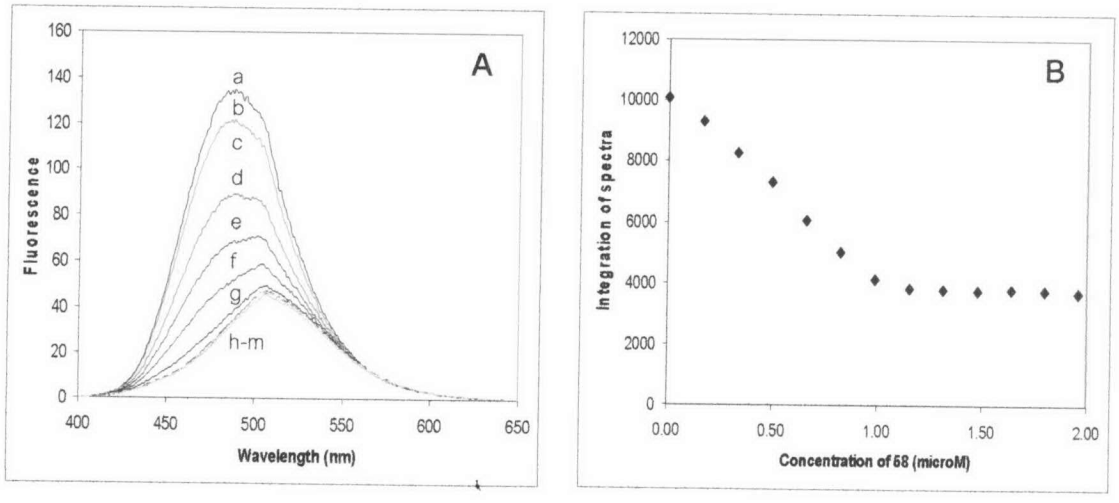

Figure 105 Spectroscopic and actin-binding property of 7-(4-aminomethyl-1*H*-1,2,3-triazol-1-yl)kabiramide C [58].

(A) Stoichiometric binding of prodan-G-actin in G-buffer with 58 at final concentration: (a) 0 μM, (b) 0.17 μM, (c) 0.33 μM, (d) 0.50 μM, (e), 0.66 μM, (f) 0.83 μM, (g) 0.99 μM, (h) 1.15 μM, (i) 1.32 μM, (j) 1.48 μM (k) 1.64 μM, (l) 1.80 μM, (m) and 1.96 μM.

(B) Plot of the integrated intensity in (A) against concentration of 58.

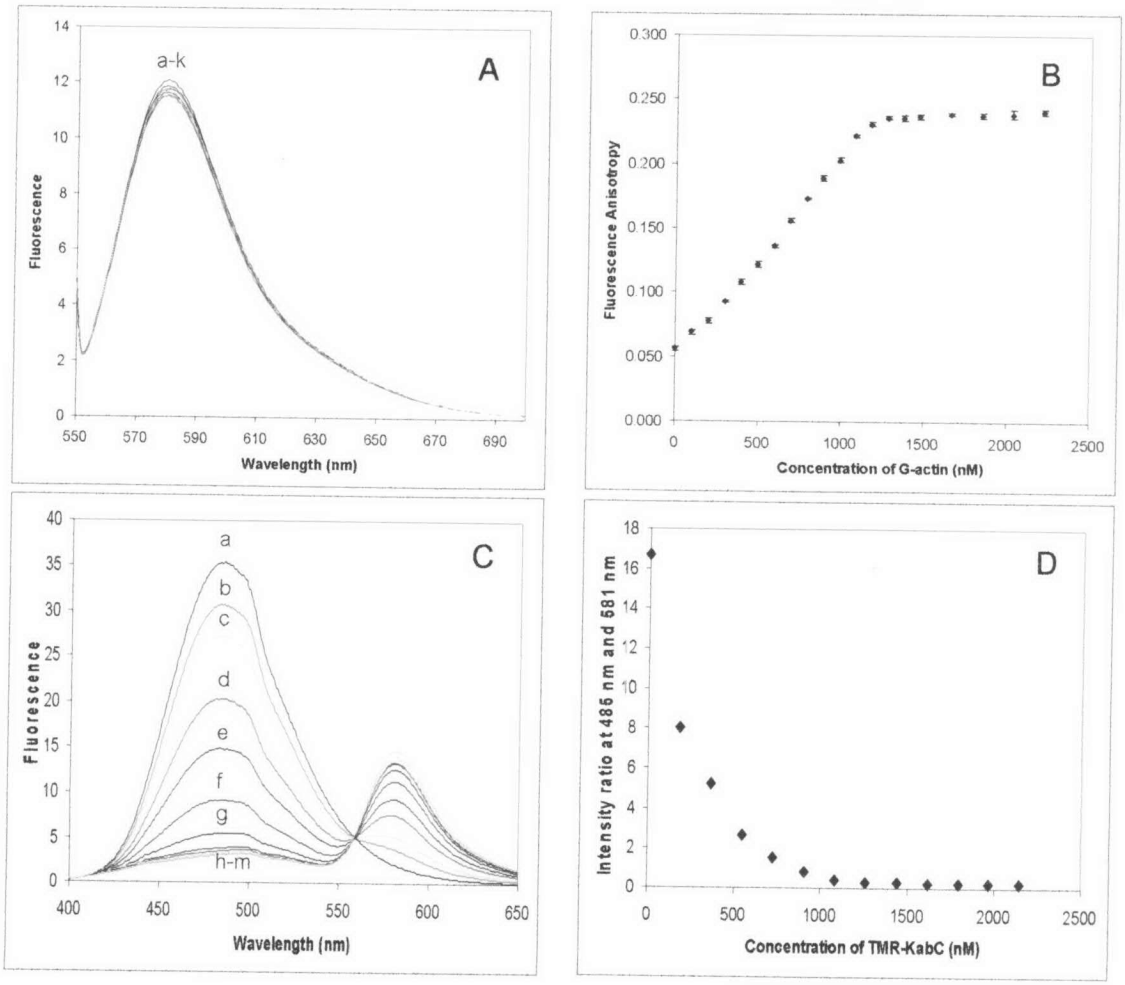

Figure 106 Spectroscopic and actin-binding properties of TMR-KabC [59].

(A) Fluorescence emission spectra of 1 μM TMR-KabC in G-buffer as a function of unlabeled G-actin concentrations: (a) 0 nM; (b) 144 nM; (c) 286 nM; (d) 423 nM; (e) 564 nM; (f) 700 nM; (g) 835 nM; (h) 968 nM; (i) 1099 nM; (j) 1228 nM; and (k) 1356 nM.

(B) Fluorescence anisotropy values of 1 μM TMR-KabC in G-buffer as a function of unlabeled G-actin concentrations.

(C) Fluorescence emission spectra of 1 μM prodan-G-actin in G-buffer as a function of TMR-KabC concentrations: (a) 0 nM; (b) 182 nM; (c) 364 nM; (d) 545 nM; (e) 725 nM; (f) 905 nM; (g) 1084 nM; (h) 1263 nM; (i) 1441 nM; (j) 1618 nM; (k) 1800 nM; (l) 1971 nM; and (m) 2147 nM.

(D) Fluorescence intensity ratio of prodan-G-actin (485 nm, 1 μM) to TMR-KabC (581 nm) as a function of TMR-KabC concentrations. The binding of TMR-KabC was monitored using the fluorescence intensity decrease in prodan resulting from KabC mediated quenching of prodan fluorescence, and the donor quenching and TMR sensitized emission due to FRET.

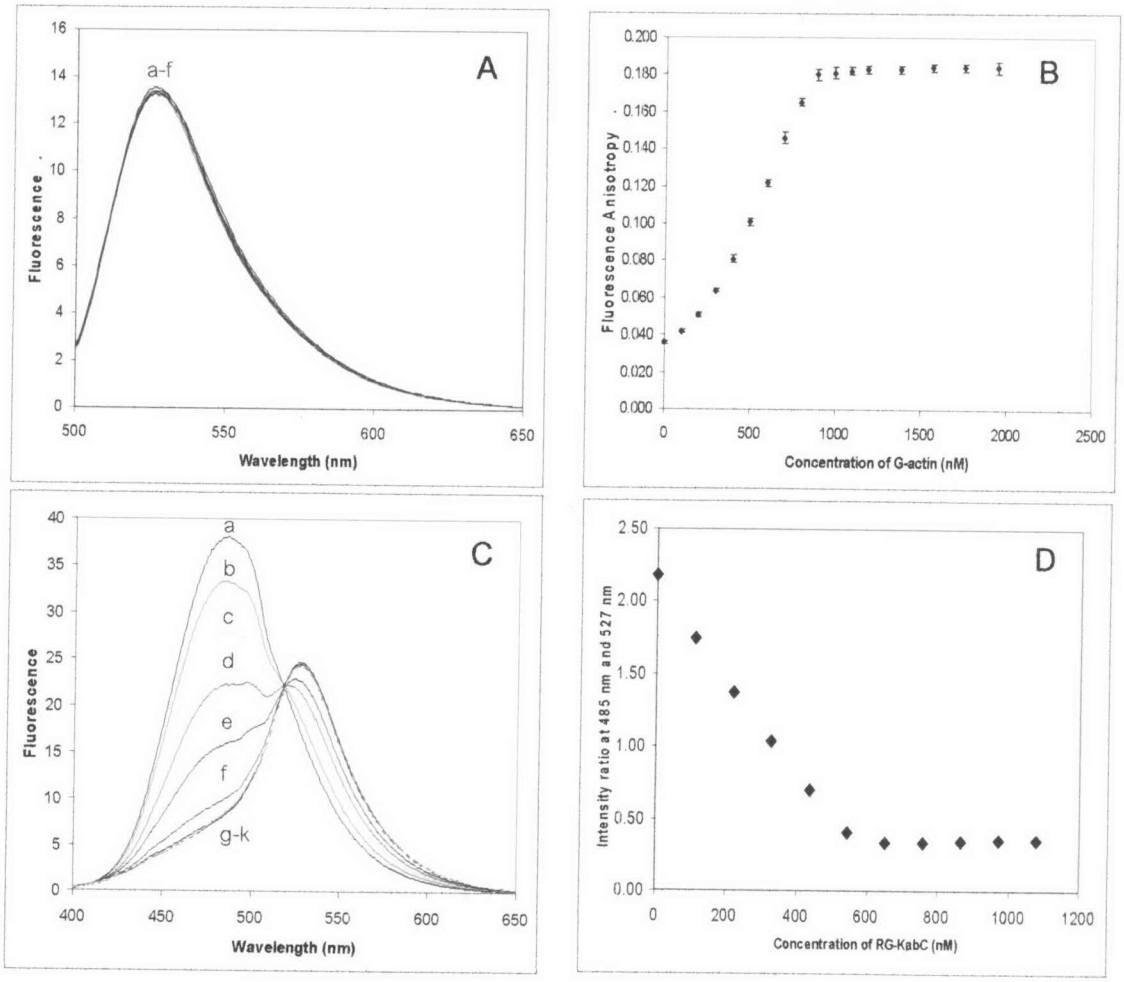

Figure 107 Spectroscopic and actin-binding properties of RG-KabC [60].

(A) Fluorescence emission spectra of 200 nM RG-KabC in G-buffer as a function of unlabeled G-actin concentrations: (a) 0 nM; (b) 72 nM; (c) 144 nM; (d) 215 nM; (e) 286 nM; (f) 356 nM.

(B) Fluorescence anisotropy values of 1 μM RG-KabC in G-buffer as a function of unlabeled G-actin concentrations.

(C) Fluorescence emission spectra of 1 μM prodan-G-actin in G-buffer as a function of RG-KabC concentrations: (a) 0 nM; (b) 109 nM; (c) 218 nM; (d) 327 nM; (e) 435 nM; (f) 543 nM; (g) 651 nM; (h) 758 nM; (i) 865 nM; (j) 971 nM; and (k) 1071 nM.

(D) Fluorescence intensity ratio of prodan-G-actin (485 nm, 1 μM) to RG-KabC (527 nm) as a function of RG-KabC concentrations. The binding of RG-KabC was monitored using the fluorescence intensity decrease in prodan resulting from KabC mediated quenching of prodan fluorescence, and the donor quenching and RG sensitized emission due to FRET.

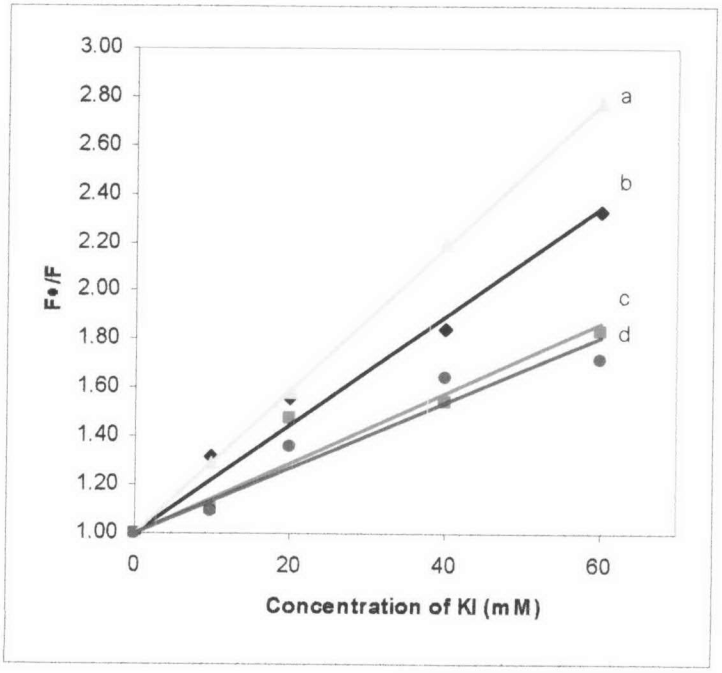

Figure 108 Stern-Volmer plot of iodide quenching behaviors of TMR-KabC, RG-KabC and G-actin complexes in G-buffer as a function of potassium iodide concentrations: (a) TMR-KabC; (b) RG-KabC; (c) TMR-KabC-G-actin complex; and (d) RG-KabC-G-actin complex.

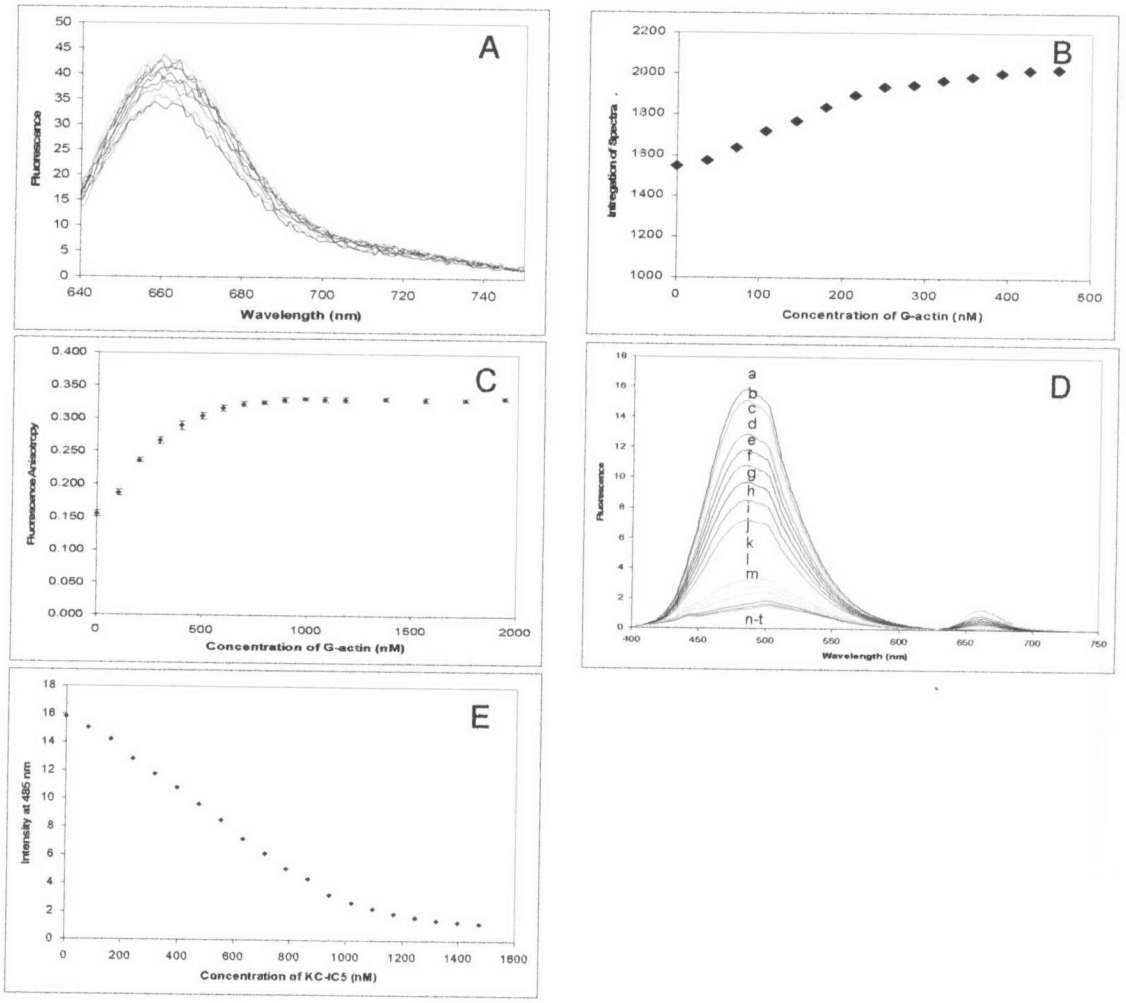

Figure 109 Spectroscopic and actin-binding properties of IC5-KabC [61].

(A) Fluorescence emission spectra of 200 nM IC5-KabC in G-buffer as a function of unlabeled G-actin concentrations.

(B) Fluorescence intensity of IC5-KabC binding to G-actin. The binding of IC5-KabC was monitored using the increase in the integrated emission intensity of IC5-KabC (200 nM, in G-buffer) on binding to actin as a function of G-actin concentrations.

(C) Fluorescence anisotropy values of 1 μM IC5-KabC in G-buffer as a function of unlabeled G-actin concentrations.

(D) Fluorescence emission spectra of 1 μM prodan-G-actin in G-buffer as a function of IC5-KabC concentrations: (a) 0 nM; (b) 80 nM; (c) 160 nM; (d) 239 nM; (e) 318 nM; (f), 397 nM; (g) 475 nM; (h) 554 nM; (i) 632 nM; (j) 709 nM; (k) 787 nM; (l) 864 nM; (m) 941 nM; (n), 1018 nM; (o) 1095 nM; (p) 1171 nM; (q) 1247 nM; (r) 1323 nM; (s) 1398 nM; and (t) 1473 nM.

(E) Fluorescence intensity of 1 μM prodan-G-actin at 485 nm as a function of IC5-KabC concentrations. The binding of IC5-KabC is detected mainly from the decrease in prodan fluorescence resulting from KabC mediated quenching of prodan fluorescence and donor quenching due to FRET to IC5.

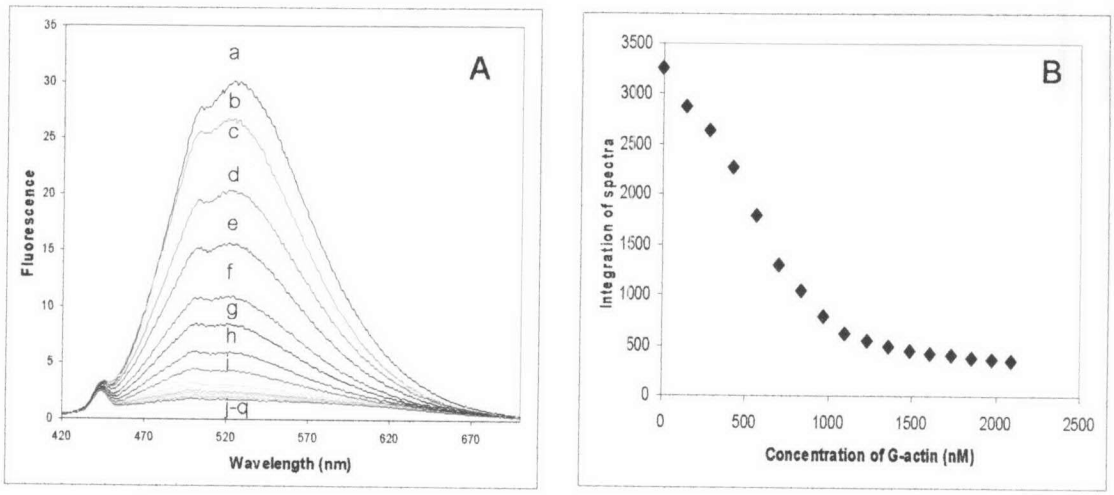

Figure 110 Spectroscopic and actin binding property of DAP-KabC [61]:

(A) Fluorescence emission spectra of 1 μM DAP-KabC in G-buffer as a function of unlabeled G-actin concentrations: (a) 0 nM; (b) 144 nM; (c) 286 nM; (d) 423 nM; (e) 564 nM; (f) 700 nM; (g) 835 nM; (h) 968 nM; (i) 1099 nM; (j) 1228 nM; and (k) 1356 nM; (l) 1483 nM; (m) 1607 nM; (n), 1731 nM; (o) 1852 nM; (p) 1973 nM; (q) 2092 nM;.

(B) Fluorescence intensity of DAP-KabC binding to G-actin. The binding of DAP-KabC was monitored using the decrease in the integrated emission intensity of DAP-KabC on binding to actin as a function of G-actin concentrations.

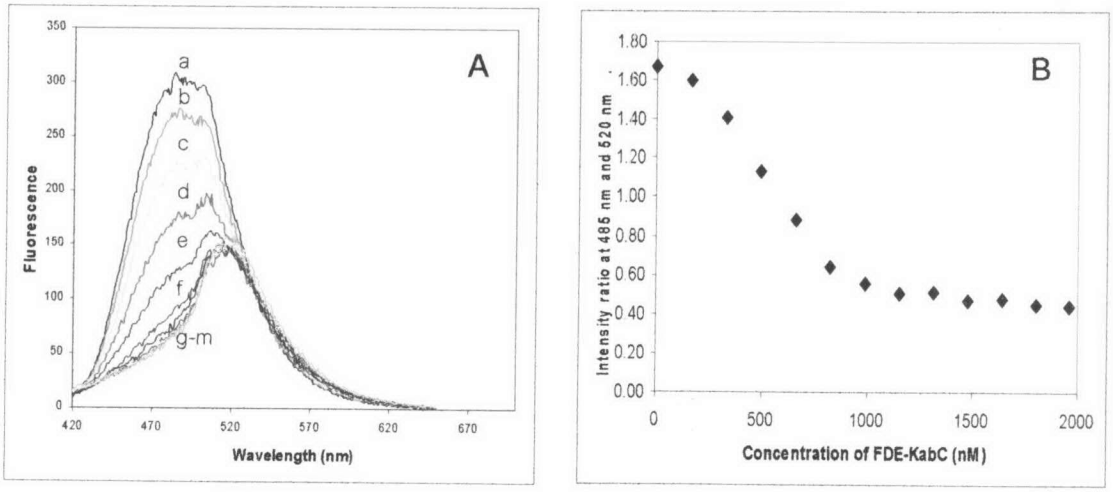

Figure 111 Spectroscopic and actin binding property of FDE-KabC [62]:

(A) Fluorescence emission spectra of 1 μM prodan-G-actin in G-buffer as a function of FDE-KabC concentrations: (a) 0 nM; (b) 1166 nM; (c) 332 nM; (d) 498 nM; (e) 662 nM; (f) 826 nM; (g) 990 nM; (h) 1153 nM; (i) 1316 nM; (j) 1478 nM; (k) 1639 nM; (l) 1800 nM; and (m) 1961 nM.

(B) Fluorescence intensity ratio of prodan-G-actin (485 nm, 1 μM) to FDE-KabC (520 nm) as a function of FDE-KabC concentrations. The binding of FDE-KabC is monitored using the fluorescence intensity decrease in prodan resulting from KabC mediated quenching of prodan fluorescence, and the donor quenching and FDE sensitized emission due to FRET.

VITA

Miss Chutima Petchprayoon was born on October 5, 1973 in Nakhonnayok Province, Thailand. She received her Bachelor Degree of Science in Pharmacy in 1996 and Master degree of Science in Pharmacy in 2000 from the Faculty of Pharmaceutical Sciences, Chulalongkorn University, Bangkok, Thailand. During 1996-1999, she was a pharmacist in Bundharik Hospital, Ubon Ratchathani Province, Thailand. She has been granted a 2001 Royal Golden jubilee Ph.D. Scholarship from the Thailand Research Fund (TRF).

Publications

1. Petchprayoon, C., Suwanborirux, K., Miller, R., Sakata, T., and Marriott, G. 2005. Synthesis and characterization of 7-(4-aminomethyl-1*H*-1,2,3-triazol-1-yl) analog of kabiramide C. J. Nat. Prod. 68(2): 157-161.
2. Petchprayoon, C., Suwanborirux, K., Tanaka, C., Tanaka, J., Yan, Y., Sakata, T., and Marriott, G. 2005. Quantitative analyses of functional interactions at the barbed (+)-end of actin using a family of fluorescent kabiramide C probes. Bioconjugate Chem. submitted.

Oral presentations

1. Petchprayoon, C. "Development of kabiramides, the actin-binding trisoxazole macrolides from the Thai marine sponge, as a cellular research tool" 22nd RGJ Seminar Series: Research Progress in Pharmacognosy and Phytochemistry, Febuary 11, 2003, Faculty of Pharmaceutical Sciences, Chulalongkorn University, Bangkok, Thailand.
2. Petchprayoon, C. "Synthesis and characterization of fluorescent derivatives of kabiramide C, an actin-binding trisoxazole macrolide from *Pachastrissa nux* sponge" RGJ-Ph.D. Congress VI, April 28-30, 2005, Pattaya, Bangkok, Thailand.

Poster presentations

1. Petchprayoon, C., and Suwanborirux, K. "Antifungal trisoxazole macrolides, kabiramides, from the Thai marine sponge, *Pachastrissa nux*" p160. The 6th JSPS-NRCT Joint Seminar: Recent Advances in Natural Medicine Research. December 2-4, 2003, Faculty of Pharmaceutical Sciences, Chulalongkorn University, Bangkok, Thailand.
2. Petchprayoon, C., Suwanborirux, K., Sakata, T.,Tanaka, J., Marriott, G. 'Mapping actin filament dynamics in vitro and in vivo with fluorescent kabiramides" p171. The American Society for Cell Biology 44th Annual Meeting. December, 4-8, 2004, Washington, DC, USA.